2. SITE 657[1]

Shipboard Scientific Party[2]

HOLE 657A

Date occupied: 27 February 1986, 2215 UTC

Date departed: 1 March 1986, 2200 UTC

Time on hole: ~48 hr

Position: 21°19.89′N, 20°56.93′W

Water depth (sea level; corrected m, echo-sounding): 4221.8

Water depth (rig floor; corrected m, echo-sounding): 4232.3

Bottom felt (rig floor; m, drill pipe): 4231.6

Distance between rig floor and sea level (m): 10.5

Total depth (rig floor, m): 4409.8

Penetration (m): 178.2

Number of cores (including cores with no recovery): 19

Total length of cored section (m): 178.2

Total core recovered (m): 126.84

Core recovery (%): 71.2

Oldest sediment cored:
Depth sub-bottom (m): 178.2
Nature: green zeolitic clay
Age: late Miocene, NN11, ~8 Ma

HOLE 657B

Date occupied: 1 March 1986, 2200 UTC

Date departed: 3 March 1986, 1215 UTC

Time on hole: ~38 hr

Position: 21°19.89′N, 20°56.93′W

Water depth (sea level; corrected m, echo-sounding): 4226.8

Water depth (rig floor; corrected m, echo-sounding): 4237.3

Bottom felt (rig floor; m, drill pipe): 4231.6

Distance between rig floor and sea level (m): 10.5

Total depth (rig floor, m): 4397.7

Penetration (m): 166.1

Number of cores (including cores with no recovery): 19

Total length of cored section (m): 166.1

Total core recovered (m): 132.48

Core recovery (%): 79.75

Oldest sediment cored:
Depth sub-bottom (m): 166.1
Nature: red brownish clay
Age: late middle Miocene, NN10, ~9–10 Ma

Principal results: Site 657 is located at 21°19.89′N, 20°56.93′W, on the lower continental rise 380 km west of Cap Blanc. Among three companion sites investigating the late Neogene history of northern trade winds and upwelling offshore from Africa, Site 657 was proposed as a "non-upwelling" site.

The site was drilled on a smooth plain of a distal turbidite fan into a well-layered, thick seismic sequence that appears relatively undisturbed. In Holes 657A and 657B in 4221 m water depth, we recovered a total of 35 advanced piston cores (APC) to depths of 149.7 meters below the seafloor (mbsf) (Hole 657A) and 166.1 mbsf (Hole 657B), and 3 extended-core-barrel (XCB) cores from Hole 657A to the total penetration of 178.2 mbsf. The drilling results are summarized in a stratigraphic section (Fig. 1).

The upper Neogene sedimentary section at Site 657 comprises two major, mainly pelagic lithostratigraphic units the upper of which is divided into five subunits. All units and subunits have marginal paleomagnetic but excellent biostratigraphic time control, despite substantial carbonate dissolution within certain intervals. A number of markers enabled us to establish a preliminary composite depth section of the two holes.

Subunit IA. 0–13.6 mbsf. Pleistocene (lowermost Brunhes) to Holocene. Pelagic sediment cycles of nannofossil ooze grading upward from darker colored greenish gray silt-bearing ooze to lighter grayish foraminifer-bearing ooze with minor intercalations of quartzose silt and sand layers. Sediment-accumulation rates average 23 m/m.y. for this interval.

Subunit IB. 13.6–26.2 mbsf. Pleistocene (lowermost Brunhes). Slump-folded greenish gray to dark greenish gray clayey nannofossil ooze with a high content (1%–2.2%) of organic carbon and a 70-cm-thick quartzose sand layer at its top (Hole 657B). The upwelling region near Site 658 offshore from Cap Blanc is considered a possible origin for Subunit IB.

Subunit IC. 26.2–96.5 mbsf. Upper Pliocene to Pleistocene (Brunhes-Matuyama boundary). Light-colored nannofossil-ooze cycles such as in Subunit IA, with numerous (up to 10 per core) thin, turbiditic and/or contouritic beds of darker colored quartzose mud, silt, and sand. Sediment-accumulation rates average 20 m/m.y. in the lower part and 45 m/m.y. in the upper part of this subunit.

Subunit ID. 96.5–124.5 mbsf. Lower Pliocene to lower–upper Pliocene. Recumbent slump fold of nannofossil-ooze cycles such as in Subunits IA and IC, but only with rare turbidites interbedded. Slump of local origin.

---

[1] Ruddiman, W., Sarnthein, M., Baldauf, J., et al., 1988. *Proc., Init. Repts. (Pt. A), ODP*, 108.

[2] William Ruddiman (Co-Chief Scientist), Lamont-Doherty Geological Observatory, Palisades, NY 10964; Michael Sarnthein (Co-Chief Scientist), Geologisch-Paläontologisches Institut, Universität Kiel, Olshausenstrasse 40, D-2300 Kiel, Federal Republic of Germany; Jack Baldauf, ODP Staff Scientist, Ocean Drilling Program, Texas A&M University, College Station, TX 77843; Jan Backman, Department of Geology, University of Stockholm, S-106 91 Stockholm, Sweden; Jan Bloemendal, Graduate School of Oceanography, University of Rhode Island, Narragansett, RI 02882-1197; William Curry, Woods Hole Oceanographic Institution, Woods Hole, MA 02543; Paul Farrimond, School of Chemistry, University of Bristol, Cantocks Close, Bristol BS8 1TS, United Kingdom; Jean Claude Faugeres, Laboratoire de Géologie-Océanographie, Université de Bordeaux I, Avenue des Facultés Talence 33405, France; Thomas Janacek, Lamont-Doherty Geological Observatory, Palisades, NY 10964; Yuzo Katsura, Institute of Geosciences, University of Tsukuba, Ibaraki 305, Japan; Hélène Manivit, Laboratoire de Stratigraphie des Continents et Océans, (UA 319) Université Paris VI, 4 Place Jussieu, 75230 Paris Cedex, France; James Mazzullo, Department of Geology, Texas A&M University, College Station, TX 77843; Jürgen Mienert, Geologisch-Paläontologisches Institut, Universität Kiel, Olshausenstrasse 40, D-2300 Kiel, Federal Republic of Germany, and Woods Hole Oceanographic Institution, Woods Hole, MA 02543; Edward Pokras, Lamont-Doherty Geological Observatory, Palisades, NY 10964; Maureen Raymo, Lamont-Doherty Geological Observatory, Palisades, NY 10964; Peter Schultheiss, Institute of Oceanographic Sciences, Brook Road, Wormley, Godalming, Surrey GU8 5UG, United Kingdom; Rüdiger Stein, Geologisch-Paläontologisches Institut, Universität Giessen, Senckenbergstrasse 3, 6300 Giessen, Federal Republic of Germany; Lisa Tauxe, Scripps Institution of Oceanography, La Jolla, CA 92093; Jean-Pierre Valet, Centre des Faibles Radioactivités, CNRS, Avenue de la Terrasse, 91190 Gif-sur-Yvette, France; Philip Weaver, Institute of Oceanographic Sciences, Brook Road, Wormley, Godalming, Surrey GU8 5UG, United Kingdom; Hisato Yasuda, Department of Geology, Kochi University, Kochi 780, Japan.

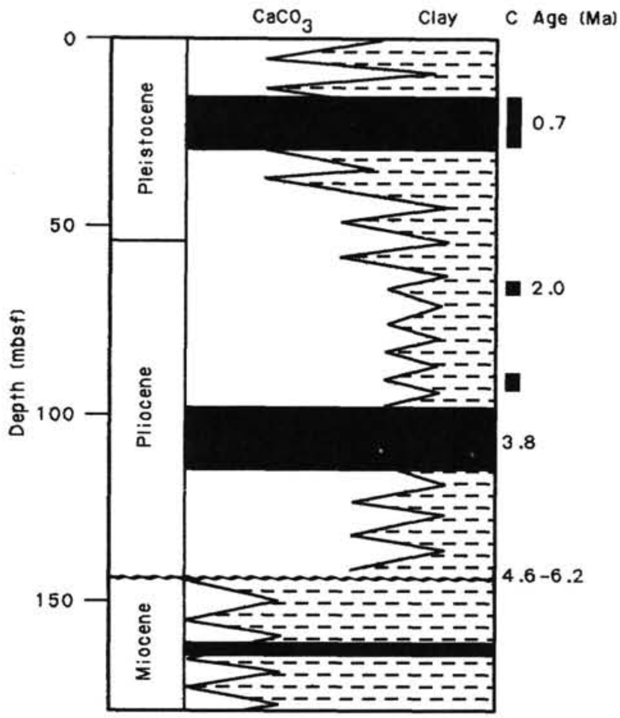

Figure 1. Summary of the stratigraphic section at Site 657. Representation of $CaCO_3$ cycles is merely schematic and based both on visual description and widely spaced shipboard laboratory analyses. *C* = organic carbon.

Subunit IE. 124.5-146.2 mbsf. Lower Pliocene. Light-colored nannofossil-ooze cycles such as in Subunits IA and IC, with interbedded turbidites and/or contourites. Sediment-accumulation rates average 31 m/m.y. in this subunit. A major hiatus of 1.6 m.y. forms the base of this unit.

Unit II. 146.2-178.2 mbsf. Upper Miocene. Pale brown to brownish red nannofossil-bearing and barren clay and silty clay with scattered thin, dark-gray quartzose sand and sandy-silt layers and a major quartz-sand bed at the base, where the drilling terminated. The unit reflects pelagic deposition of wind-borne silt near or below the carbonate compensation depth (CCD). Sediment-accumulation rates average 2.5-12 m/m.y. in this unit.

The Messinian-age hiatus at the top of Unit II corresponds in time to a major lowering of the CCD, and possibly a bottom-water-current event. Below the hiatus, shear strength strongly increased, resulting in a major reflector traceable over a distance of several hundred kilometers. A number of moderate-strength reflectors can be correlated with turbidites and with the top of the mudflow units, with seismic velocities generally ranging from 1450 to 1700 m/s.

The influence of the Canary Current is registered by planktonic foraminifers characteristic of cool water in most parts of Unit I. However, for quantitative estimates of paleoceanography, further work is required for which unexpectedly high sedimentation rates of most pelagic-sediment sections provide a good opportunity.

BACKGROUND AND SCIENTIFIC OBJECTIVES

Introduction

From a global perspective, the response of the eastern subtropical Atlantic to global climatic change is critical to paleoceanography. Here the long-term variations of two important oceanographic features, the Canary Current, a strong Eastern Boundary Current, and the oceanic upwelling offshore from northwest Africa, can be recognized from the sediments.

Moreover, sediments from the eastern Atlantic offer a unique opportunity to decipher the evolution of atmospheric circulation, which in turn controls the surface-water oceanography and reveals such major meteorological structures as the Hadley cell. Finally, the terrigenous sediments here form an important tool for connecting the history of land climates with the global history of the oceans and polar ice sheets—i.e., in north Africa, the history of the Sahara, the largest desert in the world.

Leg 108 of the Ocean Drilling Program set out to investigate some of these problems at the three companion Sites 657, 658, and 659 along two transects forming a triangle across the lower continental slope and rise and the Cape Verde Plateau (Fig. 2). The drill sites were selected to address the following scientific objectives:

1. To unravel the Neogene history of the permanent oceanic upwelling cell offshore from Cap Blanc and to separate these signals in the sedimentary record from those of the Canary Current (Fig. 3).
2. To investigate the Neogene history of the meridional trades and the zonal mid-tropospheric jet of the Saharan Air Layer. Both wind systems are documented by a specific dust supply and provide specific information on the northward paleo-advance of the Intertropical Convergence Zone during northern summers (Fig. 4).
3. To learn about the dominant mode of Milankovitch cycles controlling the history of wind regimes and upwelling in these latitudes, i.e., whether the 19,000/23,000-yr precessional cycle or the 41,000-yr obliquity cycle predominates in the wind and upwelling history.
4. To study deep-water paleoceanography at water depths between 2260 and 4220 m, particularly within the range of long-term fluctuations of the lysocline along the continental margin (Fig. 5).
5. To investigate the evolution of cold-water plankton species in low latitudes during Neogene time.

Specific Objectives and Setting

Site 657 (21°19.89′N, 20°56.93′W) lies at the lower continental rise about 400 km (220 nmi) west of Cap Blanc in a water depth of about 4221 m (Fig. 2). It lies close to the position of DSDP Site 140 (21°44.97′N, 21°47.52′W; 4483 m water depth). Its position was selected particularly for the following purposes:

1. To study the Neogene history of the Canary Current recorded in a sediment column clearly outside the influence of coastal upwelling.
2. To investigate an eolian-dust record dominated by input from the zonal flow of the Saharan Air Layer and little influenced by dust supply from the meridional trade winds.
3. To date Neogene eolian-sand turbidites (already observed at this position in cores from DSDP Site 140; Sarnthein, 1978) and fluvial-mud turbidites, which signify extreme Saharan aridity vs. humid climates.
4. To record the deep-water paleoceanography near the present lower boundary of the North Atlantic Deep Water (NADW).

The sediment morphology near Site 657 is very smooth. It is generally formed by shallow distributary fan channels of distant turbidity currents as shown by 3.5-kHz records (Figs. 6 and 7). The approximate position of the site is indicated on unpublished *Vema* and GEOTROPEX'85 cruise records (Figs. 6 and 7B). The approaching seismic lines near Site 657 are shown on the *JOIDES Resolution* records (Fig. 7A), with a close-up of Vema profile 3014 in Figure 7B and a 3.5-kHz record of the high-precision depth recorder in Figure 7C. Here the thick, layered seismic sequence appears relatively undisturbed. Several reflectors can be traced over distances of more than 180 km (100 nmi). The uppermost 0.2-s-thick sediments show a distinct fine seismic layer-

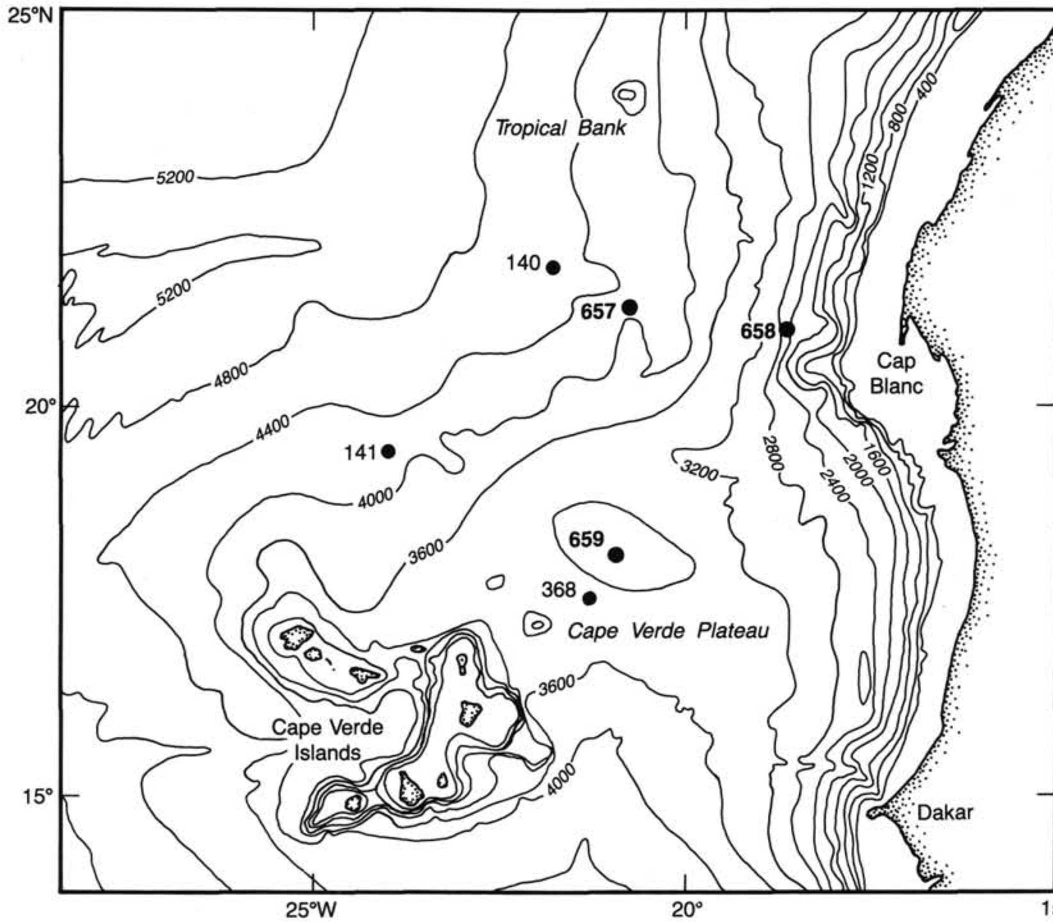

Figure 2. Location map of Sites 657, 658, and 659. Bathymetry (in meters) from Uchupi (1971).

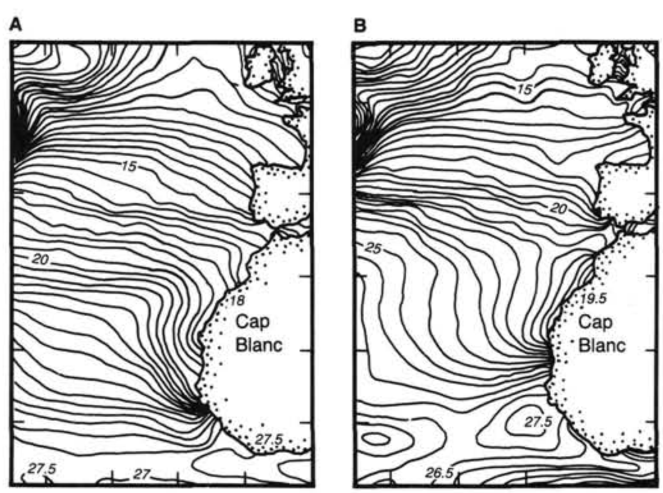

Figure 3. Permanent upwelling cell offshore from Cap Blanc as shown by zonal negative temperature anomalies during January (*A*) and July (*B*). Temperatures shown in degrees Celsius. After Sarnthein et al. (1982).

ing. At 0.2-s two-way traveltime, an apparently conformable major reflector grades laterally into distinct unconformities with erosional and onlap structures some 21.5 km (12 nmi) farther east and downlap some 36 km (20 nmi) farther west. Another major change of seismic character occurs at about 0.4 s. It separates the overlaying medium-coarse layered sequence from an extremely fine laminated sequence underneath. This change is believed to represent a pronounced lithologic change from clayey chalk and carbonate muds to mainly silty clay and diatom oozes as deduced by analogy with the results from other sites drilled in the vicinity (DSDP Sites 368 and 140; Lancelot, Seibold, et al., 1978; Hayes, Pimm, et al., 1972).

In contrast to the generally prevailing prolonged and slightly hyperbolic echos with rare and weak sub-bottom reflectors, which is indicative of a turbidite fan (Jacobi and Hayes, 1982), the 3.5-kHz echo character near Site 657 is layered.

OPERATIONS

We arrived at Site 657 after steaming for six days from Marseille, France, where the *JOIDES Resolution* departed at 1815 UTC on 21 February 1986. (All times are expressed as UTC, Universal Time Coordinated, formerly expressed as GMT, Greenwich Mean Time.) This transit provided an opportunity to check over the lab gear and discuss various questions of definition to iron out all procedural problems in the lab. We entered the Site 657 (MAU-5) survey area of *Vema* cruises 30-05, -14, and 32-05, and of *Polarstern* cruise ANT IV/1b (GEOTROPEX'85) on 10 October 1985, 0600 hr.

At Point 1 (Table 1; Fig. 6B), the *JOIDES Resolution* slowed from an average of 13 kt to 5.5 kt to allow deployment of seismic gear and commencement of a pre-site survey. The survey employed 80-in.^{3} water guns, 3.5-kHz sub-bottom profiler, and magnetometer, and continued for 36 km (20 nmi) as we approached Site 657 from the north via Points 1, 2, and 3 (Fig. 6B; Table 1). We dropped the beacon after Point 3 at 2215 hr, when we crossed the seismic line again between Points 1 and 2 and pulled the water guns and magnetometer.

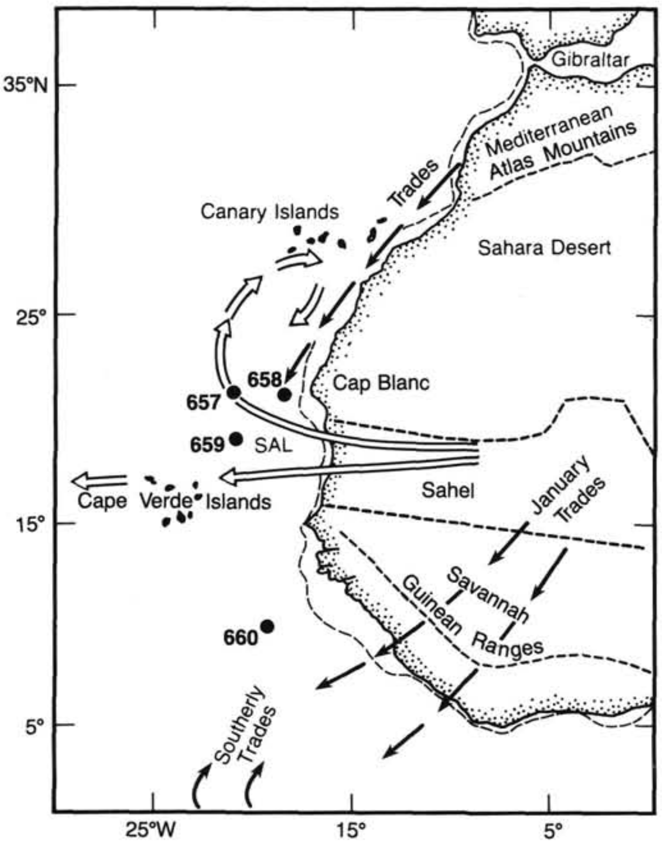

Figure 4. Atmospheric-circulation systems over the eastern Atlantic and major climatic zones in northwest Africa (after Stein and Sarnthein, 1984). Sites 657 through 660 are shown. Arrows mark flow patterns and directions of dust supply by different wind systems. Solid arrows = meridional trade winds at the surface; open arrows = mid-tropospheric zonal winds of Saharan Air Layer (*SAL*).

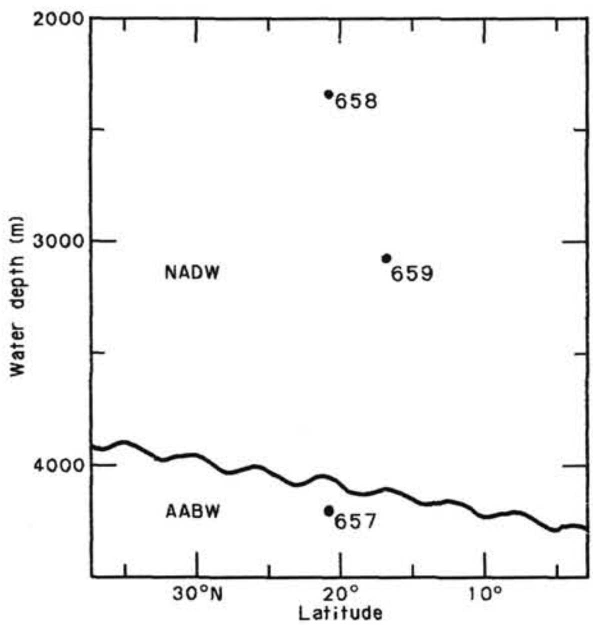

Figure 5. Deep-water masses and site positions in a transect of latitude vs. water depth along the northwest African continental margin. Antarctic Bottom Water (*AABW*) mixed with North Atlantic Deep Water (*NADW*).

We stopped over the beacon at 2240 hr and began tripping drill pipe and coring Hole 657A at 2245 hr. The first 7.2-m APC core was on deck at 1130 hr on 28 February. The mud line (water depth) for Hole 657A was established by drill pipe at 4221 m at 0900 hr. Coring continued uneventfully for 12 cores (Table 2). Core 108-657A-13H was lost, owing to a break of the sand line at the rope socket. After 4 hr the piston was successfully retrieved, and piston coring continued down to Core 108-657A-16H. We changed to XCB coring at 1300 hr on 1 March, and the first (empty) XCB core (Core 108-657A-17X) came on board at 1444 hr. Coring in Hole 657A ended when Core 108-657A-19X came on deck at 2012 hr (Table 2), because the three final XCB cores had extremely poor (0.4% to 42.6%) core recovery owing to a thick sand layer at the base of the hole. We began tripping out of Hole 657A at 2040 hr, and we cleared the mud line and finished a 25-m offset to Hole 657B at 2200 hr.

The first core of Hole 657B was on deck at 0045 hr on 2 March, and coring continued successfully for 18 APC cores until 0020 hr on 3 March, when the corer ceased to penetrate farther than 2 m because of the sand layer previously observed in Hole 657A. One final XCB core (Core 108-657B-19X; Table 2) did not provide any further recovery. We began tripping out of the hole at 1100 hr on 3 March, brought the drill string on deck, and were under way to Site 658 at 1215 hr.

Examination of cores at Site 657 indicated that some of the concern over apparent contortion by coring disturbances in Hole 657A may have been unnecessary. The upper and lowermost parts of many cores contained up to several meters of contorted sediment separated by intervals of normal-looking sediment. However, after comparing the sedimentary fabrics of cores from Holes 657A and 657B in detail, we learned that a good part of these flow structures can be ascribed to natural folding of sliding pelagic sediments. The basis for this interpretation is that specific contortion structures could be observed at approximately the same sub-bottom depths (see "Composite-Depth Section," this chapter). Nevertheless, almost 30 contorted core sections up to 3 m thick must still be ascribed to coring disturbances.

LITHOSTRATIGRAPHY AND SEDIMENTOLOGY

Introduction

Two major sedimentary units are recognized at Site 657. Unit I is composed of nannofossil ooze, with lesser amounts of sand, silt, and clay, and ranges in age from early Pliocene to Holocene. Unit II is composed primarily of silt and clay and is late Miocene in age. Each unit is described in detail in the following sections.

Unit I

Cores 108-657A-1H through -657A-16H-4; depth, 0–146.2 mbsf; thickness, 146.2 m; age, early Pliocene through Holocene.
Cores 108-657B-1H through -657B-16H, CC; depth, 0–145.2 mbsf; thickness, 145.2 m; age, early Pliocene through Holocene.

Unit I is composed of nannofossil ooze, with lesser amounts of quartzose sand, silty sand, silt, clayey nannofossil ooze, and nannofossil-bearing clay (Figs. 8 and 9). The unit is moderately to greatly disturbed by the drilling process, and in some intervals it is soupy and completely homogenized.

Unit I can be divided into five subunits:

	Hole 657A	*Hole 657B*
Subunit IA	0–13.6 mbsf	0–14.8 mbsf
Subunit IB	13.6–26.2 mbsf	14.8–27.5 mbsf
Subunit IC	26.2–96.5 mbsf	27.5–97.3 mbsf
Subunit ID	96.5–124.5 mbsf	97.3–120.0 mbsf
Subunit IE	124.5–146.2 mbsf	120.0–145.2 mbsf

Subunits IA, IC, and IE are composed predominantly (over 90%) of nannofossil ooze that contains minor amounts of foraminifers, quartz silt, clay, and sponge spicules. This sediment is commonly white, light gray, light greenish gray, greenish gray, and/or pinkish gray and commonly grades upward from silt-bearing, darker colored (e.g., greenish gray) nannofossil ooze to foraminifer-bearing, lighter colored (e.g., light greenish gray) nannofossil ooze (e.g., Core 108-657A-14H). It is slightly to moderately bioturbated, and its bedding is subhorizontal.

Quartzose sand, silty sand, and silt are minor lithologies within Subunits IA, IC, and IE. These lithologies are most common in Subunit IC (Cores 108-657A-4H through -657A-9H and 108-657B-4H through -657-9H) and Subunit IE (Cores 108-657A-15H, -657A-16H, -657B-14H, and -657B-15H; Fig. 10), and they are commonly composed of quartz, foraminifers, and minor amounts of nannofossils and contain rare broken shell debris and granule-sized clasts. These sediments are commonly dark gray, dark greenish gray, greenish gray, and light gray. They are present in subhorizontal beds that are generally very thin (1 to 5 cm) but are thicker (up to 57 cm) in Cores 108-657B-2H, -657B-9H, and -657B-14H. The individual beds have sharp, presumably erosive, basal contacts with underlying nannofossil ooze and commonly grade upward into nannofossil ooze. Reverse grading and low-angle cross-laminations occur sparsely in the lowest intervals.

Nannofossil-bearing clay is a rare lithology in Unit I and is found only in Subunit IA in Hole 657A (Core 108-657A-1H-4, 76–92 cm, 99–114 cm, and 123–147 cm). It is composed of clay minerals and quartz, and minor amounts of quartz silt and nannofossils and is gray, light gray, light olive brown, and yellow green. The sediment is slightly to moderately bioturbated, and its bedding is subhorizontal.

Subunit IB is composed of clayey nannofossil ooze, which consists of nannofossils, clay minerals, and minor amounts of quartz, foraminifers, diatoms, sponge spicules, and shell debris and has a high content (1%–2.2%) of organic carbon (see "Organic Geochemistry" section, this chapter). It is greenish gray to dark greenish gray and is slightly to moderately bioturbated. The bedding within this subunit apparently has been folded by natural depositional processes and is not the result of coring contortion.

Subunit ID consists of nannofossil ooze of similar composition and lithology to the sediment in Subunits IA, IC, and IE but contains lesser amounts of sand, silty sand, and silt beds. The bedding within this subunit apparently also has been folded by a natural depositional process and is not related to coring contortion. The core of the fold occurs in Core 108-657A-14H (approximately 123 mbsf) and in Core 108-657B-14H (approximately 117 mbsf) (see "Composite-Depth Section," this chapter).

Depositional Environment

Unit I records an open-marine environment during the Pliocene, Pleistocene, and Holocene Epochs that was dominated by pelagic deposition of nannofossils, foraminifers, and windblown silt and clay but was occasionally interrupted by the deposition of coarser grained sediment by turbidity and/or contour-parallel currents (represented by Subunits IA, IC, and IE).

However, this record of pelagic sedimentation is broken at two intervals (Subunits IB and ID) by episodes of gravitational (mass-flow) sedimentation, specifically the lateral advection and deformation (folding) of thick (12.6 and 28.0 m, respectively) beds of sediment by mudflows or slumps. The source of the sediment that makes up Subunit IB is a high-productivity upwelling area, possibly the continental slope and shelf of northwest Africa, for this sediment is rich in organic carbon. The sediment that makes up Subunit ID, however, is probably locally derived, for it is similar in composition to the sediment in Subunits IA, IC, and IE.

Unit II

Cores 108-657A-16H-5 through -657A-19X; depth, 146.2–178.2 mbsf; thickness, 32.0 m; age, late Miocene.

Cores 108-657B-17H through -657B-19H; depth, 145.2–166.1 mbsf; thickness, 20.9 m; age, late Miocene.

Unit II is composed of silty clay and nannofossil-bearing clay, with minor amounts of silty sand and sand, and is characterized by low (2%–30%) concentrations of organic carbon (see "Organic Geochemistry" section, this chapter). This unit is late Miocene in age and is separated from Unit I by a hiatus of approximately 1.6 m.y. This unit was poorly recovered at both sites.

The silty clay is present in major (50%–90%) amounts in Core 108-657B-17H and in trace (1%–10%) amounts in Core 108-657B-18H. It is generally composed of brownish red or grayish green clay minerals and quartz silt and is slightly to strongly bioturbated.

The nannofossil-bearing clay is present in major (50%–90%) amounts in Hole 657A but in minor (10%–25%) amounts in Hole 657B. This lithology is pale brown, light olive brown, and olive and is composed of clay minerals, quartz silt, and minor amounts of nannofossils. Bioturbation varies from slight to strong.

Sand and silty sand are relatively minor lithologies within Unit II. They are rarely present in Core 108-657B-17H in Section 2, 99 cm; in Section 4, 40, 68, and 136 cm; and in Section 6, 29 cm; but they are present in minor (10%–25%) amounts in Cores 108-657B-18H and -657B-19H. The sediments in this unit are generally composed of quartz, clay minerals, and minor amounts of nannofossils and are dark gray. When the core is undisturbed by drilling (as in Core 108-657B-17H), these lithologies are present in very thin (1- to 2-cm) beds with sharp basal contacts but are rarely graded.

Depositional Environment

Unit II records an open-marine environment during the late Miocene that was dominated by the deposition of windblown silt and clay and by sandy and silty-sand turbidity and contour-parallel currents. This site received a minor supply of biogenic sediment (i.e., nannofossils) from pelagic deposition. However, the low carbonate content and the extremely low sedimentation rates of the site (see "Sediment-Accumulation Rates" section, this chapter) indicate that this pelagic deposition occurred near or below the CCD. The hiatus that exists between Unit II and overlying Unit I may signify a major erosive bottom-current event.

BIOSTRATIGRAPHY

The sediments of Holes 657A and 657B range in age from late Miocene to Holocene, but a hiatus encompasses the Miocene/Pliocene boundary (Fig. 11). The water depth of 4221 m has resulted in considerable dissolution of carbonate. Dissolution occurs throughout both holes but is greater in the lower Pliocene and upper Miocene than in the Pleistocene. The foraminifers are more susceptible to dissolution than the nannofossils; their numbers are reduced in the lower Pliocene (PL1 Zone), and they are absent in the upper Miocene. Nannofossils are abundant and well preserved throughout the Pliocene and Pleistocene. In the upper Miocene the assemblages consist mainly of discoasters. With a few exceptions, diatoms are poorly preserved at this site, and many of those that do occur have been reworked from shallower areas.

Planktonic foraminifers and nannofossils provide numerous stratigraphic datums. The Pliocene/Pleistocene boundary lies near the base of Core 108-657A-6H and in the middle of Core -657B-7H (see "Sediment-Accumulation Rates" section, this chapter). The lower/upper Pliocene boundary is placed in the

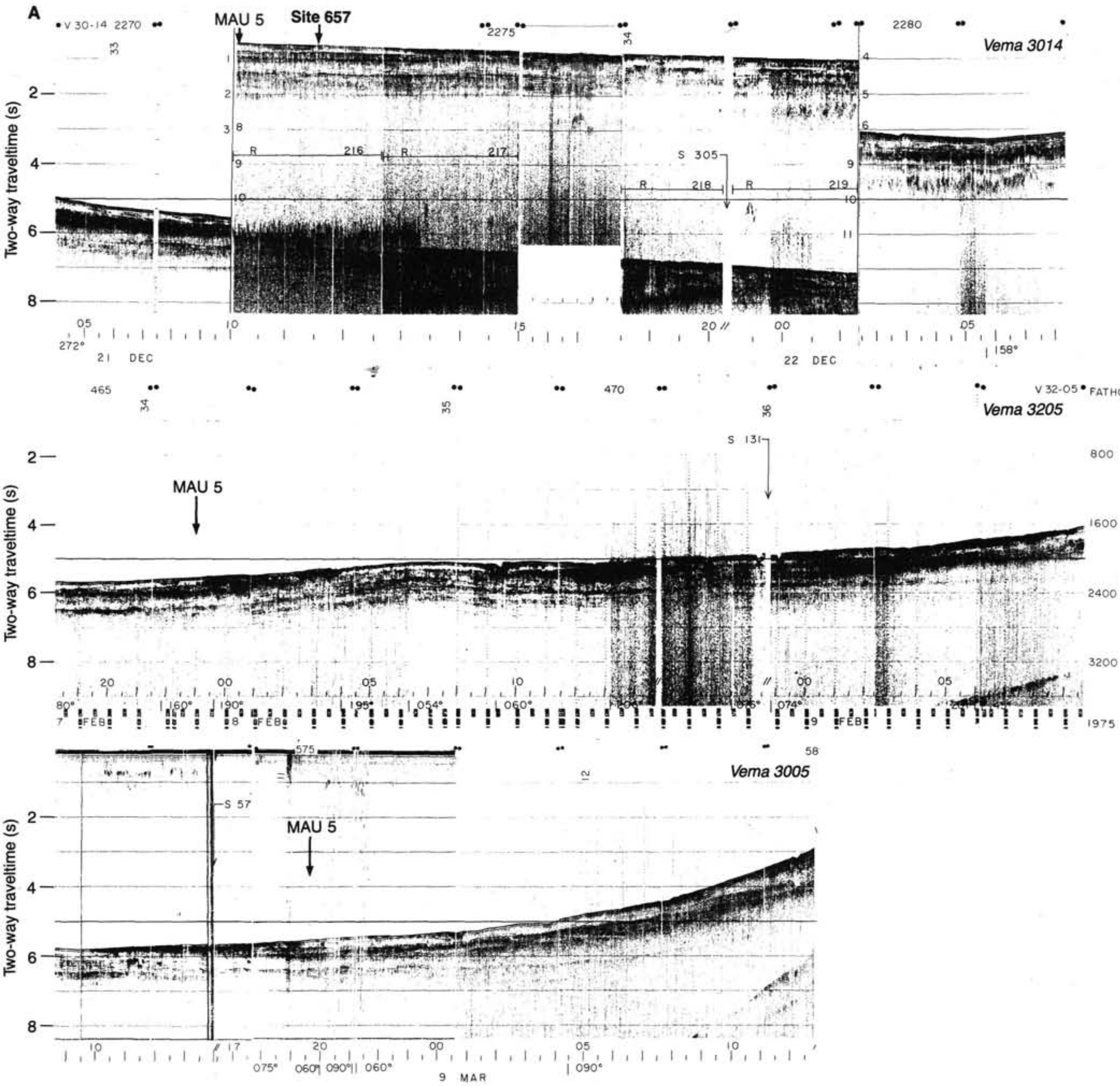

Figure 6. *Vema* seismic reflection records (*A*) and map (*B*) of seismic tracks available in the vicinity of Site 657 (= site proposal MAU 5A).

middle of Core 108-657A-11H and at the base of Core 108-657B-11H on the basis of foraminifer and paleomagnetic datums. The lowest definite Pliocene samples identified by nannofossils are in Cores 108-657A-15H and -657B-16H. A hiatus occurs at or near the Miocene/Pliocene boundary, with samples below being late Miocene in age.

Calcareous Nannofossils

Calcareous nannofossils are abundant in all samples examined from the Pliocene and Pleistocene sediments recovered from Holes 657A and 657B. Both the placolith and discoaster assemblages show slight to moderate etching in the Pliocene-Pleistocene sequence. *Ceratolithus rugosus* is the only species displaying severe calcite overgrowth. The abundances and preservational states of the Pliocene-Pleistocene nannofossil assemblages differ greatly from those of the upper Miocene.

Upper Miocene placolith assemblages are severely dissolved, resulting in an increased abundance of discoasters and ceratoliths which show neither dissolution nor overgrowth. The upper Miocene brownish and greenish clays are barren of calcareous nannofossils in some intervals.

The oldest sediment recovered at Site 657 (Hole 657B) has an age between 8.2 and 8.5 Ma. The calcareous nannofossils also indicate that the cored sequence at Site 657 contains one major hiatus, which encompasses the Miocene/Pliocene boundary and has a duration probably greater than 1 m.y. (4.6–6.2 Ma). Reworking at Site 657 is negligible, but downhole displacement of sediment was confirmed in several core-catcher samples.

Pleistocene

The Pleistocene assemblages are dominated by *Gephyrocapsa* spp., but no attempt was made to separate these at the

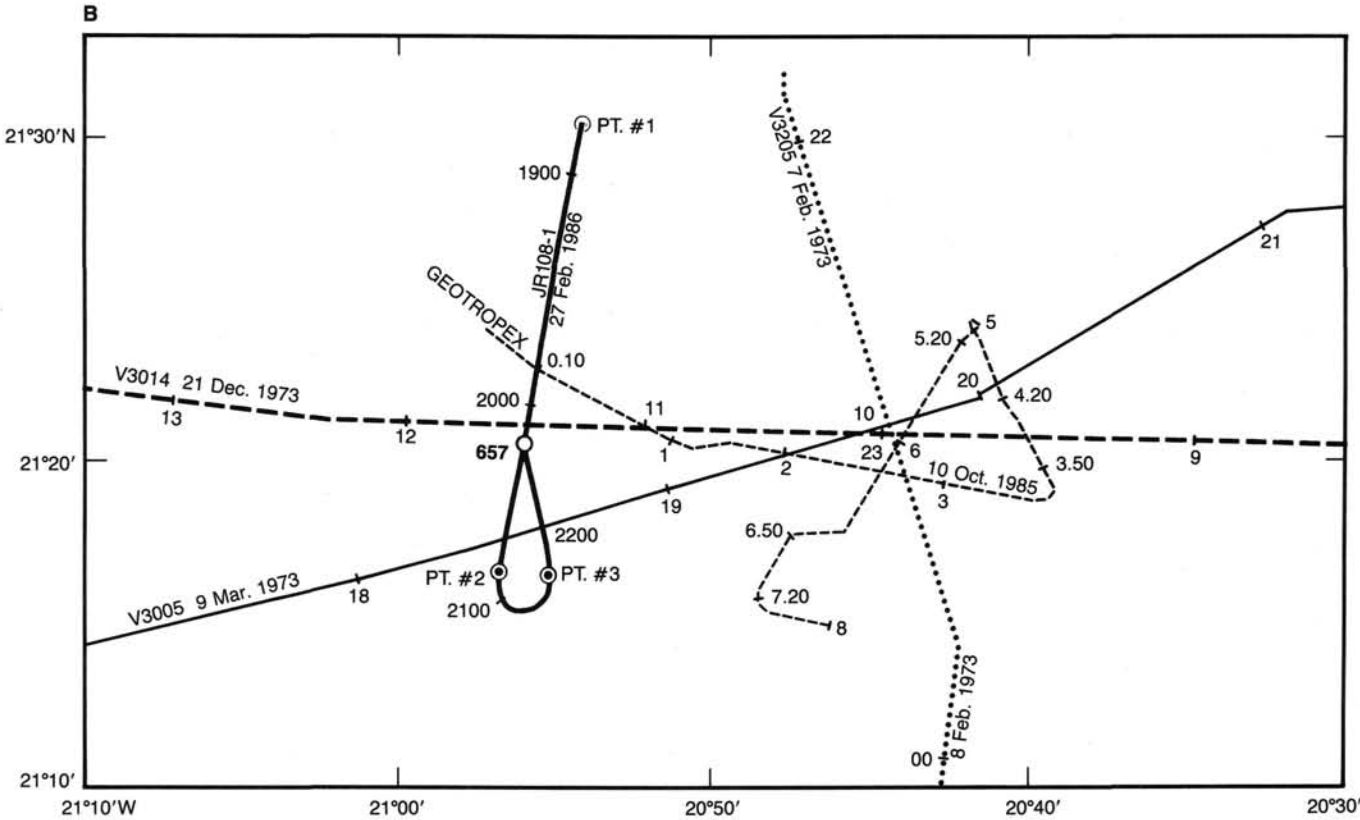

Figure 6 (continued).

species level. Other typical components are *Coccolithus pelagicus, Calcidiscus leptoporus, Helicosphaera carteri, Pontosphaera japonica, Syracosphaera* spp., and *Rhabdosphaera* spp., with lesser occurrences of *Coccolithus radiatus, Scyphosphaera* spp., and *Ceratolithus cristatus*. The lower Pleistocene assemblages contain rare to few *Helicosphaera sellii* and common *Calcidiscus macintyrei*.

On-board SEM studies indicate that the reversal in dominance between *Emiliania huxleyi* and *Gephyrocapsa* spp. can be located between Samples 108-657A-1H-2, 5 cm, and 108-657A-1H-2, 105 cm, which, according to Thierstein et al. (1977), suggests an age of 0.09 Ma at the latitude of Site 657. Low abundances of *E. huxleyi* were observed down to Sample 108-657A-1H-3, 50 cm, indicating the base of Zone NN21. *Pseudoemiliania lacunosa* was observed in Sample 657A-1H-3, 50 cm, indicating the bottom of Zone NN20 and an age of 0.47 Ma. Thus, Zone NN20 either shows a strongly reduced accumulation rate—5 m/m.y. as compared to the average Pleistocene rate of nearly 35 m/m.y.—or contains a hiatus. The latter explanation appears more tenable, considering the recovery of numerous Pliocene-Pleistocene turbidites at this site. In analogy with the above reasoning, Sample 108-657B-1H-1, 85 cm, can be assigned an age younger than 0.09 Ma, and Sample 108-657B-2H-1, 59 cm, an age older than 0.47 Ma.

Sample 108-657A-4H, CC contains abundant small *Gephyrocapsa* spp. and thus may represent the "small *Gephyrocapsa* acme zone" of Gartner (1977). This interpretation is consistent with previous (e.g., Gartner, 1977; Rio et al., in press) as well as current correlations of the acme interval to the Jaramillo subchron (see "Paleomagnetism" section, this chapter). *Helicosphaera sellii* has its highest occurrence in Cores 108-657A-5H and -657B-6H. The extinction of *C. macintyrei* is easily recognized between Samples 108-657A-6H-4, 19 cm, and -657A-6H, CC. In Hole 657B, this event occurs between 4 and 75 cm in Section -657B-7H-1. The position of the Pliocene/Pleistocene boundary can be calculated by assuming a constant sediment-accumulation rate in the interval separating the extinctions of *C. macintyrei* and *Discoaster brouweri*.

Pliocene

The final discoaster extinction is located between Samples 108-657A-7H-3, 62 cm, and -657A-7H-3, 148 cm, whereas the corresponding level in Hole 657B occurs between Samples 108-657B-7H, CC and -657B-8H-1, 50 cm. These depth intervals therefore contain the base of Zone NN18. The extinction of *D. brouweri* is accompanied by that of *Discoaster triradiatus* in both holes. The dominance of the gephyrocapsids diminishes rapidly at about the extinction level of *D. brouweri*, close to 1.9 Ma, and the small reticulofenestrids become the major assemblage element. This assemblage character is maintained to the basal Pliocene. An extreme example of this is Sample 108-657B-16H, CC, in which *Reticulofenestra minuta* outnumbers all other assemblage components by as much as an order of magnitude.

The extinction of *Discoaster pentaradiatus* occurs between Samples 108-657A-8H-4, 45 cm, and -657A-8H-5, 10 cm. *Discoaster surculus* is present in the core catcher of Core 108-657A-8H (Zone NN16). Scattered stray specimens of *Discoaster asymmetricus* were observed above the extinction of *Discoaster tamalis*, but the former increases markedly in abundance at the extinction level of the latter species. These events occur between Samples 108-657A-9H-3, 71 cm, and 108-657A-9H-3, 148 cm, and within Core 108-657B-9H.

The next-older reliable species event of the Pliocene is the extinction of *Reticulofenestra pseudoumbilica* (base of Zone NN16) at 3.56 Ma. This species is common at the top of Section 108-

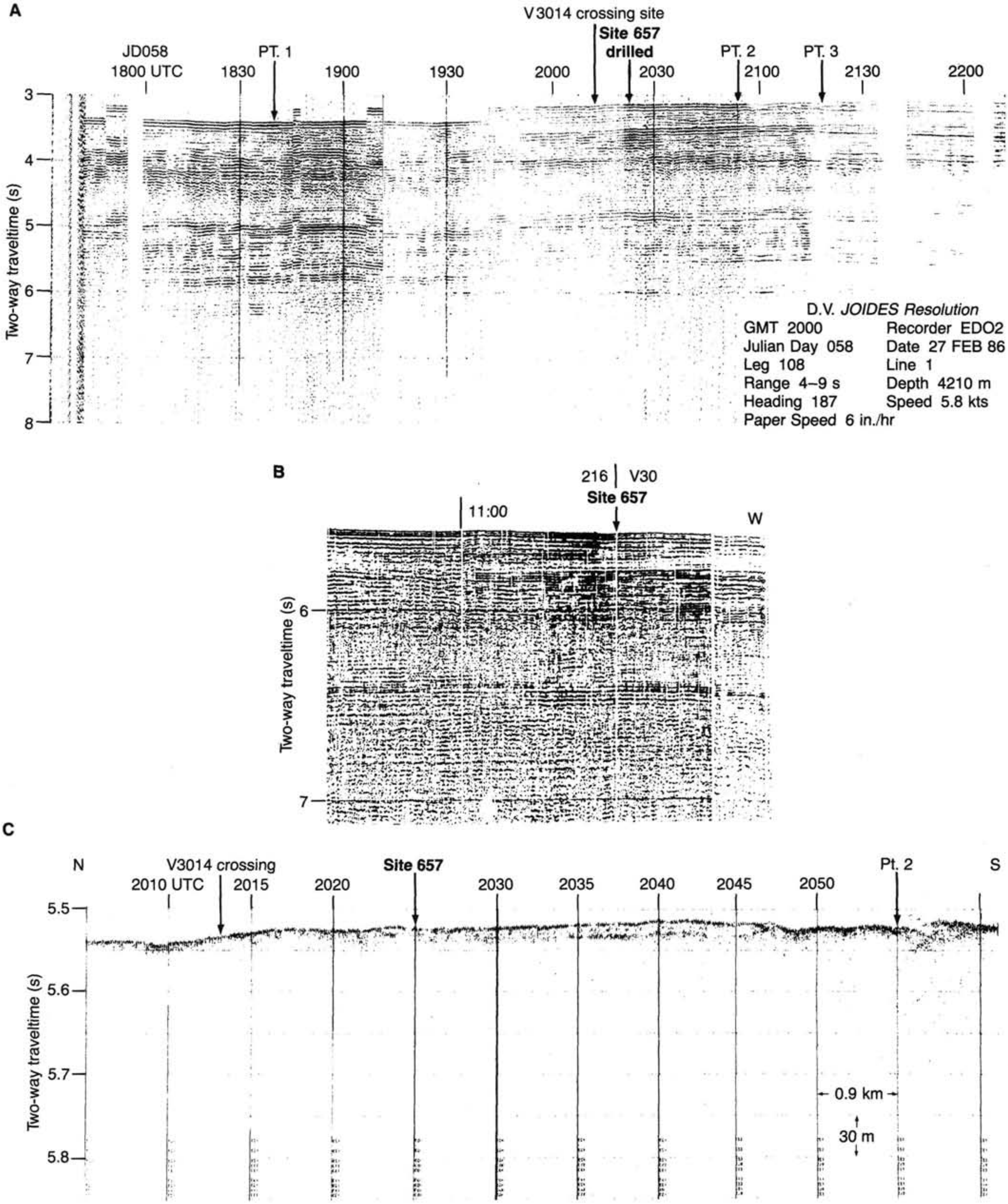

Figure 7. A. *JOIDES Resolution* seismic reflection record (close-up) near Site 657. B. Close-up of *Vema* profile 3014 near Site 657. C. Example of 3.5-kHz record from *JOIDES Resolution* near Site 657.

Table 1. Positions of site-survey turning points.

Point no.	Position
1	21°30′N, 20°54.35′W
2	21°16.5′N, 20°57′W
3	21°17′N, 20°55.35′W

Table 2. Coring summary, Site 657.

Core and type[a]	Date (1986)	Time (UTC)[b]	Sub-bottom depths (m)	Length cored (m)	Length recovered (m)	Recovery (%)
Hole 657A						
1H	Feb 28	1130	0–7.2	7.2	7.1	98.6
2H	Feb 28	1254	7.2–16.7	9.5	9.7	102.0
3H	Feb 28	1423	16.7–26.2	9.5	9.7	102.0
4H	Feb 28	1615	26.2–35.7	9.5	9.6	101.0
5H	Feb 28	1715	35.7–45.2	9.5	9.0	95.0
6H	Feb 28	1822	45.2–54.7	9.5	9.7	102.0
7H	Feb 28	1928	54.7–64.2	9.5	9.0	95.0
8H	Feb 28	2045	64.2–73.7	9.5	7.3	77.2
9H	Feb 28	2152	73.7–83.2	9.5	8.4	88.7
10H	Feb 28	2257	83.2–92.7	9.5	9.5	99.9
11H	Mar 01	0005	92.7–102.2	9.5	8.1	85.2
12H	Mar 01	0130	102.2–111.7	9.5	2.6	27.0
13H	Mar 01	0700	111.7–121.2	9.5	1.5	15.2
14H	Mar 01	0930	121.2–130.7	9.5	7.0	73.2
15H	Mar 01	1045	130.7–140.2	9.5	6.8	71.0
16H	Mar 01	1251	140.2–149.7	9.5	7.9	83.2
17X	Mar 01	1544	149.7–159.2	9.5	0.7	7.4
18X	Mar 01	1750	159.2–168.7	9.5	0	0
19X	Mar 01	2012	168.7–178.2	9.5	4.1	42.6
Hole 657B						
1H	Mar 02	0045	0–2.7	2.7	1.0	38.1
2H	Mar 02	0238	2.7–12.2	9.5	9.7	102.0
3H	Mar 02	0500	12.2–21.7	9.5	9.8	103.0
4H	Mar 02	0630	21.7–31.2	9.5	9.6	101.0
5H	Mar 02	0750	31.2–40.7	9.5	8.9	93.2
6H	Mar 02	0915	40.7–50.2	9.5	8.7	91.3
7H	Mar 02	1045	50.2–59.7	9.5	5.1	53.6
8H	Mar 02	1215	59.7–69.2	9.5	8.8	92.3
9H	Mar 02	1330	69.2–78.7	9.5	9.6	101.0
10H	Mar 02	1440	78.7–88.2	9.5	8.3	87.8
11H	Mar 02	1545	88.2–97.7	9.5	9.0	94.7
12H	Mar 02	1648	97.7–107.2	9.5	5.9	61.6
13H	Mar 02	1752	107.2–116.7	9.5	7.0	73.7
14H	Mar 02	1858	116.7–126.2	9.5	8.3	86.8
15H	Mar 02	2002	126.2–135.7	9.5	7.7	80.7
16H	Mar 02	2115	135.7–145.2	9.5	5.8	61.1
17H	Mar 02	2236	145.2–154.7	9.5	8.4	88.0
18H	Mar 03	0020	154.7–156.6	1.9	1.9	102.0
19X	Mar 03	1100	156.6–166.1	9.5	0.2	1.9

[a] H = hydraulic piston; X = extended core barrel.
[b] UTC = Universal Time Coordinated.

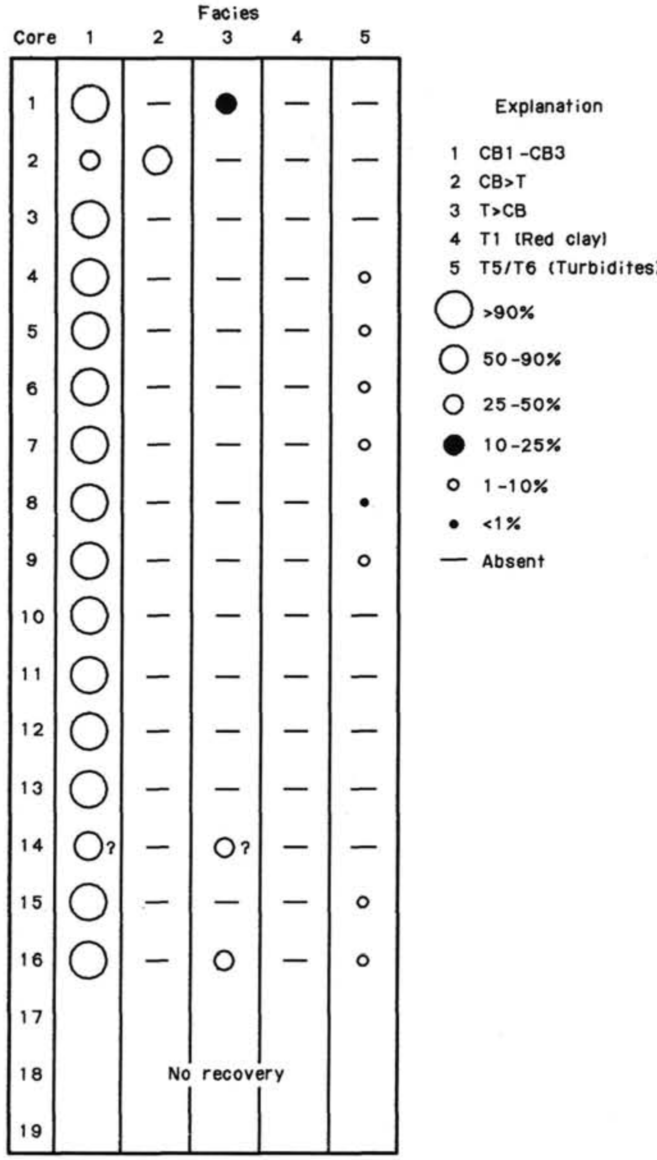

Figure 8. Summary of the lithostratigraphy of Hole 657A, showing the relative abundance of different lithologies in each core. Numerical facies designations correspond to those of Figure 5 in the "Introduction and Explanatory Notes" chapter (this volume). Relative percentages are also indicated.

657A-13H-1 but absent in Sample 108-657A-12H, CC. Unfortunately, the poor condition and recovery of Core 108-657A-12H prevent any meaningful attempt to derive a precise extinction level of *R. pseudoumbilica*. However, conditions improved in Hole 657B, and here the event was determined to have occurred between Samples 108-657B-12H-1, 40 cm, and -657B-12H-1, 120 cm.

The top of Zone NN14 was recognized by the disappearance of amaurolithids, including *Amaurolithus tricorniculatus*, within Cores 108-657A-14H and -657B-12H. The base of Zone NN14 has not been determined because of the low abundances exhibited by the marker species, *D. asymmetricus*, in the beginning of its range.

Ceratolithus rugosus is rather uncommon in Core 108-657A-15H, and the specimens observed are generally poorly preserved, displaying much secondary overgrowth. The evolutionary transition from *Ceratolithus acutus* to *C. rugosus* thus should be regarded as tentatively recognized in the upper part of Section 108-657A-15H-4, a level consequently approximating the NN12/NN13 zonal boundary. In Hole 657B, at least one well-preserved specimen of *C. acutus* and several good specimens of *C. rugosus* were observed in Sample 108-657B-15H, CC, thus indicating the base of Zone NN13.

Miocene

Discoaster quinqueramus is present in Samples 108-657A-15H-5, 40 cm, and -657A-15H, CC, together with other typically upper Miocene assemblage components, but not in Sample 108-657A-15H-5, 14 cm. *Ceratolithus acutus* was observed to occur not deeper than Sample 108-657A-15H-4, 130 cm.

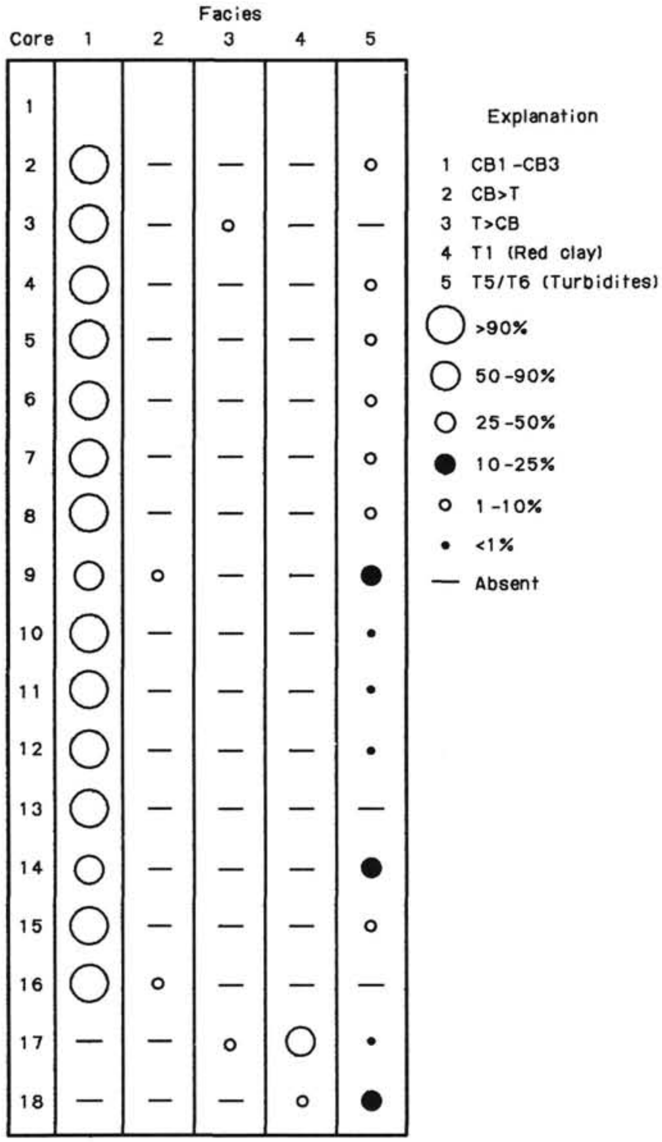

Figure 9. Summary of the lithostratigraphy of Hole 657B, showing the relative abundance of different lithologies in each core. See Figure 8 caption for further explanation.

Zone NN12 has a duration of 1 m.y. (4.6–5.6 Ma). In Core 108-657A-15H, this zone is represented by 1.5 m of sediment (from upper Section 108-657A-15H-4 to upper Section 108-657A-15H-5). The Miocene/Pliocene boundary seems to be missing, as a hiatus representing this interval occurs at Site 657. In Hole 657B, this hiatus occurs somewhere in one of the three uppermost sections of Core 108-657B-16H (Zone NN11 was confirmed in Sample 108-657B-16H-4, 50 cm, and basal Zone NN13 in Sample 108-657B-15H, CC).

Amaurolithus amplificus is present from Sample 108-657B-17H-1, 76 cm, down to Sample 108-657B-17H-2, 142 cm, whereas *A. delicatus, Amaurolithus primus*, and *Amaurolithus tricorniculatus* continue to be present in association with *D. quinqueramus* down to Sample 108-657B-17H-4, 34 cm. The upper part of Core 108-657B-17H thus represents upper Zone NN11. Calcareous nannofossils are absent in Core 108-657B-17H below Sample 108-657B-17H-4, 44 cm, including a core-catcher sample at 20 cm. An upper Zone NN11 assemblage was also observed in the core catcher of Core 108-657B-19H, although Sample 108-657B-19H, CC, 10 cm, was barren.

The uppermost 24 cm of Core 108-657B-18H contains a nannofossil assemblage belonging to Zone NN10, as indicated by the presence of *Discoaster bellus, Discoaster calcaris, Discoaster loeblichii*, and *Discoaster neohamatus*, and the absence of *D. quinqueramus*. The oldest datable sediment at Site 657 can be assigned an age between 8.2 and 8.5 Ma.

Hole 657A provides important information regarding the ranges of *A. amplificus* and *D. quinqueramus*. Berggren et al. (1985) suggest that the extinctions of these two events are synchronous. However, in Hole 657A, *D. quinqueramus* (highest observed occurrence, Sample 108-657A-15H-4, 40 cm) continues its range at least 6 m above that of *A. amplificus* (highest observed occurrence, Sample 108-657A-16H-5, 0 cm). All amaurolithids mentioned above begin to appear between Samples 108-657A-16H-6, 90 cm, and 108-657A-16H-6, 110 cm. The presence of *D. quinqueramus* without amaurolithids in the latter sample, and in Samples 108-657A-16H, CC, -657A-17X, CC, and -657A-18X, CC, indicate lower Zone NN11 and an age younger than 8.2 Ma but older than 6.5 Ma. Sample 108-657A-19X, CC consists of a sand containing some obviously displaced Pleistocene nannofossils. Three- and four-rayed varieties of *D. quinqueramus* were observed in Sample 108-657A-17X, CC.

Planktonic Foraminifers

Planktonic foraminifers are generally abundant through the Pliocene and Pleistocene at this site, but dissolution has affected all samples to some degree. Through the Pliocene and Pleistocene, dissolution varies from slight to moderate and may have selectively removed some species in the more dissolved intervals. In some samples, such as 108-657A-15H, CC and -657B-14H, CC, dissolution has significantly reduced the numbers of foraminifers. Samples containing large amounts of detrital sand (108-657A-3H, CC and -657A-8H, CC; -657B-2H, CC and -657B-4H, CC) also have reduced abundances of foraminifers. Below Cores 108-657A-16H and -657B-17X, the sediment is barren of foraminifers except for a few contaminants.

The influence of the Canary Current, or changes in the position and intensity of the upwelling cells offshore from Africa, can clearly be seen in the foraminiferal fauna. Many of the tropical species are absent, allowing cool subtropical and temperate species, such as *Neogloboquadrina pachyderma* (dextral) and *Globigerina bulloides*, to dominate. The proximity of warm water is, however, indicated by the scattered occurrence of tropical species such as *Sphaeroidinella dehiscens* and *Pulleniatina obliquiloculata*.

The Pleistocene *Globorotalia truncatulinoides* Zone is represented in both holes, but the base is difficult to identify owing to the absence of *G. truncatulinoides* and the rare occurrence of *Globigerinoides obliquus* around the boundary. In Hole 657A the base lies above Sample 108-657A-7H-6, 79–81 cm, and in Hole 657B it lies in Core 108-657B-6H. The fauna of this zone is dominated by *N. pachyderma* (dextral), with variable amounts of *Globigerinoides ruber, G. bulloides, Globorotalia inflata*, and *Neogloboquadrina dutertrei*.

The late Pliocene was dominated by *N. pachyderma* (dextral) and *Neogloboquadrina acostaensis*, with variable numbers of *Globigerina decoraperta* and *Globorotalia puncticulata*. The PL5/PL6 zonal boundary is marked at the last occurrence (LO) of *Globorotalia miocenica*, which occurs between Samples 108-657A-7H, CC and -657A-8H-2, 21–23 cm, and within Core 108-657B-8H. The age of this boundary is 2.2 Ma. The first occurrence (FO) of *G. inflata* has an age of 2.1 Ma in the North Atlantic (Weaver and Clement, 1986), and this datum occurs between Samples 108-657A-7H, CC and -657A-8H-2, 21–23 cm, and in Core 108-657B-8H. Zone PL4 represents a short time span and was recognized in only one sample (108-657B-10H-3, 36–38 cm). The top of the PL3 Zone is identified on the LO of *Sphaeroidinellopsis seminulina*, which lies between Samples

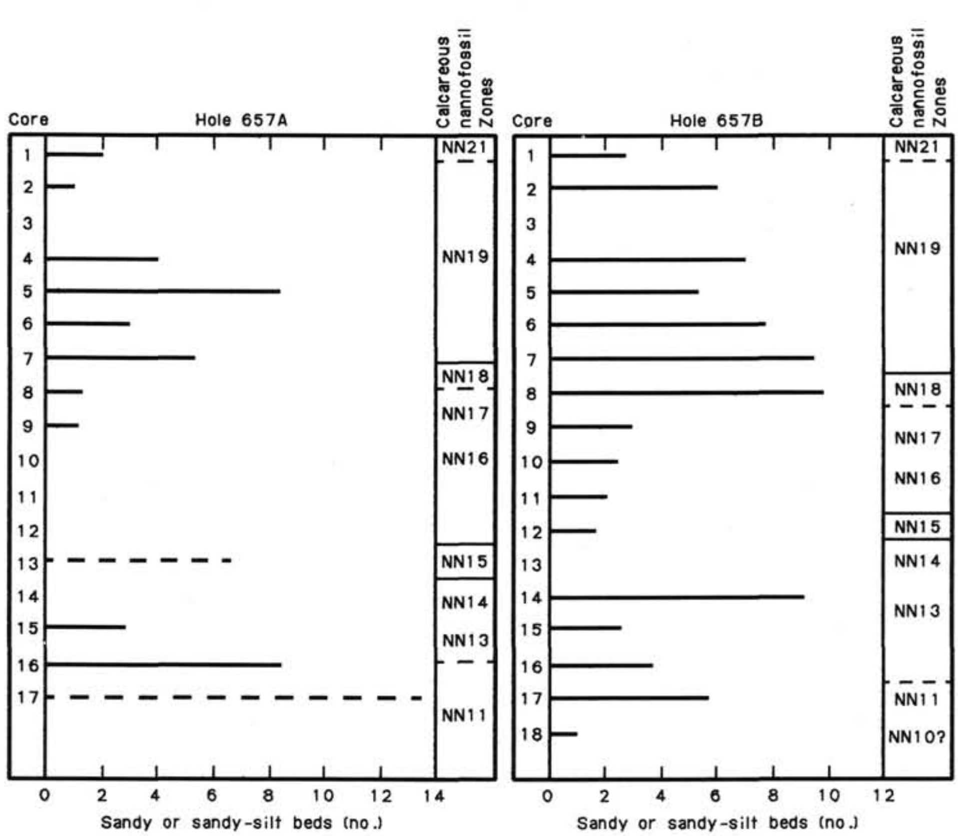

Figure 10. Number of sandy or sandy-silt beds (turbidites or contourites?) in each core in Holes 657A and 657B. Calcareous-nannofossil zones are indicated (see "Biostratigraphy" section, this chapter).

108-657A-9H, CC and -657A-10H-1, 130–132 cm, and between Samples 108-657B-10H-3, 6–8 cm, and -657B-10H, CC. This datum has an estimated age of 3.0 Ma. The top of Zone PL2 marks the base of the late Pliocene at 3.4 Ma and is identified by the LO of *Globorotalia margaritae*. This datum occurs in Cores 108-657A-12H and -657B-12H. However, Weaver and Clement (1986) found this to be a diachronous datum, occurring progressively earlier away from the tropics in the North Atlantic.

The early Pliocene was also dominated by *N. pachyderma* (dextral) and *N. acostaensis* with some influxes of sinistral *N. pachyderma*. In the younger part of the early Pliocene, *G. puncticulata* is also common. The PL2/PL1 zonal boundary, at 3.9 Ma, is based on the LO of *Globigerina nepenthes*, which is rare at this site. The LO of this species is between Samples 108-657A-14H, CC and -657A-15H-1, 87–89 cm, and lies in Core 108-657B-14H. Weaver and Clement (1986) showed that *G. puncticulata* has a synchronous FO, at 4.15 Ma, in the subtropical to temperate North Atlantic. Because this species shows a relatively long overlap with *G. margaritae* and a short overlap with *G. nepenthes*, we feel confident that the LOs of *G. margaritae* and *G. nepenthes* fall near 3.4 and 3.9 Ma, respectively, at this site. The first appearance of *G. puncticulata* is between Samples 108-657A-15H-1, 87–89 cm, and -657A-15H-3, 80–82 cm, and in Core 108-657B-15H. Dissolution becomes progressively more severe through the PL1 Zone, and the lowest stratigraphic sample that can be dated as belonging to this zone is 108-657A-16H-3, 111–113 cm. Below this, no age-diagnostic foraminifers were found.

Benthic Foraminifers

Benthic foraminifers at Site 657A are divided into two assemblages. One is a deep-water assemblage, indicating middle to abyssal depths. The characteristic species of this assemblage are *Planulina wuellerstorfi, Melonis pompilioides, Laticarinina pauperata, Oridorsalis tener, Cibicidoides kullenbergi*, and *Gyroidinoides soldanii*, which occur mainly in the calcareous-foraminifer–nannofossil ooze (Samples 108-657A-1H, CC and -657A-5H, CC). In these samples, benthic foraminifers are few or rare, and the preservation is moderate or good. The other group is a shallow-water assemblage, indicating neritic to upper bathyal conditions. This assemblage is accompanied by or associated with terrigenous sand and is further subdivided into two groups. When the sediment consists mainly of coarse-grained sand (core-catcher Samples 108-657A-3H, -657A-8H, and -657A-19H), the assemblage is represented by *Ammonia beccarii, Elphidium macellum*, and *Cibicides lobatulus*. When the sediment consists of very fine- or fine-grained sand (Sample 108-657A-2H, CC), the assemblage is characterized by *Chilostomella oolina, Cassidulina carinata*, and *Bulimina aculeata*. *Ammonia* and *Elphidium* do not occur in this assemblage. In both cases in which the sediment includes sand, benthic foraminifers are rare to common, and the preservation is poor or moderate. In Samples 108-657A-3H, CC and -657A-8H, CC, the shallower species, such as *A. beccarii, Spiroloculina soldanii*, and *E. macellum*, are broken and poorly preserved. These species occur together with species indicating middle to abyssal depths, such as *G. soldanii, O. tener*, and *Martinotiella* sp. The latter assemblage seems to be autochthonous, and the former seems to have been transported by sand turbidites from the shelf.

Diatoms

Rare to abundant diatoms were observed in core-catcher samples examined from Cores 108-657A-1H through -657A-4H and 108-657B-1H through -657B-5H. Preservation is generally poor; however, the preservation is moderate in Samples 108-657B-1H, CC and -657B-2H, CC. The diatom assemblage is a mixture of

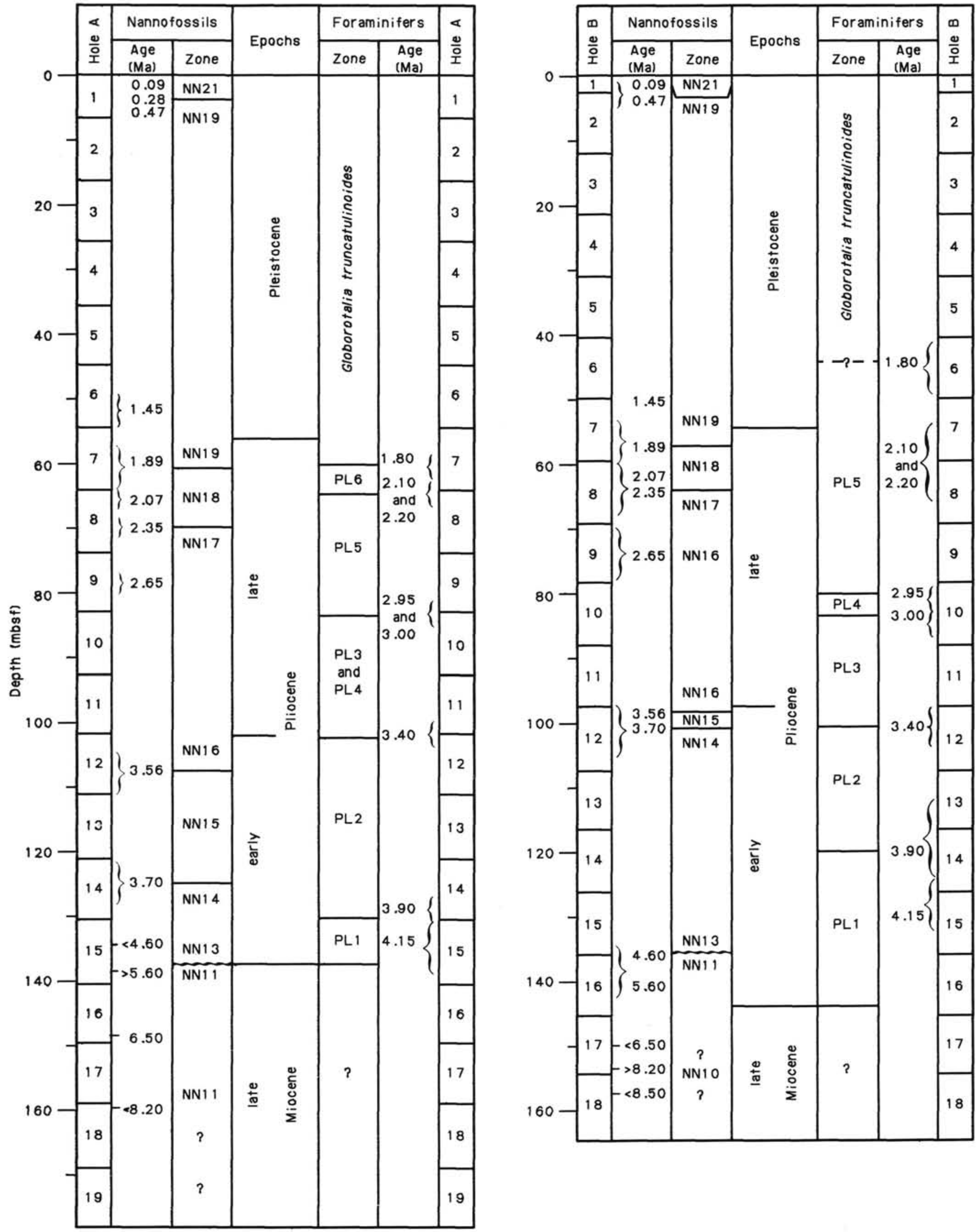

Figure 11. Correlation of microfossil zones and epoch boundaries with cores and depths (mbsf) in Holes 657A and 657B.

pelagic, coastal, and freshwater species. The rare occurrence of biostratigraphic indicators and the mixed nature of the assemblage make age determinations tentative.

The occurrence of *Pseudoeunotia doliolus* in Samples 108-657A-3H, CC and -657B-1H, CC through -657B-3H, CC suggests a late Pliocene to Holocene age for these samples (*Pseudoeunotia doliolus* or *Nitzschia reinholdii* Zone). The absence of *N. reinholdii* suggests placement within the *P. doliolus* Zone (0–0.65 m.y.); however, the paucity of *Nitzschia* spp. in the samples may reflect ecological exclusion of *N. reinholdii.*

The occurrence of numerous neritic and freshwater species suggests possible downslope transport and resedimentation. The extensive fragmentation of diatoms and sponge spicules suggests mechanical breakage and also supports redeposition.

With the exception of rare specimens of freshwater *Melosira* spp. in Sample 108-657A-6H, CC and a single specimen of *Rhizosolenia styliformis* in Sample 108-657A-13H, CC, core-catcher samples examined from Cores 108-657A-5H through -657A-18X, -657B-6H through -657B-17H, and -657B-19X are barren of diatoms.

Sample 108-657A-19X, CC contains rare diatoms with poor preservation. No age-diagnostic species were observed. Sample 108-657B-18X, CC contains coarse sand and was not examined.

PALEOMAGNETISM

Magnetostratigraphy

All core sections from the two holes at Site 657 that were in suitable condition were measured at 5-cm intervals using the cryogenic magnetometer. Of these, approximately half were also demagnetized at 5 mT (the ODP official limit) and measured again. Owing to severe core disturbance, strong lithologic contrast, and magnetic overprinting, the whole-core measurements proved of little practical use. A few cores (e.g., from Hole 657B) were of tantalizingly high quality. These enabled us to predict quite well the remanence of the discrete subsamples as illustrated in Figure 12. We show the vector data of the whole core by the continuous line and that from the discrete samples, close to the Matuyama-Brunhes transition, by dots. These data demonstrate the potential of the whole-core method. However, ow-

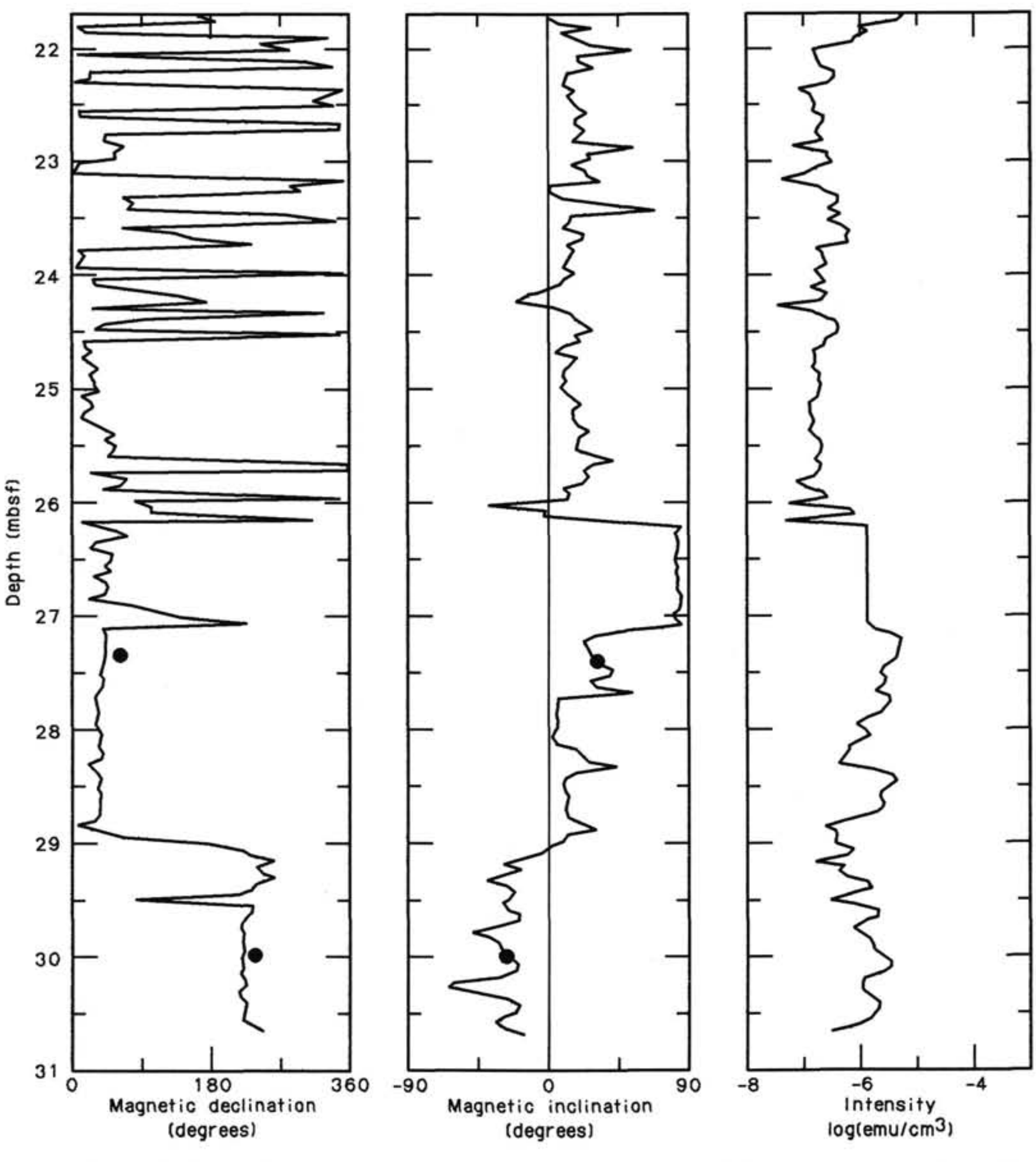

Figure 12. Declination, inclination, and intensity variations as a function of depth recorded from Core 108-657A-4H.

ing to the nature of whole-core measurements, which juxtapose disturbed and undisturbed sediments indiscriminately, subsampling and/or extensive editing of the data set is required.

For these reasons, one subsample per core section was routinely measured on the spinner magnetometer for a total of more than 100 samples. In order to detect downcore variations in magnetic properties, at least one sample per core was subjected to stepwise demagnetization. In general, 5-10 mT was sufficient to remove the soft overprint in the vertical direction.

In Figures 13 through 16 we plot the magnetic-inclination data from the discrete samples. Data from Hole 657A are shown in Figure 13, from Hole 657B in Figure 14, and the combined results in Figure 15. The inclinations expected at the site latitude (about 37°N) are shown as dashed lines in Figures 13 and 14. Above about 60 mbsf, the measured inclinations are in fair agreement with the expected values for normal and reversed polarities, indicating some stability of magnetic remanence. Below 60 mbsf, the positive inclinations are, for the most part, too steep, while the negative inclinations are too shallow. Such behavior suggests incomplete removal of a high coercivity overprint. Rock magnetic studies investigating the mineralogy are essential to determine how and/or whether this overprint might be removed.

Evident in Figures 13 and 14 are the incomplete core recovery and the insufficient density of subsamples in order to provide a reliable magnetostratigraphy. The situation is somewhat improved by combining the data from Holes 657A and 657B (Fig. 15). We present a tentative correlation with the geomagnetic-polarity time scale, which is consistent with the paleontological results. Below about 140 mbsf, the sediment-accumulation rates appear to be much slower than in the upper part of the site. Therefore, we plot the portion of data from Hole 657B below 147 mbsf at a larger scale in Figure 16. We show a tentative correlation that appears reasonable and is consistent with the available biostratigraphic constraints.

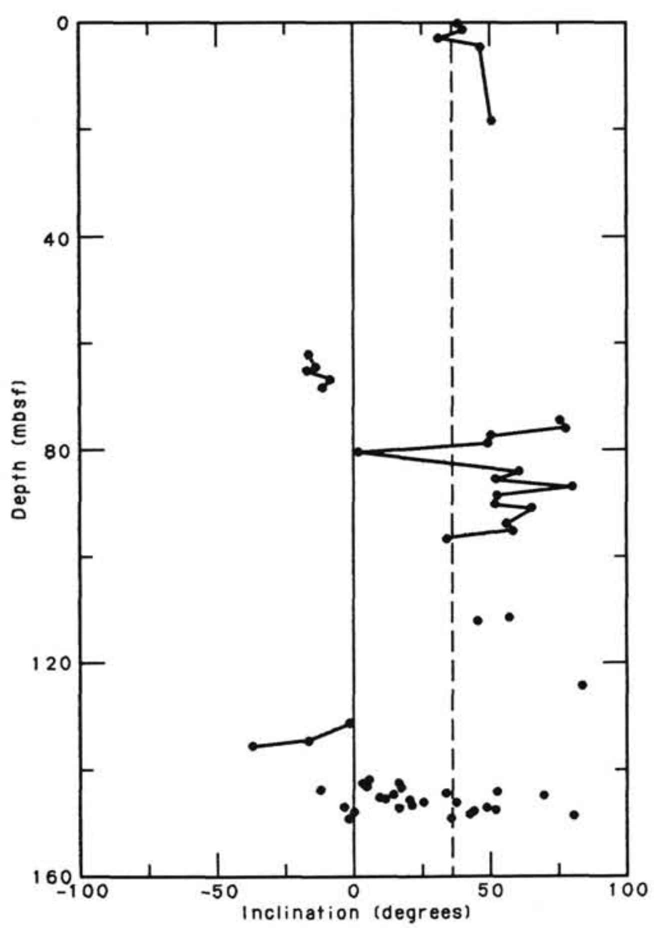

Figure 13. Inclination data obtained from discrete samples of cores in Hole 657A. The inclination value of the geocentered dipole at the site latitude is shown by the dashed line.

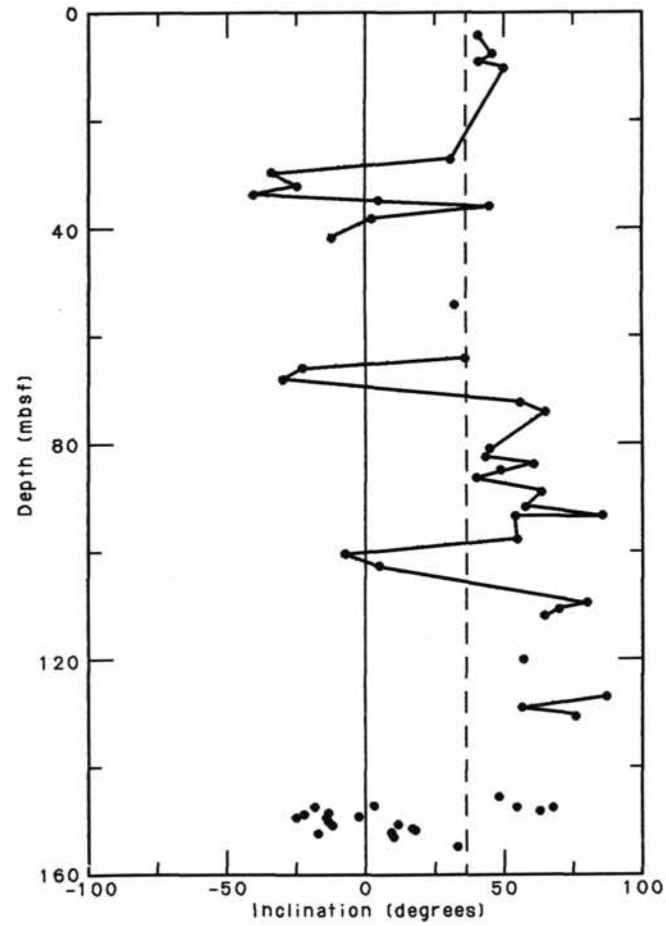

Figure 14. Inclination data obtained from discrete samples of cores in Hole 657B. The inclination value of the geocentered dipole at the site latitude is shown by the dashed line.

Magnetic Susceptibility

We measured the whole-core volume susceptibility at 5-cm intervals throughout the hydraulic-piston-cored lengths of Holes 657A and 657B, excluding badly disturbed intervals. The susceptibility reflects variations in the concentration of magnetic material in the sediment. Susceptibilities generally were low (approximately 10^{-5} to 10^{-4} SI units) except for the Miocene brown silty clays (up to approximately 10^{-2} SI units) (Cores 108-657A-16H and -657B-16H and below in both holes).

In most sections the susceptibility record shows a pattern of high-frequency variation at approximately 1 to 5 cycles per meter (Fig. 17).

Detailed correlation of susceptibility variations between Holes 657A and 657B is not straightforward, which is possibly a consequence of the poorer quality of the core material from Hole 657A. However, it is possible to correlate broad trends of susceptibility changes over several tens of meters, and some detailed between-core correlations are possible (Fig. 18).

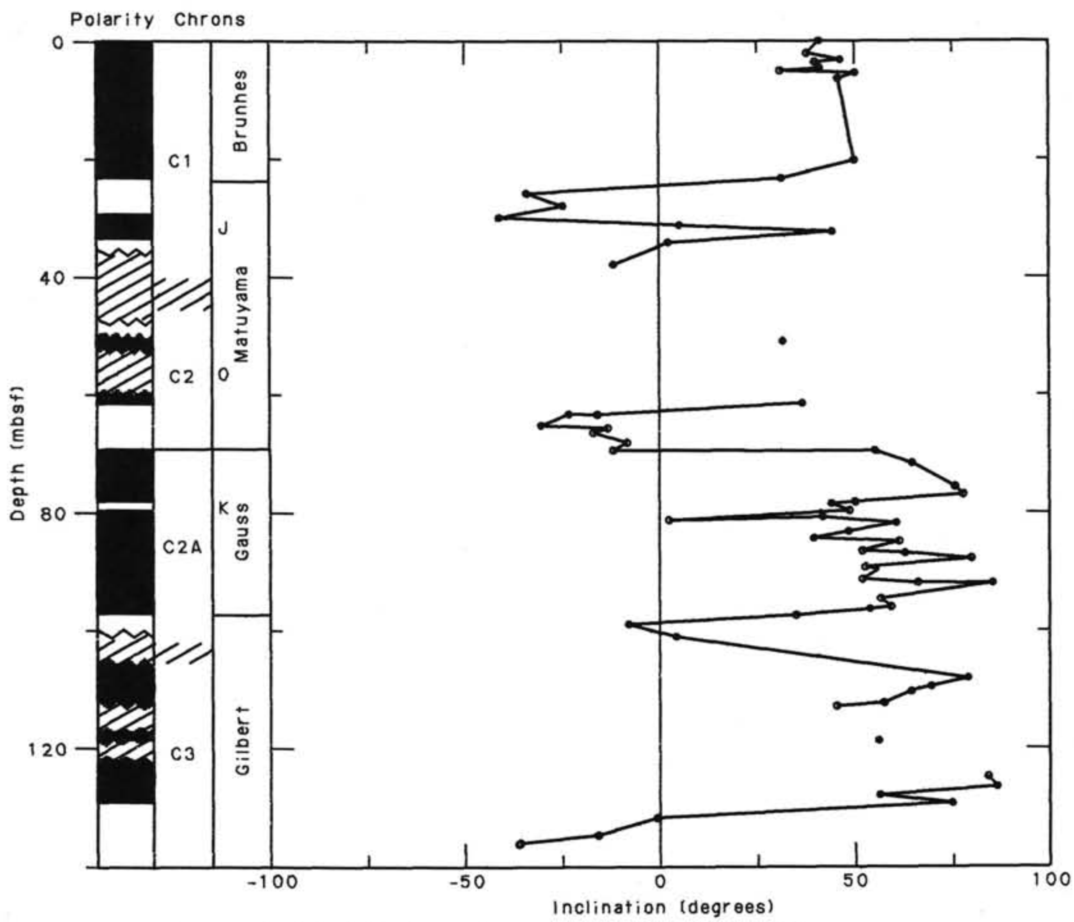

Figure 15. Combined record of the inclination variations from Holes 657A and 657B.

SEDIMENT-ACCUMULATION RATES

The sediment-accumulation-rate curves for Hole 657B are shown in Figures 19 and 20 and are based on the datums listed in Table 3. The curve is drawn for Hole 657B because it had more datums identified than Hole 657A. Comparison of depths of datums between Holes 657A and 657B can be found in "Composite-Depth Section," this chapter. Figure 19 includes no sedimentologic interpretations, whereas Figure 20 takes into account two mudflow units between 15 and 27 and 98 and 120 mbsf, respectively, giving a more accurate representation of the accumulation rates. Sedimentation rates between 0 and 3.8 Ma (0–98 mbsf in Hole 657B) average about 23 m/m.y. (excluding mudflow), although this number may be artificially high owing to the presence of numerous small turbidites. There appears to be an increase in the sedimentation rate between 0.7 and 1.0 Ma (27–42 mbsf in Hole 657B) to 50 m/m.y. Sedimentation rates below the lower mudflow unit, between 3.8 and 4.6 Ma (120–145 mbsf in Hole 657B), average 31 m/m.y.

A hiatus is inferred from 4.6 to 6.2 Ma at 137 m in Hole 657A and at 145 m in Hole 657B. While uncertainty in the depth placement of the *Ceratolithus rugosus* and *Discoaster quinqueramus* datums would allow this hiatus to be as shallow as 135.7 m (in Hole 657B), we chose to place it at the level of lithologic change from red clay to carbonate-rich facies (145.2 mbsf). Below the hiatus, nannofossil and paleomagnetic datums indicate a sedimentation rate of 12 m/m.y. from 6.2 to 6.7 Ma (145–151 mbsf in Hole 657B), and the presence of three nannofossil species at 154.8 mbsf indicates a rate of 2.5 m/m.y. from 6.7 to 8.5 Ma (151–155 mbsf in Hole 657B). No datums were identified below 160 mbsf in Hole 657A nor below 155 mbsf in Hole 657B.

INORGANIC GEOCHEMISTRY

Interstitial-water samples were squeezed from four sediment samples taken routinely from every fifth core recovered from Hole 657A. Values for pH and alkalinity were measured in conjunction, using a Metrohm 605 pH-meter followed by titration with 0.1N HCl. Salinities were measured using an optical refractometer, and chlorinities determined by titration with silver nitrate to a potassium chromate end-point. Calcium, magnesium, and sulfate analyses were carried out by ion chromatography on a Dionex 2120i instrument. Results from all these analyses are presented in Table 4. Note the increase in salinity and chlorinity at the lowermost level.

ORGANIC GEOCHEMISTRY

For Hole 657A, the physical-property samples (about 5 to 9 per core) were used for determinations of total-organic-carbon (TOC) and carbonate contents. Several of these samples also were analyzed by Rock-Eval pyrolysis. For Hole 657B, only the carbonate contents were determined.

Organic and Inorganic Carbon

Inorganic-carbon (IC) contents were determined using the Coulometrics Carbon Dioxide Coulometer. Total-carbon (TC) values were obtained by means of the Perkin Elmer 240C Elemental Analyser. Then, TOC values were calculated by the difference between total carbon and inorganic carbon. Analytical methods are discussed and data presented in the chapter enti-

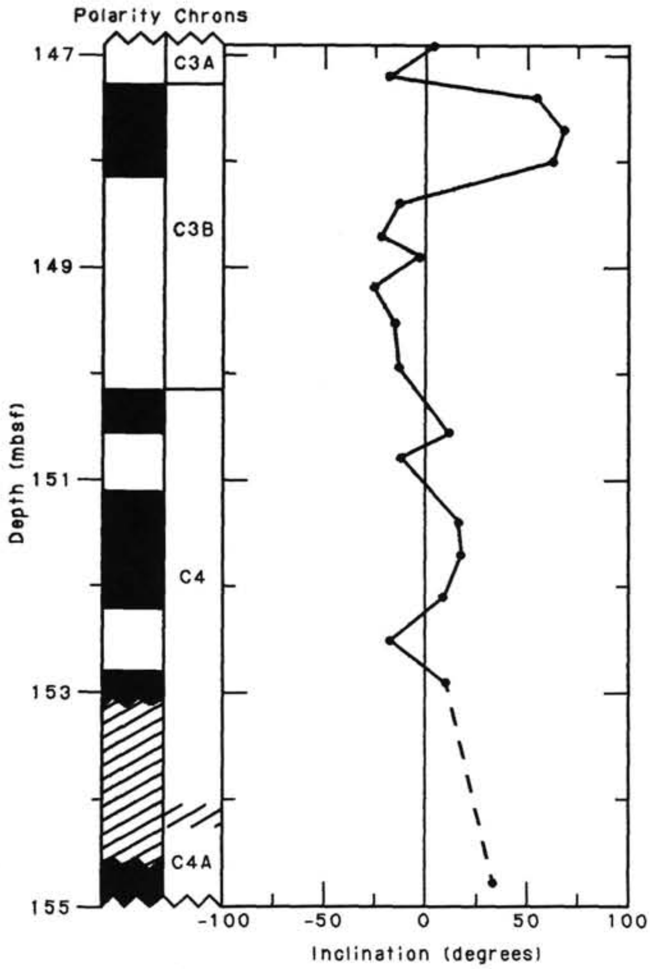

Figure 16. Inclination data obtained from Hole 657B below 147 mbsf plotted at a larger scale than in Figure 15.

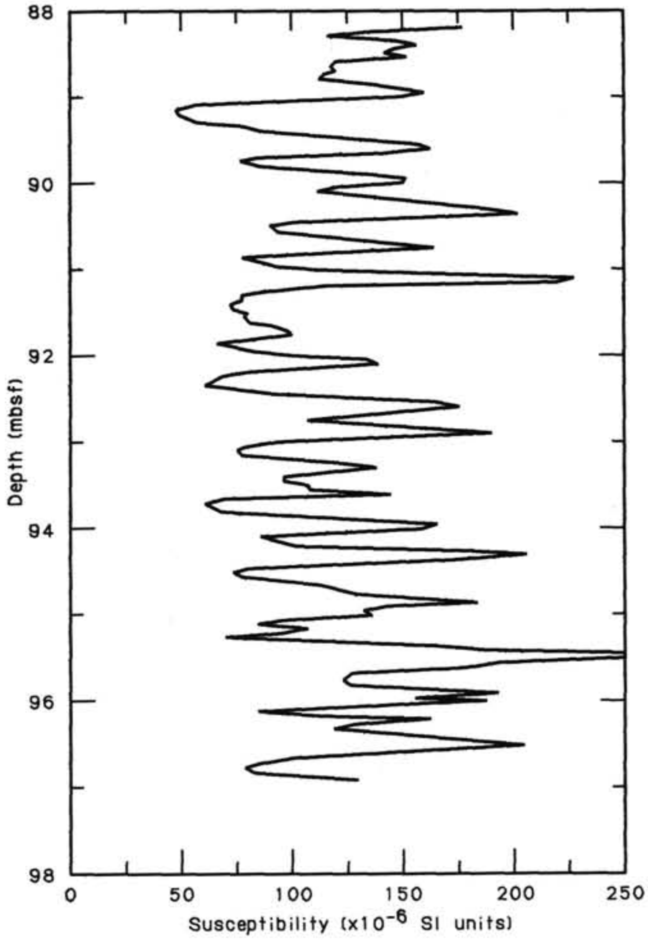

Figure 17. High-frequency type of susceptibility record. Core 108-657B-11H.

tled, "Total Organic Carbon and Carbonate Analyses, ODP Leg 108," this volume.

In general, the TOC values from Hole 657A are relatively low (less than 0.5%) with two exceptions: (1) single high TOC spikes of up to 3.3% occur at 5.6, 66.9, and 89.1 mbsf, and (2) an interval of high organic-carbon content with TOC values between 1% and 2.2% was recorded between 11 and 21 mbsf (i.e., in Subunit IIB; see "Lithostratigraphy and Sedimentology" section, this chapter; Fig. 21).

On the basis of carbonate content, the sediment sequence at Site 657 can be divided into two parts that correspond to lithologic Units I and II (see "Lithostratigraphy and Sedimentology" section, this chapter). Unit I (Hole 657A, 0 to 146.2 mbsf; Hole 657B, 0 to 145.2 mbsf) is characterized by high-amplitude variations of $CaCO_3$ between 20% and almost 90%, with lower values concentrated in the upper 40 m of the sequence (Fig. 21). All the TOC maxima fall into intervals of low carbonate values (Fig. 21). Unit II (Hole 657A, 146.2 to 178.2 mbsf; Hole 657B, 145.2 to 173.7 mbsf) is characterized by low carbonate values ranging between 2% and 37% (Fig. 21).

Rock-Eval Pyrolysis

Rock-Eval pyrolysis (Espitalié et al., 1977) was used to characterize the type and maturity of the organic matter in some of the organic-carbon-rich samples. The results are shown in Figure 22 in the form of a "van Krevelen diagram" (Tissot and Welte, 1984). This diagram implies that samples with lower TOC values are characterized by high oxygen-index (OI) values and low hydrogen-index (HI) values, indicating that the organic matter is highly oxidized. The samples from the interval between 11 and 21 mbsf characterized by high TOC values have high HI values between 260 and 320 mbsf (Fig. 22; Table 5), suggesting a type II/III mixture—i.e., a mixture of marine and terrigenous organic matter (Tissot and Welte, 1984).

The maximum temperatures of pyrolysis yield (T_{max} values) range between 382° and 413°C, indicating that the organic matter found in sediments from Site 657 is immature.

Discussion

The sediments at Site 657 are dominated by low TOC values of less than 0.5%, which are typical for open-marine environments (e.g., McIver, 1975; Müller et al., 1983). On the other hand, several time intervals at Site 657 are characterized by sediments with high TOC values (1%–3.3%). Using the correlation between HI values and the amount of marine and terrigenous macerals shown for immature sediments from the Cenozoic and Mesozoic Atlantic Ocean (Stein et al., 1986), the content of marine organic matter at Site 657 can be roughly estimated to vary between 25% and 60% (Table 5). That means that some of the samples at Site 657 contain up to 2% *marine* organic carbon. Contents of 2% marine organic carbon are unusual for open-marine environments and require special environmental conditions such as high oceanic productivity or rapid burial of organic carbon (C_{org}) by turbidites (e.g., Cornford, 1979; Arthur et al., 1984; Stein et al., 1986). Because the high TOC spikes at

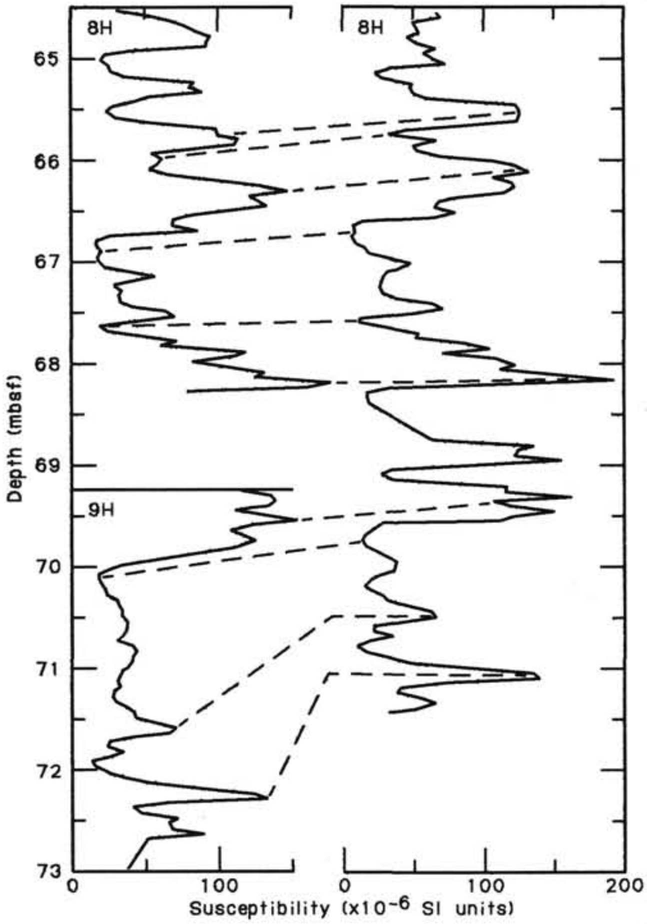

Figure 18. Example of detailed between-hole susceptibility corrections. Cores 108-657B-8H and 108-657B-9H on left; Core 108-657A-8H on right.

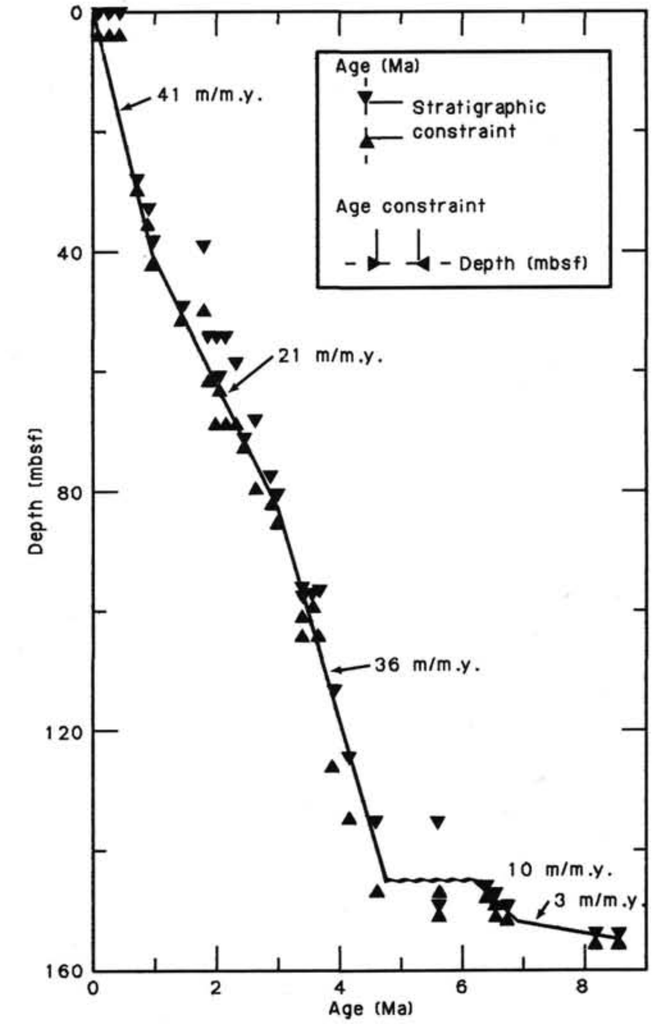

Figure 19. Accumulation-rate curve for Hole 657B without sedimentologic interpretation.

5.6, 66.9, and 89.1 mbsf coincide with turbidites (see "Lithostratigraphy and Sedimentology" section, this chapter, and core photographs), and the interval of high TOC values between 11 and 21 mbsf coincides with a thick mudflow sequence (see "Principal Results" and "Lithostratigraphy and Sedimentology" sections, this chapter), rapid burial of organic matter may have caused the high preservation rate of marine TOC. Furthermore, the high content of marine organic matter and the high amount of biogenic opal (see "Lithostratigraphy and Sedimentology" section, this chapter) indicate that the source area of the turbidites and the mudflow probably was the upper continental slope/shelf area off northwest Africa, which is characterized by high oceanic productivity. For further environmental interpretations (e.g., fluvial nutrient supply vs. upwelling as causes for the high productivity), more detailed sedimentological and organic-geochemical investigations are necessary.

The lower carbonate values in the upper 40 m (i.e., about the last 1 Ma; see "Biostratigraphy" section, this chapter) may have been caused by increased terrigenous sediment supply (i.e., by dilution), as suggested from the increased bulk sedimentation rates. On the other hand, the extremely low carbonate values in Unit II may have resulted from increased dissolution, owing to the site's position near the CCD during the late Miocene. This is supported by the markedly reduced sedimentation rates during that time (see "Sediment-Accumulation Rates" section, this chapter).

PHYSICAL PROPERTIES

The techniques used for the shipboard physical-property measurements at Site 657 are outlined in the "Introduction and Explanatory Notes" (this volume). Tables 6 through 9 show data for index properties, vane shear strength, and compressional-wave velocity (Hamilton Frame) from Holes 657A and 657B. Most of these data are presented graphically in Figures 23 through 30 (the calcium carbonate profile is shown in Figure 27 for comparison with the other properties). Thermal-conductivity measurements were made only on cores from Hole 657A down to a depth of 90.4 mbsf. The data show an average thermal conductivity of 1.2544 W/m/°C. All the data presented in this section are uncorrected and unscreened (i.e., the sub-bottom depths have not been corrected for inter-hole correlation, and any bad data points have not been removed). The best indication of inaccuracies in the gravimetric and volume analysis comes from an examination of the grain-density data. In carbonate and clays with low siliceous contents, the grain-density values should lie close to 2.7 g/cm^3. Grain densities obtained using this technique are not particularly accurate, but they do provide a qualitative assessment of index-property data. The scatter in the grain-density data (Fig. 28) dropped significantly below a depth of 90 mbsf in Hole 657A. At this point, the drying proce-

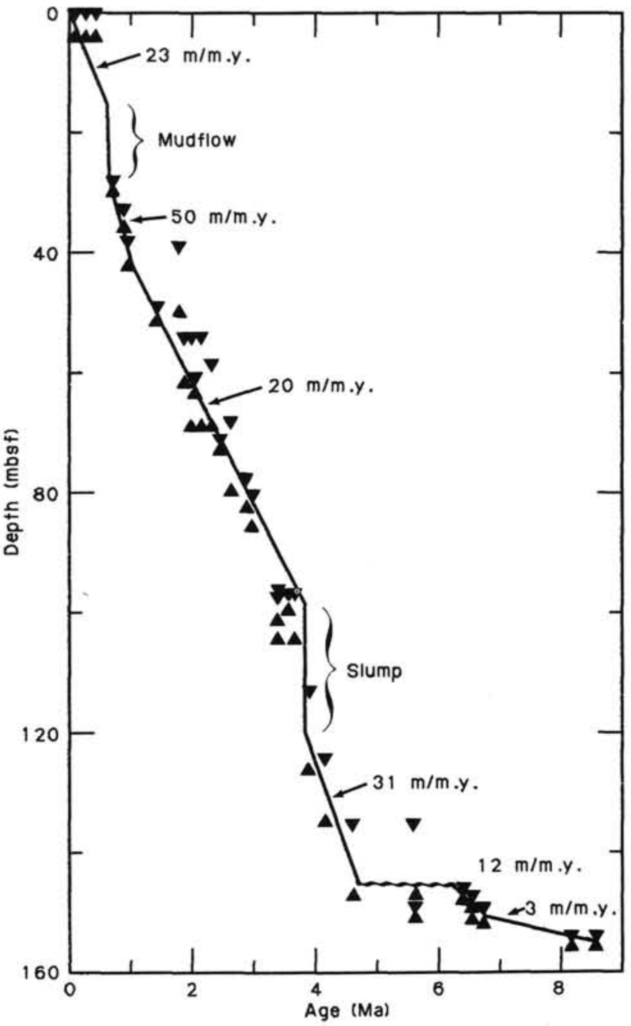

Figure 20. Accumulation-rate curve for Hole 657B adjusted for two mudflow units between 15 and 27 and 98 and 120 m.

dure was changed after we noted some evidence that the finer grained sediments were not being completely dried. The procedure was changed from 4 hr in the freeze drier to 8 hr in the freeze drier plus 2 hr in the oven at 110°C.

The wet-bulk-density plots (Fig. 23) show a generally increasing density with depth from 1.55 g/cm^3 near the surface to 1.95 g/cm^3 at a depth of 160 mbsf. The large variations in sediment lithology at this site are reflected in the large fluctuations in the wet-bulk density and related parameters (dry-bulk density, water content, and porosity).

Only hand-held "Torvane" shear-strength measurements were performed on cores from Site 657. Much of the cored material had suffered a significant degree of disturbance; hence, the shear-strength profiles (Fig. 29) are probably a better indication of relative degrees of remolding than of formation shear strength.

The profiles for compressional-wave (*P*-wave) velocity obtained using the Hamilton Frame (Fig. 30) show a slight positive gradient (especially below 100 mbsf). Velocities range from 1.53 km/s near the surface to 1.64 km/s at 160 mbsf. The *P*-wave-velocity data correlate strongly with the bulk density (as would be expected in unlithified sediments).

All the whole-core sections were continuously logged using the GRAPE and PWL. Continuous downhole plots are not available at this stage, but two sections are shown for illustrative purposes in Figure 31. Figure 31A shows the GRAPE and PWL data for Section 108-657B-15H-2; Figure 31B shows the data for Section 108-657B-3H-3. It can be seen that the signal-to-noise ratio for the PWL is far superior to the GRAPE. In particular, Section 108-657B-15H-2 (Fig. 31A) illustrates how the PWL can resolve subtle changes in lithology that are not resolved by the GRAPE. However, there are occasions when the PWL does not provide complete profiles. This occurred at Site 657 whenever a significant amount of air or other gas was present in the core or between the core and the liner. Additional problems occurred when the liners were broken, when the tape on the outside of the liner sometimes prohibited a good acoustic coupling between the core and the transducers. These problems do not affect the GRAPE.

Table 3. Biostratigraphic and magnetostratigraphic events, their stratigraphic placement, and their estimated ages for Hole 657B.

Datum	Depths (mbsf)	Age (Ma)
Emiliania huxleyi acme begins	0.9-3.3	0.09
FO *E. huxleyi*	0.9-3.3	0.28
LO *Pseudoemiliania lacunosa*	0.9-3.3	0.47
Brunhes/Matuyama (C1-C1r)	29.0	0.73
Top Jaramillo (C1r-1)	33.8-35.0	0.91
Base Jaramillo (C1r-1)	39.3-41.7	0.98
LO *Calcidiscus macintyrei*	50.2-51.0	1.45
LO *Globigerinoides obliquus*	40.1-49.4	1.80
LO *Discoaster brouweri*	55.2-61.2	1.89
FO *Globorotalia inflata*	55.3-68.5	2.00
FO *Discoaster triradiatus* acme	61.9-62.78	2.07
LO *Globorotalia miocenica*	55.3-68.5	2.20
LO *Discoaster pentaradiatus*	59.7-68.5	2.35
Top Gauss (C2/C2A)	72.3	2.47
LO *D. tamalis*	69.2-78.8	2.65
LO *D. altispira*	78.7-81.8	2.90
LO *Saphaeroidinellopsis seminulina*	81.8-84.8	3.00
Base Gauss (C2A/C2Ar)	98.5-100.5	3.40
LO *Globorotalia margaritae*	97.2-103.6	3.40
LO *Reticulofenestra pseudoumbilica*	98.1-98.9	3.56
LO *Amaurolithus tricorniculatus*	97.7-103.6	3.70
LO *Globigerina nepenthes*	114.2-125.0	3.90
FO *G. puncticulata*	125.0-133.9	4.15
FO *Ceratolithus rugosus*	135.7-146.0	4.60
LO *Discoaster quinqueramus*	135.7-146.0	5.60
Top C3B	146.9-147.2	6.37
C3B/C3B-r	148.0-148.4	6.50
Top C4	149.9-150.6	6.70
Within upper NN11	150.0	5.60
Within upper NN11	150.0	6.50
Within NN10	154.8	8.20
Within NN10	154.8	8.50

FO = first occurrence; LO = last occurrence. See "Introduction and Explanatory Notes" chapter (this volume) for further explanations.

SEISMIC STRATIGRAPHY

High-resolution seismic reflection profiles (3.5 and 12 kHz) and 20- to 500-Hz reflection profiles were recorded at Site 657 (see "Background and Scientific Objectives" section, this chapter). The 50- to 500-Hz seismic record is characterized by a two-part section (Fig. 32; Table 10). The upper seismic unit (unit 1) extends 0.185 s below the seafloor (143 m at 1554 m/s) and consists of a number of strong reflectors and a few weaker, slightly divergent reflectors. Seismic unit 2 consists in its upper part of three strong, continuous reflectors below a thin transparent zone; only this uppermost part was drilled at Site 657.

The source of these reflectors was determined from (1) well-known sound velocities of the sediment profiles (see "Physical Properties" section, this chapter) and (2) a number of sedimentological events resulting in increased shear strength and anoma-

Table 4. Results of inorganic geochemical analyses conducted for Site 657.

Core/ section	Depth (m)	pH	Alkalinity (meq/dm^3)	Salinity (‰)	Chlorinity (mmol/L)	SO_4^{2-} (mmol/L)	Mg^{2+} (mmol/L)	Ca^{2+} (mmol/L)
1H-4	5.95	7.75	4.25	34.5	550	22.9	50.0	28.3
6H-3	49.57	7.59	5.69	34.3	556	18.6	50.5	14.9
11H-3	97.10	7.63	4.71	35.2	586	16.9	51.3	17.5
16H-5	147.60	7.69	3.94	37.7	621	16.1	50.8	16.5

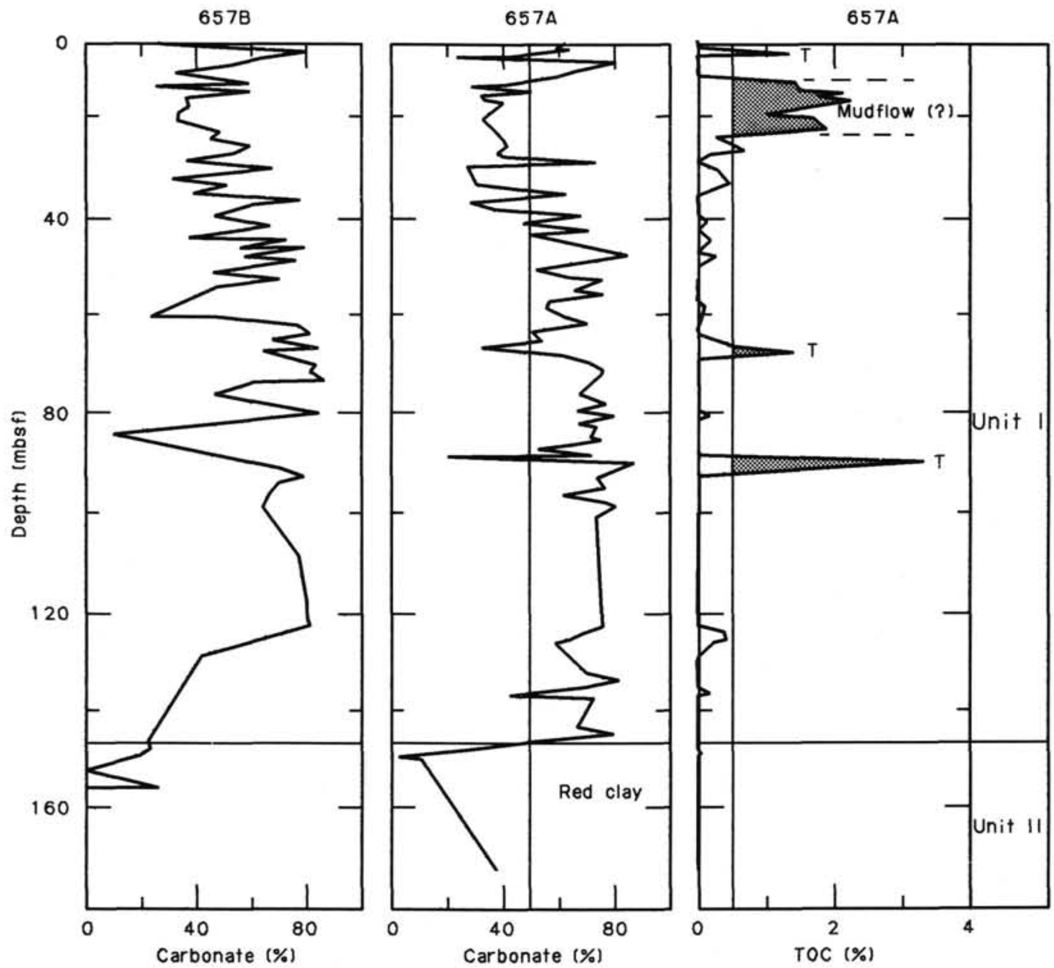

Figure 21. Total-organic-carbon (TOC) and carbonate records of Hole 657A and carbonate record of Hole 657B. T = turbidite.

lously high P-wave velocities at well-defined sub-bottom depths. In addition, a number of irregularities in the seismic record has confirmed the sedimentological interpretation of several reflectors. The details of our seismic correlation are summarized in Table 10.

Seismic unit 1 correlates with lithostratigraphic Unit I, and the upper part of seismic Unit 2 with lithostratigraphic Unit II. Also, the base of the slump fold of lithostratigraphic Unit ID is well marked in the seismic record by reflector 7. On the seismic record, the slump fold between reflectors 6 and 7 pinches out just south of Site 657, halfway to point 2 (Fig. 32, right-hand side). Reflectors 2a and possibly 4 and 9 can be correlated with major turbiditic sand layers, some of them covering irregular topography. Reflectors 1 and 2 are artifacts. A processed record of the *JOIDES Resolution* seismic line possibly will provide more detailed evidence for our correlation attempt.

COMPOSITE-DEPTH SECTION

The lithologic units recovered from Holes 657A and 657B are essentially identical (see "Lithostratigraphy and Sedimentology" section, this chapter). The interbedded clay–nannofossil-ooze profiles of the two holes, which lie only some 8 m apart, could be correlated in detail by means of biostratigraphic markers, paleomagnetics, sand layers from turbidites, and fold structures. However, the nominal sub-bottom depths (based on the drilling record) of several distinct lithostratigraphic features were offset by up to more than 5 m between Holes 657A and 657B (Fig. 33). The offset is not constant from core to core but becomes reversed twice downcore. The amount of displacement cannot be related to irregular small-scale seafloor topography, according to evidence from both well-stratified seismic and sub-bottom profiler records. Thus, we assume that the differences in

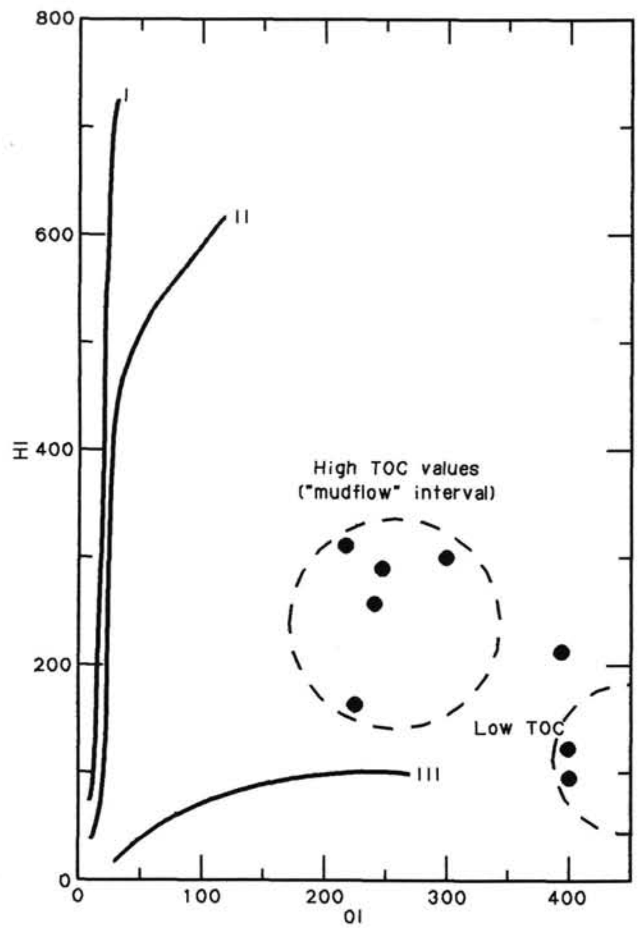

Figure 22. Hydrogen Index (*HI*) vs. oxygen index (*OI*), or van Krevelen diagram, of organic matter from Hole 657A.

Table 5. Rock-Eval pyrolysis results and estimated amounts of marine organic matter from Hole 657A, according to Stein et al. (1986).

Sample	TOC (%)	HI	OI	T_{max}	Marine C_{org} (%)
657A-2H-3-121	1.41	164	221	413	40
2H-4-121	1.47	315	293	408	60
2H-5-115	1.74	297	247	411	60
2H-6-040	2.24	324	216	412	60
3H-1-121	0.98	281	315	411	60
3H-3-121	1.87	261	239	413	60
3H-5-121	0.51	216	398	411	50
4H-4-120	0.45	124	738	382	30
8H-1-120	0.54	96	704	390	25

TOC = total organic carbon; HI = hydrogen index; OI = oxygen index; T_{max} = maximum temperature; C_{org} = organic carbon.

Table 6. Data for index properties, Hole 657A.

Section	Depth (mbsf)	Grain density (g/cm^3)	Wet water content (%)	Dry water content (%)	Wet-bulk density (g/cm^3)	Dry-bulk density (g/cm^3)	Porosity (%)
1-2	2.7	2.28	54.01	117.46	1.40	0.67	74.01
1-3	4.2	2.70	49.13	96.59	1.51	0.79	72.39
1-4	5.7	2.72	25.21	33.71	1.95	1.48	48.10
2-1	8.4	2.68	47.39	90.09	1.53	0.83	70.84
2-2	9.9	2.72	42.83	74.91	1.47	0.86	61.48
2-3	11.4	2.27	37.16	59.14	1.57	1.01	56.88
2-4	12.9	2.62	46.87	88.21	1.54	0.84	70.48
2-5	14.3	2.29	37.61	60.29	1.58	1.01	58.06
2-6	15.0	2.53	44.76	81.02	1.56	0.89	68.31
3-1	17.9	2.31	32.74	48.67	1.65	1.13	52.62
3-2	18.5	2.20	40.15	67.07	1.50	0.92	58.76
3-3	20.9	2.57	45.25	82.66	1.55	0.87	68.59
3-4	22.4	2.65	26.72	36.46	1.88	1.39	48.92
3-5	23.9	2.57	27.16	37.28	1.86	1.37	49.17
3-6	25.4	2.61	24.88	33.13	1.91	1.45	46.36
3-7	26.0	2.59	24.41	32.29	1.92	1.47	45.84
4-1	27.4	2.39	35.68	55.46	1.63	1.07	56.59
4-2	28.0	2.36	24.36	32.21	1.39	1.06	32.97
4-3	30.4	2.40	37.03	58.81	1.60	1.03	57.73
4-4	31.9	2.43	39.78	66.05	1.57	0.97	61.07
4-5	33.4	2.19	29.90	42.66	1.63	1.16	47.68
4-6	34.0	2.71	41.65	71.39	1.62	0.97	65.95
4-7	35.7	2.73	42.78	74.78	1.59	0.93	66.40
5-1	36.9	2.64	42.18	72.96	1.63	0.96	66.99
5-2	38.4	2.71	44.70	80.83	1.61	0.92	70.22
5-3	39.9	2.29	35.75	55.64	1.60	1.05	55.87
5-4	41.4	2.42	36.33	57.06	1.62	1.05	57.58
5-5	42.0	2.35	36.49	57.45	1.62	1.05	57.55
5-6	44.4	2.46	34.75	53.25	1.65	1.10	55.88
6-1	46.2	2.60	38.09	61.52	1.59	1.01	59.15
6-2	47.0	2.58	41.30	70.37	1.58	0.95	63.78
6-3	49.7	2.51	33.50	50.37	1.69	1.15	55.35
6-4	50.9	3.12	43.89	78.22	1.68	0.97	71.94
6-5	51.5	2.10	34.84	53.48	1.55	1.03	52.79
6-6	53.9	2.55	37.65	60.37	1.64	1.04	60.20
6-7	54.5	2.23	32.53	48.21	1.57	1.08	49.94
7-1	55.9	2.45	41.82	71.87	1.55	0.93	63.41
7-2	57.4	2.60	38.76	63.29	1.64	1.03	62.00
7-3	58.9	2.16	25.46	34.16	1.64	1.23	40.65
7-4	60.5	2.47	27.63	38.18	1.76	1.29	47.42
7-5	61.8	2.36	34.67	53.08	1.64	1.09	55.58
7-6	63.3	2.42	32.44	48.02	1.70	1.17	53.84
8-1	65.4	2.54	39.52	65.35	1.64	1.02	63.40
8-2	66.9	2.08	41.75	71.67	1.63	0.98	66.58
8-3	68.3	2.23	20.74	26.17	1.81	1.45	36.70
8-4	69.9	2.44	38.21	61.84	1.64	1.04	61.26
8-5	70.54	2.31	33.12	49.51	1.61	1.10	52.09
9-1	74.9	2.27	30.22	43.31	1.66	1.18	48.98
9-2	76.4	2.54	35.03	53.91	1.67	1.11	57.21
9-3	78.3	2.69	26.33	35.74	1.92	1.43	49.23
9-4	79.4	2.43	36.88	58.42	1.64	1.06	59.06
9-5	80.9	2.12	25.30	33.88	1.65	1.25	40.76
9-6	81.5	2.38	30.57	44.02	1.68	1.18	50.08
10-1	84.4	2.23	28.75	40.35	1.66	1.20	46.52
10-2	85.9	2.42	27.20	37.37	1.74	1.28	46.25
10-3	87.4	2.20	30.19	43.24	1.62	1.15	47.68
10-4	88.9	2.67	33.61	50.63	1.75	1.19	57.57
10-6	91.9	2.85	37.49	59.96	1.71	1.09	62.69
11-1	93.9	2.69	37.54	60.11	1.68	1.07	61.43
11-2	95.4	2.77	33.67	50.75	1.82	1.23	59.68
11-3	96.9	2.72	41.03	69.57	1.62	0.98	64.76
11-4	97.6	2.65	37.01	58.77	1.68	1.08	60.69
11-5	99.9	2.68	36.19	56.71	1.78	1.16	62.83
14-1	122.4	2.70	30.67	44.25	1.84	1.29	54.94
14-2	123.9	2.62	31.85	46.74	1.81	1.25	56.25
14-3	125.4	2.73	32.54	48.23	1.84	1.26	58.50
14-4	126.0	2.66	29.99	42.84	1.83	1.30	53.47
15-1	131.9	2.88	28.87	40.59	1.92	1.39	54.18
15-2	133.4	2.78	32.27	47.64	1.82	1.26	57.40
15-3	134.9	2.78	31.93	46.92	1.86	1.29	58.09
15-4	136.4	2.75	28.50	39.86	1.86	1.35	51.84
15-5	137.9	2.89	32.49	48.13	1.82	1.25	57.73
16-2	142.9	2.72	27.52	37.97	1.94	1.42	52.02
16-3	144.4	2.72	34.04	51.60	1.77	1.19	58.77
16-4	145.9	2.72	29.08	41.01	1.87	1.34	53.01
16-5	147.4	2.49	31.10	45.14	1.79	1.25	54.19
16-6	148.9	2.76	30.99	44.92	1.90	1.33	57.58
16-7	149.4	2.90	27.94	38.77	1.93	1.41	52.61
19-3	172.1	2.68	24.40	32.28	1.93	1.48	46.09

the nominal sub-bottom depths are artifacts of the coring process and ODP conventions for recording depths.

We have, therefore, attempted to adjust the core depths from the two holes in order to arrive at a preliminary composite-depth section of well-preserved, uncontorted cores (Fig. 33; Table 11). The following criteria and rationales define our procedure:

1. The top of Core 108-657B-2H was moved from 2.7 to 3.0 mbsf with respect to Hole 657A, based on a close definition of the top of Zone NN19.

2. Based on the presence of the same thick turbiditic sand layer and an 8-m-thick mudflow with a further 10 m of turbiditic sand and mud below, we believe that Cores 108-657A-2H, -657A-3H, -657A-4H, etc., should be moved down by 1.5 m relative to Hole 657B. The strongly contorted two upper sections

Table 7. Data for index properties, Hole 657B.

Section	Depth (mbsf)	Grain density (g/cm^3)	Wet water content (%)	Dry water content (%)	Wet-bulk density (g/cm^3)	Dry-bulk density (g/cm^3)	Porosity (%)
2-2	5.30	2.72	28.80	40.45	1.87	1.35	52.61
2-2	5.41	2.59	59.14	144.75	1.39	0.60	80.42
2-3	6.91	2.70	42.80	74.83	1.59	0.93	66.44
2-4	8.41	2.66	45.69	84.12	1.54	0.86	68.74
2-5	9.91	2.66	47.63	90.96	1.53	0.83	71.00
2-6	11.50	2.61	43.25	76.21	1.58	0.92	66.49
3-1	13.41	2.65	50.45	101.82	1.49	0.76	73.35
3-2	14.05	2.71	48.96	95.92	1.49	0.79	71.24
3-2	15.02	2.83	33.13	49.55	1.81	1.23	58.57
3-3	16.41	2.58	46.97	88.59	1.62	0.89	74.28
3-4	17.91	2.71	46.10	85.53	1.57	0.87	70.74
3-5	19.41	2.67	45.79	84.48	1.67	0.93	74.59
3-6	20.91	2.75	44.90	81.50	1.60	0.91	70.29
4-1	22.91	2.71	48.94	95.83	1.53	0.81	73.18
4-3	25.91	2.82	33.22	49.75	1.81	1.23	58.80
4-4	27.41	2.77	44.86	81.36	1.65	0.94	72.32
4-5	28.91	2.62	42.42	73.69	1.68	0.99	69.40
4-6	30.41	2.71	44.06	78.75	1.59	0.91	68.17
5-1	32.41	2.66	42.82	74.87	1.61	0.94	67.26
5-2	33.91	3.03	46.23	85.98	1.67	0.93	75.55
5-3	35.41	2.62	42.43	73.71	1.66	0.98	68.64
5-4	36.91	2.75	41.66	71.41	1.66	0.99	67.35
5-5	37.64	2.71	40.76	68.81	1.67	1.01	66.36
6-1	41.91	2.64	41.66	71.41	1.63	0.97	66.17
6-3	44.30	2.69	23.51	30.74	1.99	1.54	45.77
6-3	44.91	2.68	40.78	68.86	1.69	1.02	67.19
6-4	46.40	2.70	43.76	77.81	1.62	0.94	69.38
6-5	47.91	2.61	42.68	74.46	1.67	0.98	69.39
6-6	48.54	2.72	41.68	71.46	1.65	0.99	67.03
6-6	48.99	2.60	27.92	38.74	1.87	1.37	50.97
7-1	51.41	2.80	41.27	70.28	1.68	1.01	67.58
7-2	52.91	2.91	39.95	66.52	1.69	1.04	65.89
7-3	54.41	2.76	37.32	59.55	1.74	1.11	63.44
8-1	60.87	2.72	43.32	76.42	1.59	0.93	67.33
8-1	60.93	3.29	39.45	65.16	1.74	1.08	66.89
8-2	62.41	2.71	38.66	63.04	1.68	1.05	63.34
8-3	63.91	2.72	38.72	63.19	1.69	1.06	63.87
8-4	65.42	2.75	38.72	63.18	1.71	1.07	64.59
8-5	66.91	2.70	39.62	65.63	1.67	1.03	64.54
8-6	67.54	2.72	39.89	66.37	1.66	1.02	64.45
9-1	70.41	2.67	43.24	76.19	1.61	0.94	68.13
9-2	71.91	2.49	41.80	71.81	1.57	0.94	64.05
9-3	73.41	3.06	36.31	57.02	1.78	1.16	63.14
9-4	74.04	2.67	34.83	53.45	1.78	1.18	60.41
9-5	76.41	1.22	39.75	65.98	1.73	1.07	67.14
9-6	77.91	2.86	32.55	48.25	1.89	1.29	59.91
10-1	79.91	2.71	41.27	70.27	1.71	1.03	68.88
10-2	81.41	2.33	47.61	90.87	1.66	0.90	77.07
10-3	82.91	2.76	39.96	66.56	1.69	1.04	66.08
10-4	84.41	2.34	42.48	73.85	1.56	0.92	64.62
10-5	85.91	2.78	39.31	64.77	1.70	1.05	65.13
10-6	86.61	2.80	40.10	66.94	1.67	1.02	65.36
11-1	89.41	2.70	38.32	62.12	1.68	1.06	62.88
11-2	90.91	2.72	35.97	56.17	1.68	1.10	59.08
11-4	93.91	2.64	36.28	56.93	1.81	1.18	64.27
11-5	95.41	2.65	34.80	53.37	1.80	1.19	61.09
11-6	96.04	2.75	36.25	56.87	1.83	1.19	64.76
12-1	98.91	2.76	37.32	59.54	1.71	1.09	62.30
12-2	100.41	2.76	35.48	55.00	1.79	1.18	62.13
12-3	101.95	2.69	34.32	52.24	1.76	1.18	58.93
12-4	102.55	2.92	35.44	54.88	1.79	1.18	61.94
13-1	108.45	2.77	38.30	62.08	1.70	1.07	63.54
13-2	109.91	2.76	35.10	54.07	1.73	1.15	59.31
13-3	111.41	2.69	36.78	58.18	1.70	1.10	61.05
13-4	112.91	2.67	36.44	57.33	1.75	1.14	62.33
13-5	113.55	2.73	37.11	59.02	1.77	1.14	64.13
14-1	117.91	2.73	35.95	56.12	1.75	1.14	61.29
14-2	119.41	2.67	35.18	54.28	1.74	1.15	59.81
14-3	120.91	2.67	35.97	56.18	1.73	1.13	60.81
14-4	122.41	2.71	34.00	51.52	1.76	1.19	58.57
14-5	123.91	2.75	32.56	48.28	1.78	1.22	56.61
15-1	127.41	2.70	33.02	49.29	1.78	1.22	57.50
15-2	128.91	2.84	30.48	43.84	1.87	1.32	55.67
15-3	130.41	2.86	31.39	45.76	1.88	1.31	57.72
15-4	131.91	2.74	32.79	48.80	1.79	1.22	57.20
16-1	136.91	2.71	26.71	36.45	1.91	1.41	49.70
16-2	138.09	2.68	25.85	34.86	1.94	1.46	49.00
16-3	139.91	2.78	28.26	39.39	1.89	1.37	52.11
16-4	140.52	2.73	29.15	41.14	1.87	1.35	53.26
17-1	145.80	2.80	30.72	44.35	1.91	1.34	57.27
17-2	147.91	2.69	28.87	40.58	1.87	1.35	52.66
17-3	149.41	2.83	29.94	42.74	1.89	1.35	55.38
17-4	150.91	2.66	31.63	46.26	1.83	1.27	56.38
17-5	152.41	2.64	31.21	45.38	1.84	1.28	56.02
18-1	155.91	2.65	20.75	26.18	2.02	1.61	40.89

Table 8. Data for shear strength, Site 657.

Section	Depth (mbsf)	Shear strength (kPa)
Hole 657A		
1-3	4.2	4.0
2-1	8.4	4.0
2-2	9.9	3.0
2-3	11.4	15.0
2-4	12.9	31.0
2-5	14.3	45.0
2-6	15.0	41.0
3-1	17.9	14.0
3-2	18.5	37.0
3-3	20.9	48.0
3-4	22.4	52.0
3-5	23.9	18.0
3-6	25.4	48.0
3-7	26.0	62.0
4-1	27.4	17.5
4-2	28.0	21.0
4-3	30.4	33.0
4-4	31.9	35.0
4-5	33.4	24.0
4-6	34.0	17.0
4-7	35.7	19.5
5-1	36.9	25.0
5-2	38.4	22.5
5-3	39.9	26.0
5-4	41.4	18.0
5-5	42.0	28.5
5-6	44.4	17.5
6-1	46.2	14.5
6-2	47.0	31.5
6-3	49.7	36.0
6-4	50.9	30.0
6-5	51.5	22.0
6-6	53.9	29.0
6-7	54.5	19.5
7-1	55.9	00.0
7-2	57.4	16.0
7-3	58.9	21.0
7-4	60.5	27.5
7-5	61.8	31.5
7-6	63.4	30.0
8-1	65.4	40.0
8-2	66.9	23.5
8-3	68.34	28.0
8-4	69.9	25.0
8-5	70.54	21.0
9-1	74.9	11.0
9-2	76.4	1.0
9-3	77.9	15.0
9-4	79.4	21.0
9-5	80.9	25.0
9-6	81.5	31.0
10-1	84.4	0.0
10-2	85.9	18.0
10-3	87.4	10.0
10-4	88.9	36.0
10-6	91.9	25.0
11-1	93.9	30.0
11-2	95.4	20.0
11-3	96.9	45.0
11-4	97.6	15.0
11-5	99.9	15.5
14-1	122.4	37.5
14-2	123.9	30.0
14-3	125.4	42.0
14-4	126.0	52.5
15-1	131.9	60.5
15-2	133.4	26.0
15-3	134.9	72.0
15-4	136.4	83.5
15-5	137.9	48.0
16-2	142.9	65.0
16-3	144.4	33.0
16-4	145.9	81.0
16-5	146.7	150.0
16-5	147.4	98.0
16-6	148.8	162.5
16-6	148.9	100.1
16-7	149.3	142.5
16-7	149.4	75.0
Hole 657B		
2-2	5.41	4.0
2-3	6.91	6.0
2-4	8.41	11.0
2-5	9.91	16.0
2-6	11.50	15.0
3-1	13.41	13.0
3-2	14.05	7.0
3-2	15.02	0.0
3-3	16.41	13.0
3-4	17.91	16.0
3-5	19.41	15.0
3-6	20.91	24.0
4-1	22.91	13.0
4-2	24.41	14.0
4-3	25.91	16.0
4-4	27.41	15.0
4-5	28.91	34.0
4-6	30.41	32.0
5-1	32.41	30.0
5-2	33.91	34.0
5-3	35.41	38.0
5-4	36.91	22.0
5-5	37.64	32.5
5-6	39.91	38.0
6-1	41.91	18.5
6-2	43.41	20.0
6-3	44.30	23.0
6-4	46.40	29.5
6-5	47.91	29.0
6-6	48.54	38.5
7-1	51.41	32.5
7-2	52.91	28.0
7-3	54.41	37.5
8-1	60.87	41.0
8-1	60.93	44.5
8-2	62.41	28.0
8-3	63.91	27.0
8-4	65.42	0.0
8-5	66.91	30.0
8-6	67.54	34.5
9-1	70.41	23.0
9-2	71.91	29.0
9-3	73.41	28.0
9-4	74.04	24.5
9-5	76.41	60.0
9-6	77.91	48.0
10-1	79.91	33.0
10-2	81.41	26.0
10-3	82.91	18.0
10-4	84.41	24.5
10-5	85.91	14.5
10-6	86.61	23.0
11-1	89.41	22.5
11-2	90.91	22.5
11-3	92.41	22.5
11-4	93.91	29.0
11-5	95.41	40.0
11-6	96.04	34.0
12-1	98.91	39.0
12-2	100.41	33.5
12-3	101.95	37.0
12-4	102.55	34.5
13-1	108.45	25.5
13-2	109.91	36.0
13-3	111.41	25.0
13-4	112.91	25.0
13-5	113.55	28.5
14-1	117.91	33.0
14-2	119.41	35.0
14-3	120.91	37.0
14-4	122.41	43.0
14-5	123.91	65.0
15-1	127.41	47.0
15-2	128.91	70.0
15-3	130.41	84.0
15-4	131.91	78.0
15-5	133.41	74.0
16-1	136.91	70.5
16-2	138.90	75.0
16-3	139.91	98.5
16-4	140.52	89.0
17-1	145.80	66.0
17-2	147.91	86.0
17-3	149.41	96.0
17-4	150.91	85.0
17-5	152.41	103.0

Table 9. Data for compresional-wave velocity, Site 657.

Section	Depth (mbsf)	*P*-wave velocity (km/s)	Section	Depth (mbsf)	*P*-wave velocity (km/s)
Hole 657A			Hole 657B		
1-2	2.70	1.51	2-2	5.41	1.51
1-2	3.63	1.51	2-3	6.91	1.52
1-2	3.85	1.57	2-4	8.41	1.52
1-3	4.20	1.47	2-5	9.91	1.56
1-4	5.70	1.69	2-6	11.50	1.56
1-4	6.50	1.58	3-1	13.40	1.51
1-5	7.80	1.54	3-2	14.05	1.39
2-1	8.40	1.56	3-2	15.02	1.67
2-2	9.90	1.57	3-3	16.41	1.56
2-3	11.40	1.58	3-4	17.91	1.55
2-4	12.90	1.56	3-5	19.41	1.54
2-5	13.30	1.59	3-6	20.91	1.56
2-5	14.30	1.57	4-1	22.91	1.54
2-6	15.00	1.57	4-2	24.41	1.54
3-1	17.90	1.60	4-3	25.91	1.62
3-2	18.50	1.58	4-4	27.41	1.56
3-3	20.90	1.56	4-5	28.91	1.55
3-4	22.40	1.70	4-6	30.41	1.56
3-5	23.90	1.68	5-1	32.41	1.53
3-6	25.40	1.70	5-2	33.91	1.52
3-7	26.00	1.71	5-3	35.41	1.54
4-1	27.40	1.51	5-4	36.91	1.59
4-2	28.00	1.43	5-5	37.64	1.58
4-3	30.40	1.45	5-6	39.91	1.55
4-4	31.90	1.51	6-1	41.91	1.54
4-5	33.40	1.51	6-2	43.41	1.56
4-6	34.00	1.55	6-3	44.30	1.56
4-7	35.70	1.58	6-4	46.40	1.55
5-1	36.90	1.55	6-5	47.91	1.54
5-2	38.40	1.49	6-6	48.54	1.55
5-3	39.90	1.51	7-1	51.41	1.54
5-4	41.40	1.54	7-2	52.91	1.57
5-5	42.00	1.52	7-3	53.70	1.54
5-6	44.40	1.58	7-3	54.41	1.61
6-1	46.20	1.56	8-1	60.87	1.52
6-2	47.00	1.54	8-1	60.93	1.55
6-3	49.70	1.56	8-2	62.41	1.53
6-4	50.90	1.59	8-3	63.91	1.54
6-5	51.50	1.60	8-4	65.42	1.54
6-6	53.90	1.62	8-5	66.91	1.54
6-7	54.54	1.57	8-6	67.54	1.56
7-1	55.90	1.55	9-1	70.41	1.53
7-2	57.40	1.58	9-2	71.91	1.59
7-3	58.90	1.62	9-3	73.41	1.62
7-4	60.49	1.57	9-4	74.04	1.58
7-5	61.90	1.57	9-5	76.41	1.55
7-6	63.40	1.58	9-6	77.91	1.58
8-1	65.40	1.55	10-1	79.91	1.54
8-2	66.90	1.56	10-1	81.08	1.55
8-3	68.34	1.62	10-2	81.41	1.53
8-4	69.90	1.58	10-3	82.91	1.56
8-5	70.54	1.59	10-4	84.41	1.56
9-1	74.90	1.54	10-5	65.91	1.56
9-2	76.40	1.57	10-6	86.61	1.57
9-3	76.87	1.78	11-1	89.41	1.54
9-3	77.90	1.57	11-2	90.91	1.53
9-4	79.40	1.55	11-3	92.41	1.53
9-5	80.90	1.58	11-4	93.91	1.55
9-6	81.54	1.57	11-5	95.41	1.56
10-1	84.40	1.58	11-6	96.04	1.56
10-2	85.90	1.58	12-1	98.91	1.54
10-3	87.40	1.58	12-2	100.41	1.53
10-4	88.90	1.61	12-3	101.95	1.56
10-4	89.13	1.57	12-4	102.55	1.58
10-6	91.90	1.60	13-1	108.45	1.56
11-1	93.90	1.59	13-2	109.91	1.56
11-3	96.90	1.59	13-3	111.41	1.56
11-5	99.90	1.57	13-5	113.55	1.57
14-1	122.40	1.59	13-4	112.91	1.57
14-2	123.90	1.59	14-1	117.91	1.56
14-3	125.40	1.57	14-2	119.41	1.56
14-4	126.04	1.60	14-3	120.91	1.55
15-1	131.90	1.63	14-4	122.41	1.57
15-2	133.40	1.59	14-5	123.91	1.58
15-3	134.90	1.60	15-1	127.41	1.57
15-4	136.40	1.66	15-2	128.91	1.59
15-5	137.00	1.60	15-3	130.41	1.59
16-2	142.90	1.69	15-4	131.91	1.58
16-3	143.80	1.65	15-5	133.41	1.57
16-3	144.00	1.72	16-1	136.91	1.65
16-3	144.40	1.58	16-2	138.90	1.65
16-4	145.90	1.65	16-3	139.91	1.61
16-5	147.20	1.68	16-4	140.52	1.65
16-6	148.70	1.66	17-1	145.80	1.59
16-7	149.20	1.67	17-2	147.91	1.62
19-3	172.10	1.50	17-3	149.41	1.62
			17-4	150.91	1.61
			17-5	152.41	1.63

of Core 108-657A-2H may contain the lost stratigraphic record we observe in the middle part of Core 108-657B-2H. The sedimentary record of Cores 108-657A-4H to -657A-6H and 108-657B-5H to -657B-7H does not provide firm links between the two holes. However, nearly full recovery makes breaks of the record unlikely. On the other hand, gaps probably occur between Cores 108-657A-6H and -657A-7H and between Cores 108-657B-5H and -657B-7H—i.e., near 1.4–1.5 m.y.

3. Susceptibility (see "Paleomagnetism" section, this chapter) provides a most reliable correlation between Cores 108-657A-7H through -657A-9H and Cores 108-657B-7H through -657B-9H at both holes between 60 and 73 mbsf. Accordingly, from 64 to 69 m, the sedimentary record in Hole 657B lies at an equal depth as in Hole 657A, but it is displaced 1.5 m deeper below 69 mbsf. This evidence appears to conflict with that from some biostratigraphic datum levels in Cores 108-657A-6H to -657A-9H and Cores 108-657A-6H to -657B-9H, which show the opposite tendency (e.g., 52 mbsf, composite depth; see "Biostratigraphy" section, this chapter).

4. Based on the top of a nannofossil-ooze section barren of turbiditic sands in Cores 108-657A-10H and -657A-11H and Cores 108-657B-10H and -657B-11H at 83.5 mbsf, composite depth, we place the equivalent sediment record of Core 108-657A-10H at least 2 m up relative to Core 108-657B-10H. This shift is contrary to the outlined magnetic record but is approximately confirmed by the base of Zone PL5. The discrepancy with the core correlation higher up may be ascribed to a possibly spurious 2-m-thick interval of under-recovery at the base of Core 108-657A-8H. The following Cores 108-657A-10H and -657A-11H and Cores 108-657B-10H and -657B-11H form a probably complete section with little under-recovery and little disturbance. Accordingly, the mode of correlation between the holes at 83.5 mbsf is retained.

5. The top of a 22-m-thick sediment fold near 99 mbsf, composite depth, suggests a correlation of Core 108-657A-11H, 96.5 mbsf, with Core 108-657B-12H, 98 mbsf. However, the base of the mudflow lies 4.5 m deeper in Hole 657A than in Hole 657B. Likewise does the whole lithostratigraphic sequence behave farther below, as shown by a number of markers, such as turbiditic sand layers and the transition from nannofossil ooze to brownish red clay near 145 mbsf. We assume that the extra core length between Cores 108-657A-11H and -657A-14H relative to Cores 108-657B-12H to -657B-14H can be explained by the extremely low recovery in Cores 108-657A-12H and -657A-13H; these may be artifacts of the coring process and the ODP convention for recording core depth. Unfortunately, the marked hiatus at the top of the Miocene found at the base of Cores 108-657A-15H and -657B-16H (see "Biostratigraphy" section, this chapter) does not fit with the outlined core correlation.

6. In general, our correlations and adjustments do not always lead to an overlap of sections of "good core" between the holes, but they do allow us to resolve the major gaps in continuous core recovery.

7. By the adjustments, the driller's total sub-bottom depth is reduced by 1 m in Hole 657A and expanded by 4.5 m in Hole 657B.

The composite section (Fig. 33) is a first approximation to the *in-situ* stratigraphy and should reveal the best match with seismic stratigraphy (see "Seismic Stratigraphy" section, this chapter). In addition, it shows how a number of voids and contorted sections in cores with poor recovery can be bypassed successfully by sampling the companion hole. The actual recovery of relatively undeformed core amounts to approximately 85% for the two holes together. Sediment-accumulation rates were recalculated for Site 657 using the new composite-depth estimate and are shown in Figure 34.

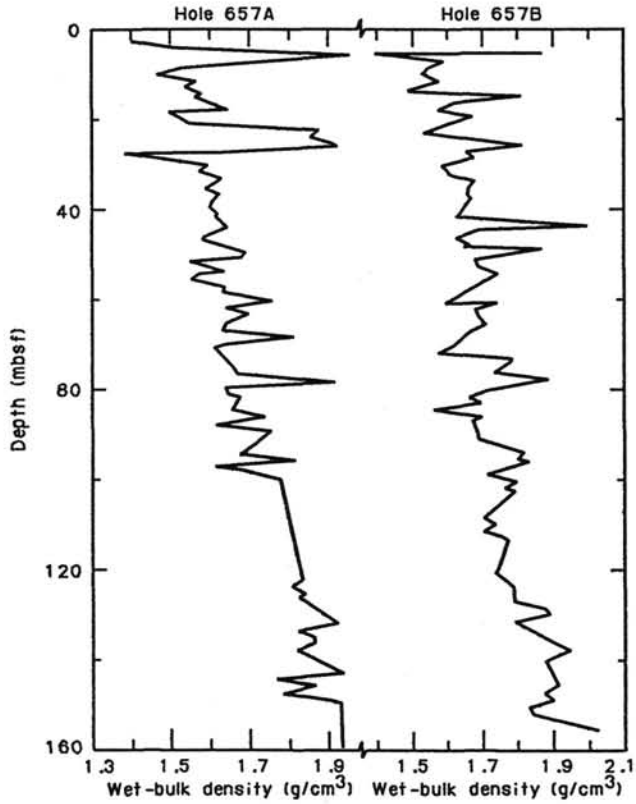

Figure 23. Wet-bulk-density profiles for Holes 657A and 657B.

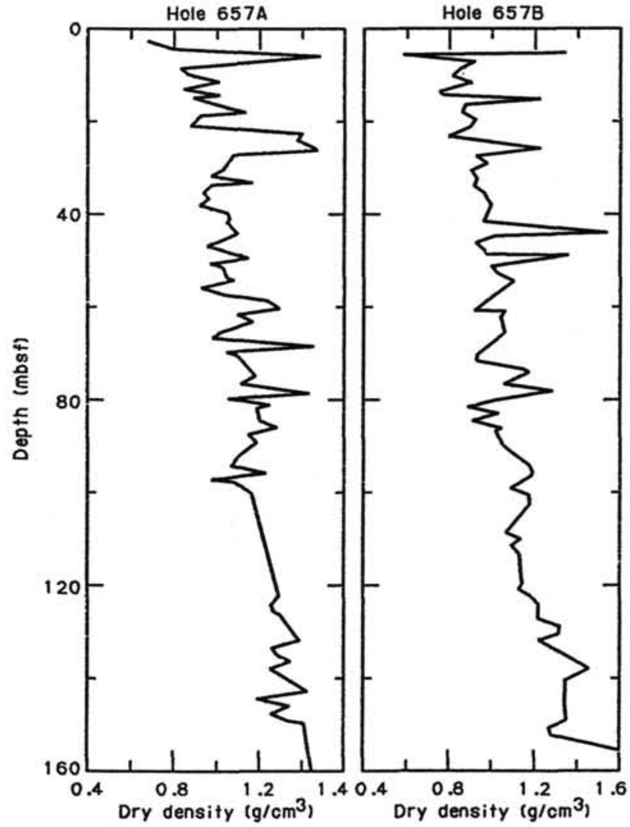

Figure 24. Dry-bulk-density profiles for Holes 657A and 657B.

REFERENCES

Arthur, M. A., Dean, W. E., and Stow, D.A.V., 1984. Models for the deposition of Mesozoic-Cenozoic fine-grained organic-carbon-rich sediments in the deep sea. *In* Stow, D. A., and Piper, D.J.W. (Eds.), *Fine-Grained Sediments: Deep-Water Processes and Facies*: Geol. Soc. London Spec. Publ., 15:527–560.

Backman, J., and Shackleton, N. J., 1983. Quantitative biochronology of Pliocene and early Pleistocene calcareous nannofossils from the Atlantic, Indian and Pacific oceans. *Mar. Micropaleontol.*, 8:141–170.

Berggren, W. A., Kent, D. V., and Van Couvering, J. A., 1985. Neogene geochronology and chronostratigraphy. *In* Snelling, N. J. (Ed.), *The Chronology of the Geological Record*: Geol. Soc. London Mem. 10, 211–259.

Cornford, C., 1979. Organic deposition at a continental rise: organic geochemical interpretation and synthesis at DSDP Site 397, Eastern North Atlantic. *In* von Rad, U., Ryan, W.B.F., et al., *Init. Repts. DSDP*, 47, Pt. 1: Washington (U.S. Govt. Printing Office), 503–510.

Estipalié, J., Madec, M., Tissot, B., Mennig, J. J., and Leplat, P., 1977. Source rock characterization method for petroleum exploration. *Proc. 9th Annu. Offshore Technol. Conf.*, Houston, May 2–5: 439–448.

Gartner, S., Jr., 1977. Calcareous nannofossil biostratigraphy and revised zonation of the Pliocene. *Mar. Micropaleontol.*, 2:1–25.

Hayes, D. E., Pimm, A. C., et al., 1972. Site 140. *In* Hayes, D. E., Pimm, A. C., et al., *Init. Repts. DSDP*, 14: Washington (U.S. Govt. Printing Office), 179–215.

Jacobi, R., and Hayes, D., 1982. Bathymetry, microphysiography and reflectivity characteristics of the west African margin between Sierra Leone and Mauritania. *In* von Rad, U., Hinz, K., Sarnthein, M., and Seibold, E. (Eds.), *Geology of the Northwest African Continental Margin*: Berlin-Heidelberg (Springer-Verlag), 182–212.

Lancelot, Y., Seibold, E., et al., 1978. Site 368: Cape Verde Rise. *In* Lancelot, Y., Seibold, E., et al., *Init. Repts. DSDP*, 41: Washington (U.S. Govt. Printing Office), 233–326.

McIver, R., 1975. Hydrocarbon occurrence from JOIDES Deep Sea Drilling Project. *Proc. 9th Pet. Congr.*, 269–280.

Müller, P., Erlenkeuser, H., and von Grafenstein, R., 1983. Glacial-interglacial cycles in oceanic productivity inferred from organic carbon contents in eastern North Atlantic sediment cores. *In* Thiede, J., and Suess, E. (Eds.), *Coastal Upwelling: Its Sediment Record*, Part B: New York (Plenum), 365–398.

Peters, K. E., and Simoneit, B.R.T., 1982. Rock-Eval pyrolysis of Quaternary sediments from Leg 64, Sites 479 and 480, Gulf of California. *In* Curray, J. R., Moore, D. G., et al., *Init. Repts. DSDP*, 64, Pt. 2: Washington (U.S. Govt. Printing Office), 925–931.

Rio, D., Backman, J., and Raffi, I., in press. *Calcareous Nannofossil Biochronology and the Pliocene/Pleistocene Boundary*: Micropaleontol. Press Spec. Publ.

Sarnthein, M., 1978. Neogene sand layers off northwest Africa: composition and source environment. *In* Lancelot, Y., Seibold, E., et al., *Init. Repts. DSDP*, 41, Suppl.: Washington (U.S. Govt. Printing Office), 939–959.

Sarnthein, M., Thiede, J., Pflaumann, U., Erlenkeuser, H., Fütterer, D., Koopmann, B., Lange, H., and Seibold, E., 1982. Atmospheric and oceanic circulation patterns off northwest Africa during the past 25 million years. *In* von Rad, U., Hinz, K., Sarnthein, M., and Seibold, E. (Eds.), *Geology of the Northwest African Continental Margin*: Berlin-Heidelberg (Springer-Verlag), 545–604.

Stein, R., Rullkötter, J., and Welte, D., 1986. Accumulation of organic-carbon-rich sediments in the Late Jurassic and Cretaceous Atlantic Ocean—A synthesis. *Chem. Geol.*, 56:1–32.

Stein, R., and Sarnthein, M., 1984. Late Neogene events of atmospheric and oceanic circulation offshore northwest Africa: high-resolution record from deep-sea sediments. *Palaeoecol. Africa*, 16:9–36.

Thierstein, H. R., Geitzenauer, K. R., Molfino, B., and Shackleton, N. J., 1977. Global synchroneity of late Quaternary coccolith datum levels: validation by oxygen isotopes. *Geology*, 5:400–404.

Tissot, B. P., and Welte, D. H., 1984. *Petroleum Formation and Occurrence* (2nd ed.): Berlin-Heidelberg (Springer-Verlag).

Uchupi, E., 1971. Bathymetric atlas of the Atlantic, Caribbean, and Gulf of Mexico. Woods Hole Oceanogr. Inst., Ref. 71-72, unpubl. manuscr.

Weaver, P.P.E., and Clement, B. M., 1986. Synchroneity of Pliocene planktonic foraminiferal datums in the North Atlantic. *Mar. Micropaleontol.*, 295–307.

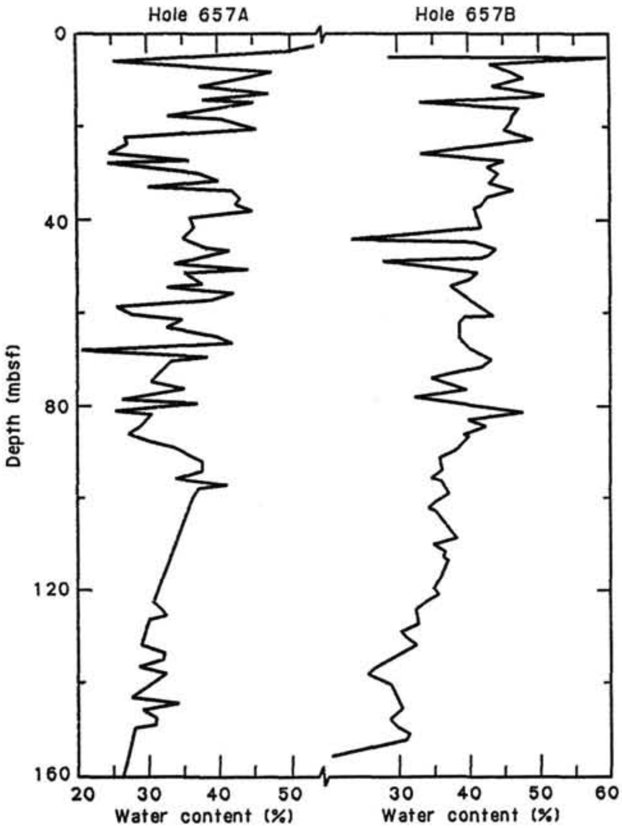

Figure 25. Water-content profiles for Holes 657A and 657B.

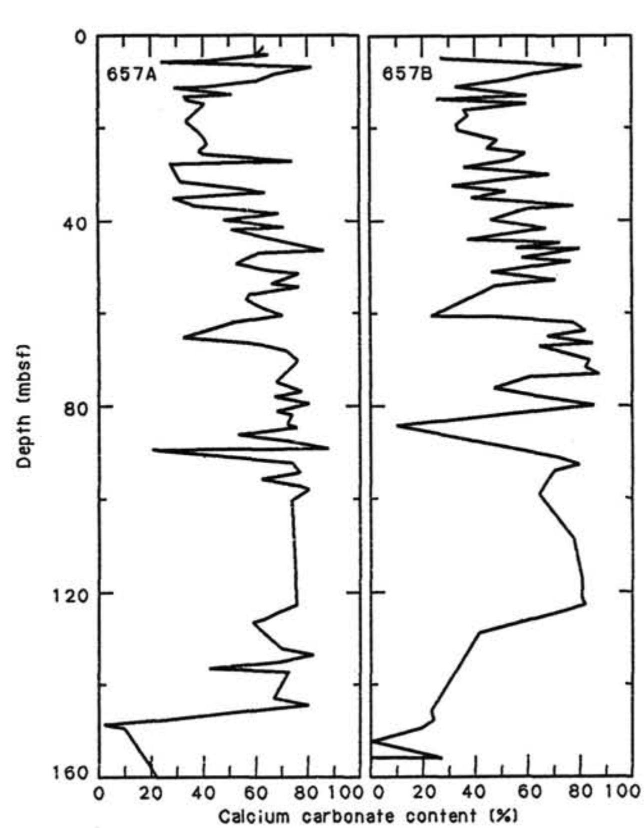

Figure 27. Calcium carbonate content profiles for Holes 657A and 657B.

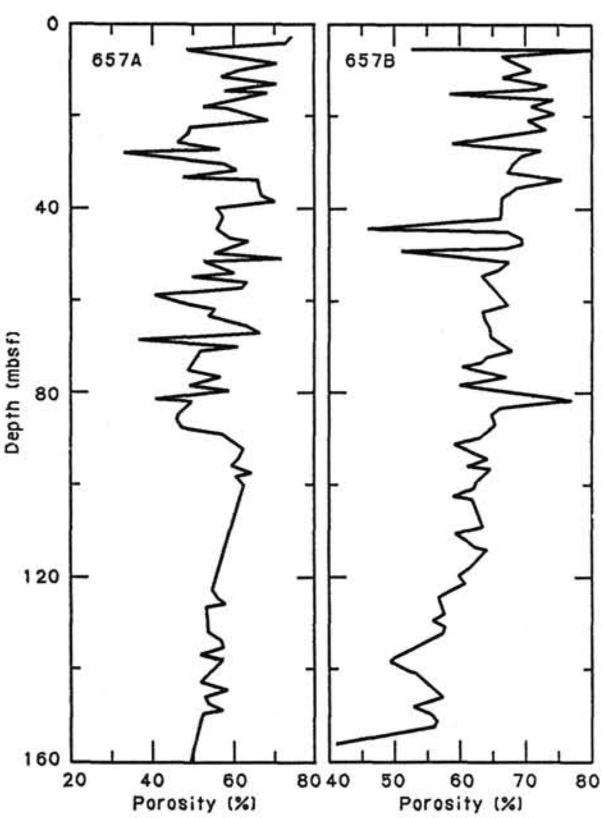

Figure 26. Porosity profiles for Holes 657A and 657B.

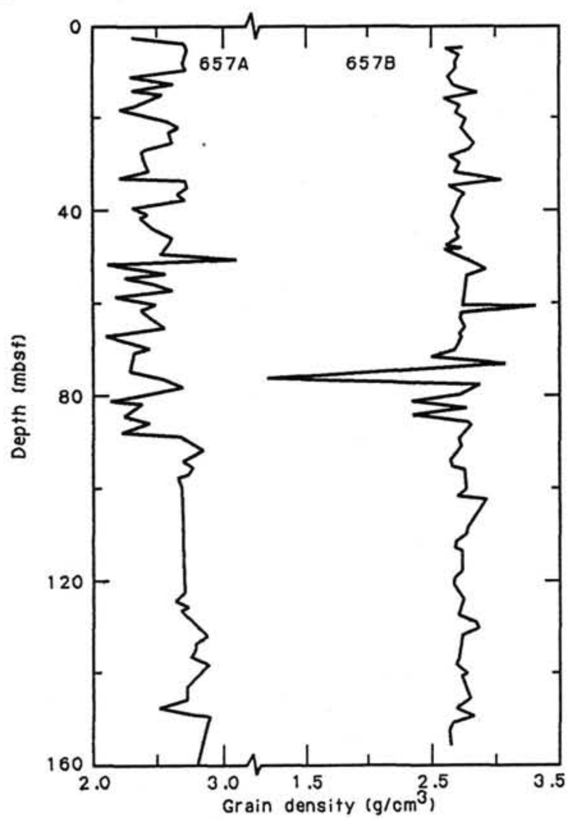

Figure 28. Grain-density profiles for Holes 657A and 657B.

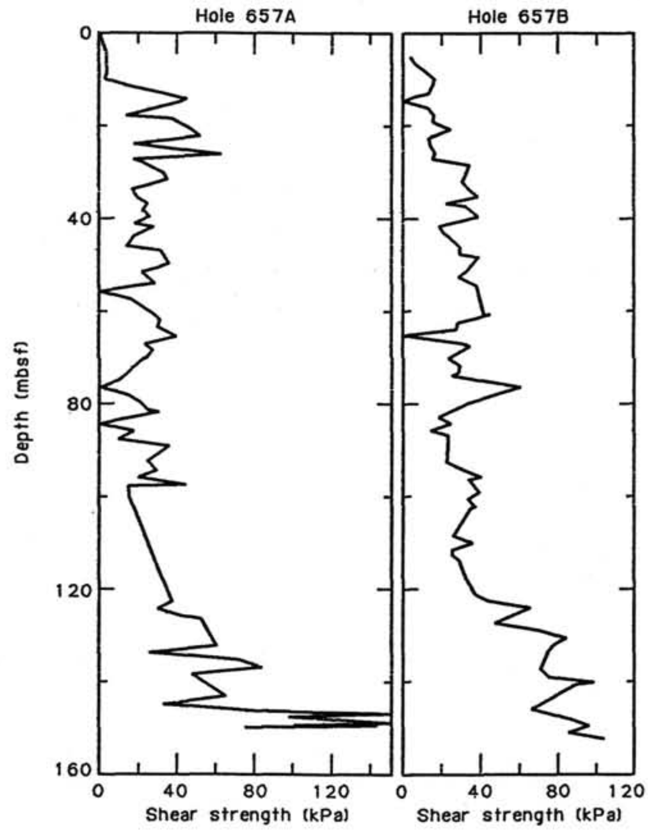

Figure 29. Vane-shear-strength profiles for Holes 657A and 657B.

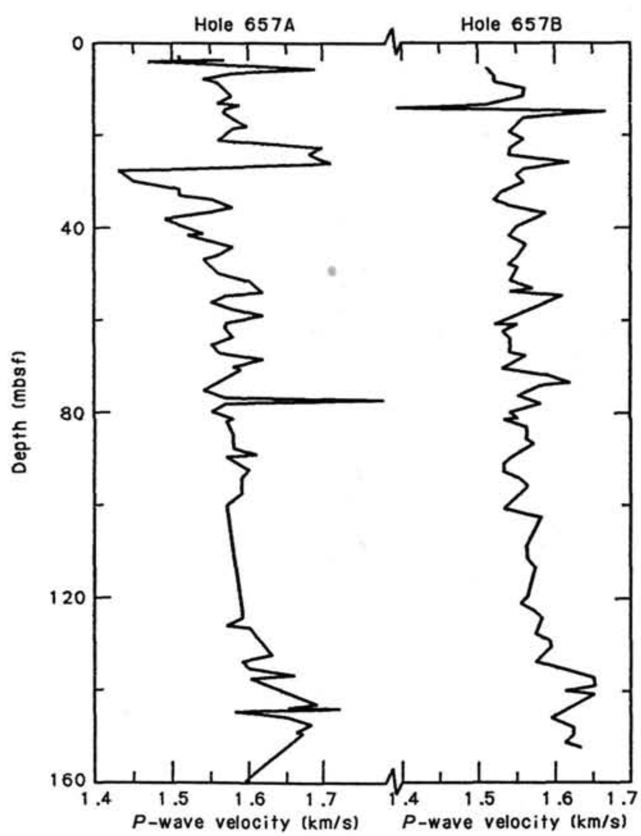

Figure 30. *P*-wave-velocity profiles for Holes 657A and 657B.

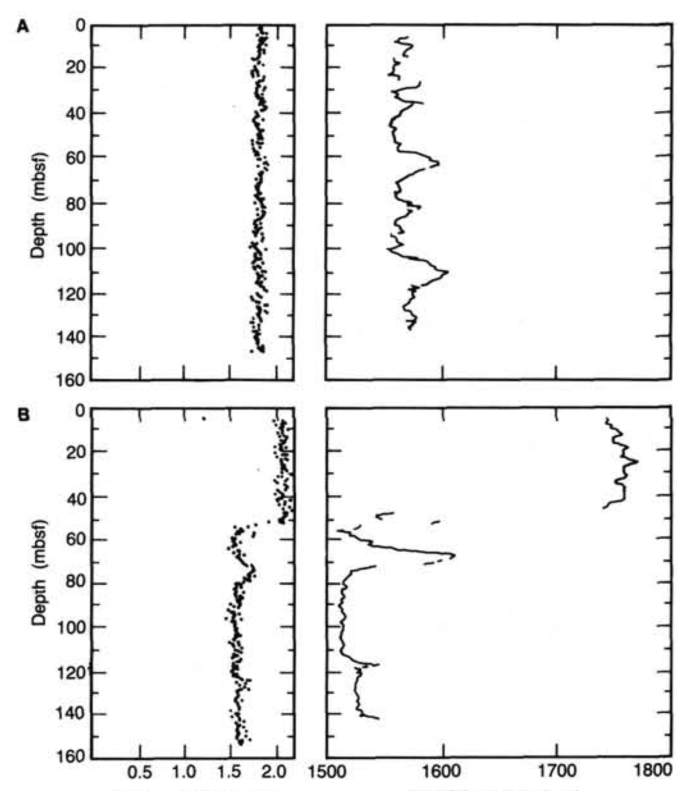

Figure 31. PWL and GRAPE examples, Sections 108-657B-15H-2 (*A*) and 108-657B-3H-2 (*B*).

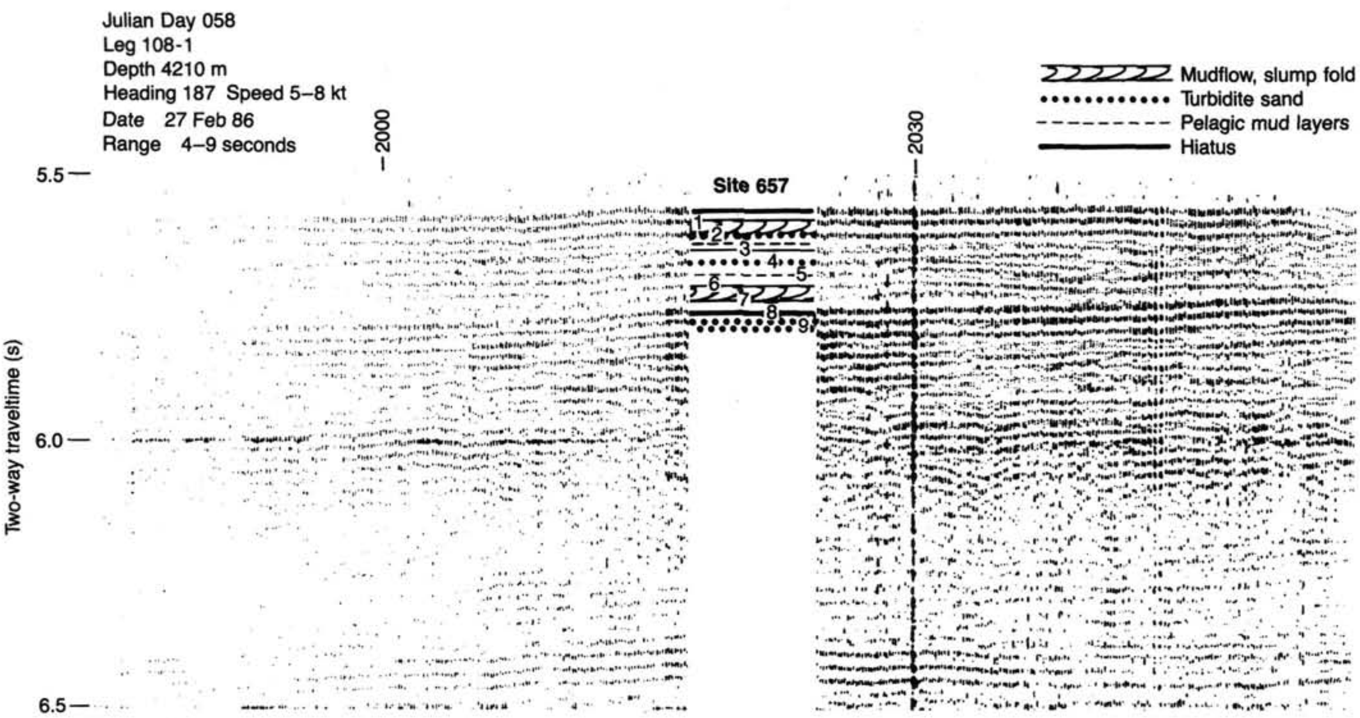

Figure 32. Interpretation of seismic line 108-1, obtained during the approach to Site 657 and recorded on the EDO 2 recorder. Numbers designate reflectors (see Table 10, this chapter).

Table 10. Seismic correlations (50 to 500 Hz), Site 657.

Reflector	Sub-bottom depth (s)	Depth (mbsf)	Source	Age (Ma)	Lithostratigraphic unit
1	0.02	15.5	Artifact		IA
					IB
2	0.045	34.6	Artifact		
2a	0.06	46.6	Turbidite sand	1.2	
3	0.07	56.0	Unknown (void in cores)	1.5	IC
4	0.095	73.8	?Turbidite sand	2.4	
5	0.12	91.7	Pelagic carbonate-poor mud	3.3	
6	0.14	108.8	Upper slump fold	3.6	
7	0.16	124.3	Base of slump fold	3.6	ID
8	0.185	143.0	Major hiatus	4.6–6.2	IE
9	0.22	161.6	Top of turbidite	8.5	II

Table 11. Summary of biostratigraphic and lithologic markers used to arrive at composite depths for Holes 657A and 657B.

Criteria	Hole 657A (depth, mbsf)	Hole 657B (depth, mbsf)	Composite depth (mbsf)
Top Zone NN19	3.5	3.3	3.5
Turbidite sand	5.7	5.2	5.5–5.7
Top thick turbidite	10.0	11.3	11.6
Top mudflow	13.1	14.9	15.2
Base mudflow	26.2	27.7	28.0
LO *Calcidiscus macintyrei*	49.8	50.2–51.0	51.2–53.0
LO *Discoaster*	59.9–60.7	59.7–60.0	63.3–63.5
D/T marker	63.4–64.25	62.0–63.0	62.6–63.3
Magnetic susceptibility	66.0	66.0	68.8
Magnetic susceptibility	69.5	69.5	73.0
Magnetic susceptibility	71.0	72.0	76.0
Base Zone PL5	82.1	78.7	83.5
Base occurrence of turbiditic sands	82.1	80.0	83.5
Top slump fold	96.5	97.7	98.0–101.3
Core slump fold	123.0	117.2	122.2–121.0
Base slump fold	124.5	120.0	123.7
Base turbidite sand	126.1	121.5	125.4
Turbidite sand	131.8	127.4	131.0–131.3
Turbidite sand	136.0	132.0	135.2–136.0
Base turbidite sand	143.5	138.7	142.8–143.3
Top brown clay	146.0	141.5	145.4
Top sand bed	159.2	154.9	159.1

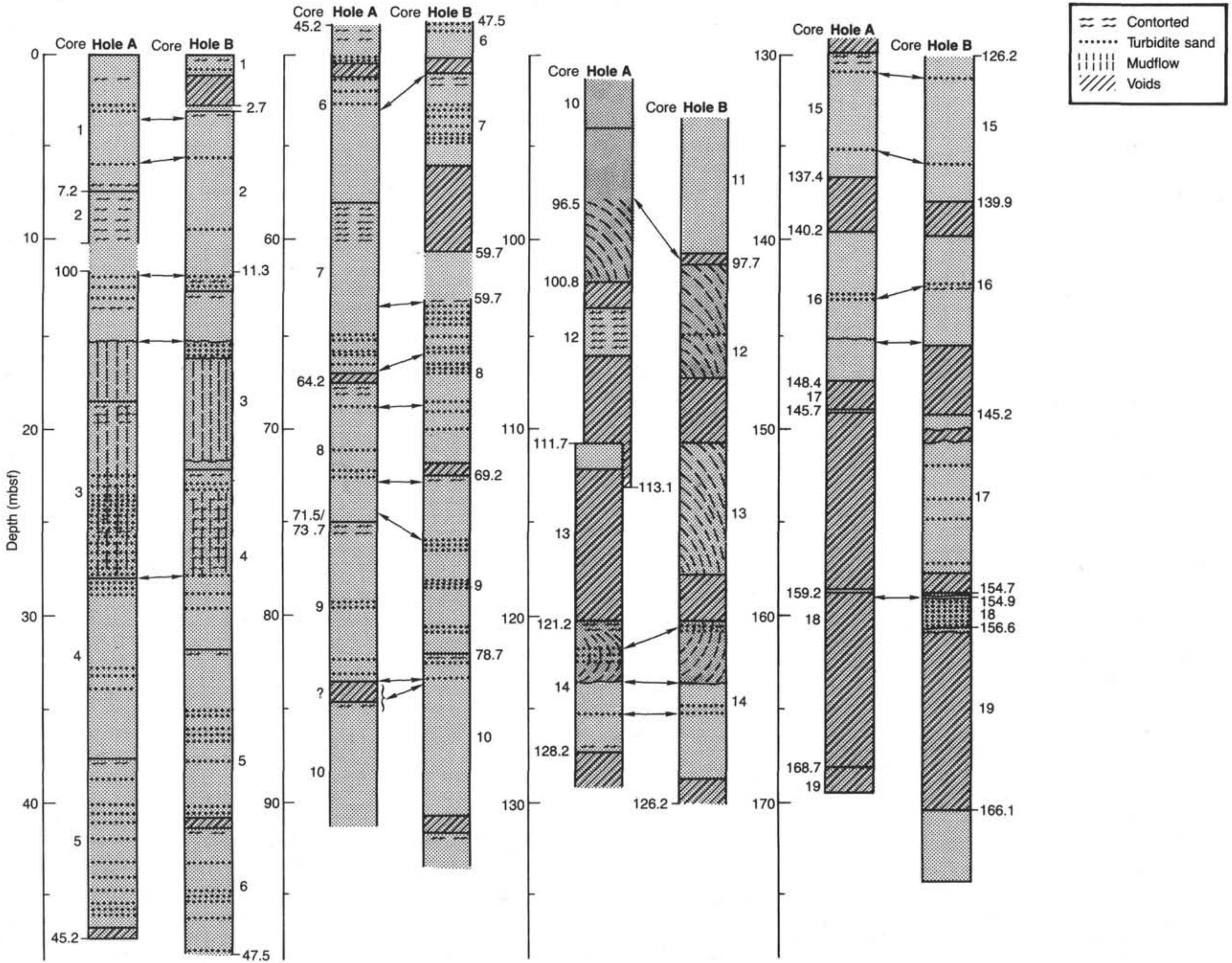

Figure 33. Composite-depth section of Site 657, Holes 657A and 657B. Composite-depth estimates at the margin, actual depth of penetration, and core numbers along the graphs of the single holes.

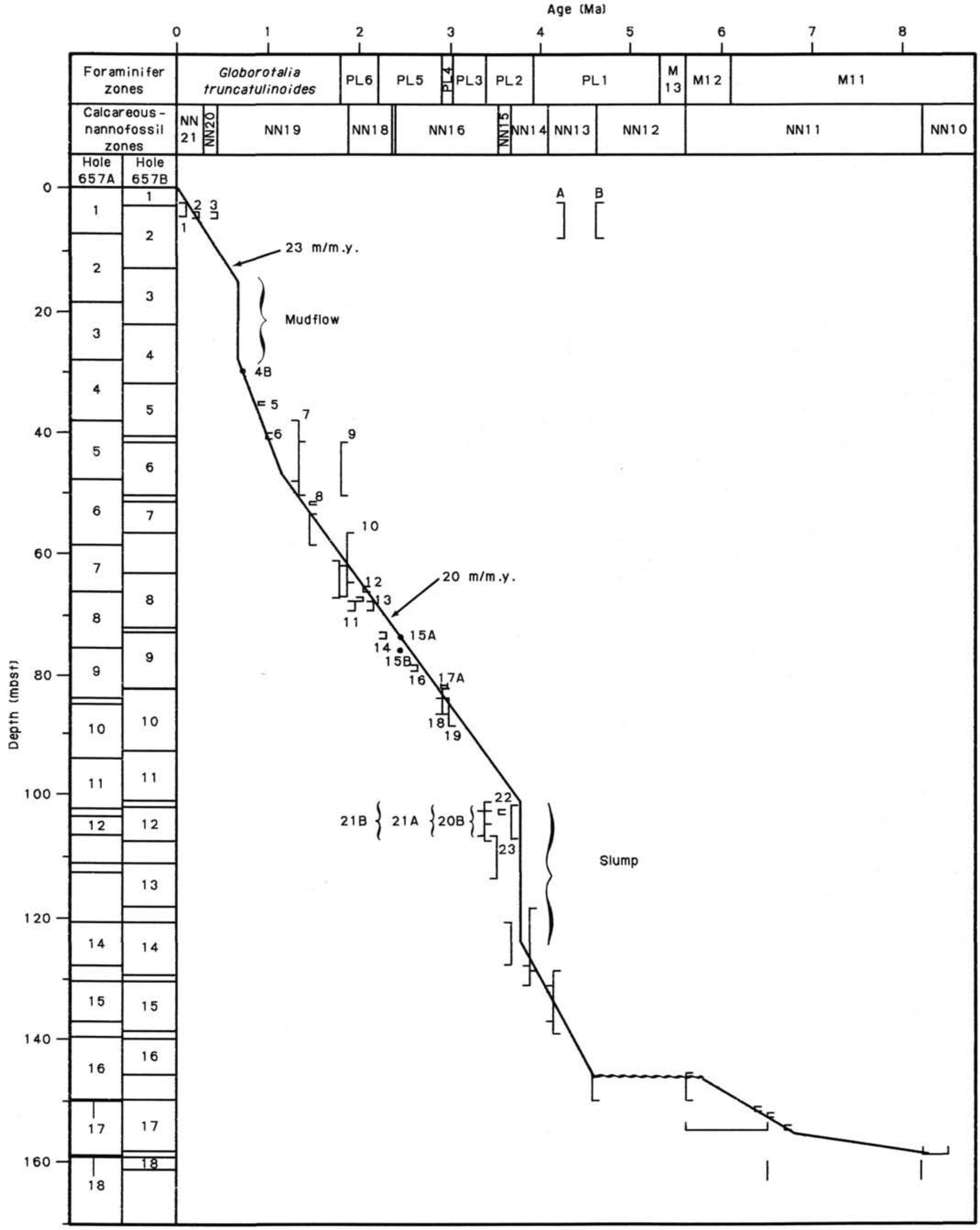

Figure 34. Age-depth section of Site 657 using biostratigraphic data from "Biostratigraphy" section (this chapter) and new composite-depth estimates.

SITE 657 HOLE A CORE 1 H CORED INTERVAL 4221.1-4228.3 mbsl; 00-7.2 mbsf

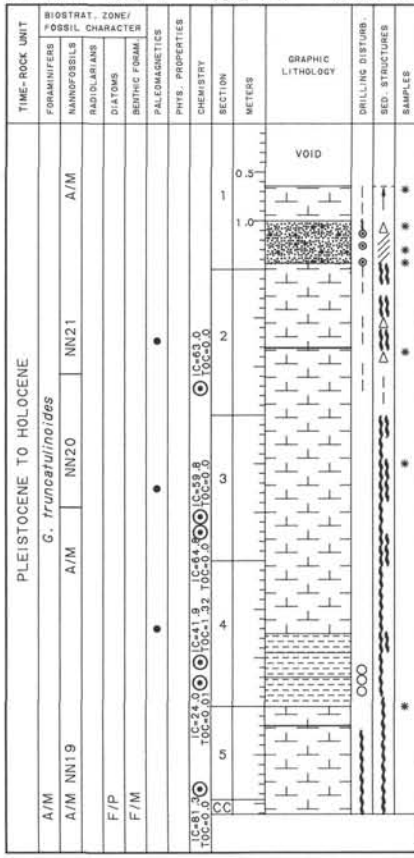

LITHOLOGIC DESCRIPTION

FORAMINIFER-BEARING NANNOFOSSIL OOZE

Foraminifer-bearing nannofossil ooze, generally pale-yellow (2.5Y 7/4), light-gray (2.5Y 7/1, 7/2), and pinkish-gray (7.5YR 6/2). Minor amounts of silt and scattered black-stained (pyritic?) foraminifers. Slightly to moderately bioturbated.

Minor lithologies: Section 1, 99–141 cm: foraminifer silty sand, greenish-gray (5GY 5/1, 6/1), graded, with low-angle cross-lamination at base. Section 2, 80 cm, and Section 5, 21 cm: silt and clay-bearing foraminifer ooze, light-gray (2.5Y 7/2). Section 4, 76–92, 99–114, and 123–147 cm: nannofossil-bearing clay, generally dusky-yellow-green (5GY 5/2) to grayish-yellow-green (5Y 7/2). Minor void in Section 2, 147–150 cm. Section 5: nannofossil ooze, generally light-gray (5Y 7/1) to light-greenish-gray (5G 7/1).

SMEAR SLIDE SUMMARY (%):

	1, 77 D	1, 110 D	1, 135 D	1, 146 D	2, 88 M	3, 53 D	5, 5 D
TEXTURE:							
Sand	60	40	70	30	60	25	5
Silt	10	30	20	20	20	20	5
Clay	30	30	10	50	20	55	90
COMPOSITION:							
Quartz	20	60	60	15	15	15	Tr
Feldspar	—	Tr	—	—	—	—	—
Clay	—	—	—	—	20	—	—
Accessory minerals	—	Tr	Tr	Tr	—	—	—
Foraminifers	30	20	30	30	60	25	10
Nannofossils	50	20	10	55	5	60	90
Sponge spicules	—	—	—	—	Tr	—	—

Chemistry: IC here refers to weight % $CaCO_3$.

SITE 657 HOLE A CORE 2 H CORED INTERVAL 4228.3-4237.8 mbsl; 7.2-16.7 mbsl

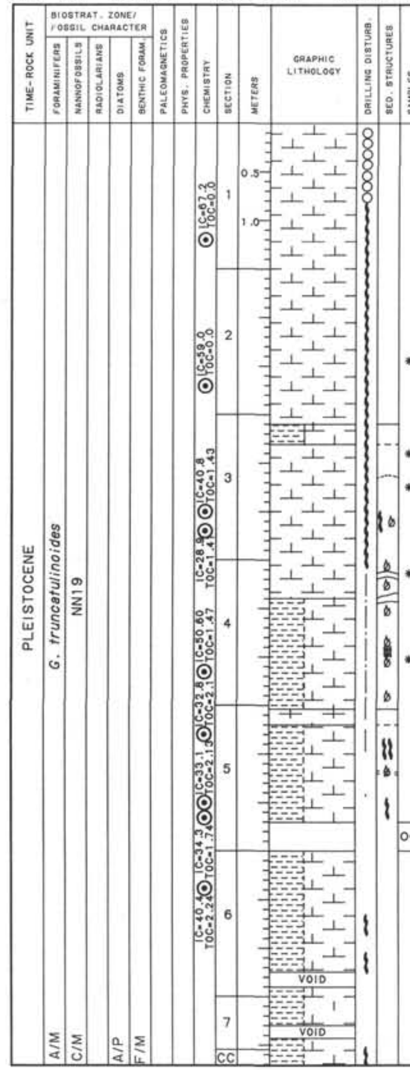

LITHOLOGIC DESCRIPTION

FORAMINIFER-BEARING NANNOFOSSIL OOZE and CLAYEY NANNOFOSSIL OOZE

Foraminifer-bearing nannofossil ooze, light-gray to greenish-gray (5GY 7/1, 5G 7/1), homogeneous, black (N2) blebs (pyrite?, Mn?).

Clayey nannofossil ooze, dark-greenish-gray to greenish-gray (10Y 4/2, 10Y 5/2), slightly to moderately bioturbated: scattered shell debris; deformed, 122-cm-thick shell-debris layers in Sections 3 and 4.

Minor lithologies: Section 3, 30–60 cm: spicule- and clay-bearing nannofossil ooze. Section 4, 28–40 cm: clay- and foraminifer-bearing nannofossil ooze. Section 5, 4–21 cm: foraminifer-nannofossil ooze, white to light-gray (2.5Y 8/0, 5Y 7/1), homogeneous.

SMEAR SLIDE SUMMARY (%):

	2, 90 D	3, 44 M	3, 77 D	4, 17 M	4, 102 M
TEXTURE:					
Sand	10	10	10	25	20
Silt	20	30	20	25	80
Clay	70	60	70	50	—
COMPOSITION:					
Quartz	Tr	10	10	10	60
Mica	—	—	—	—	Tr
Clay	—	15	30	—	10
Accessory minerals	—	—	—	—	Tr
Pyrite	—	—	Tr	Tr	Tr
Glauconite	—	—	Tr	—	Tr
Foraminifers	20	Tr	10	—	10
Nannofossils	80	50	50	70	5
Diatoms	—	—	—	Tr	—
Radiolarians	—	—	—	Tr	—
Sponge spicules	—	15	Tr	5	15
Bioclasts	—	10	—	—	—

SITE 657 HOLE A CORE 3 H CORED INTERVAL 4237.8-4247.3 mbsl; 16.7-26.2 mbsf

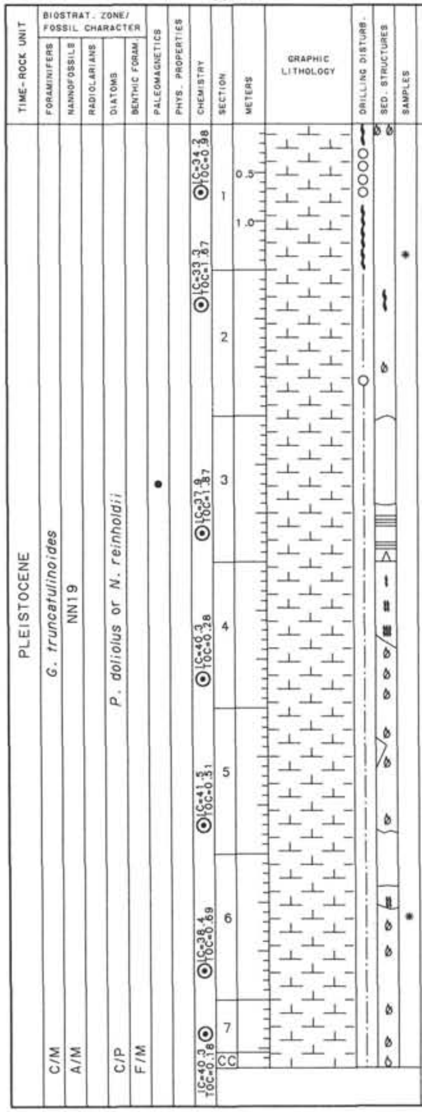

LITHOLOGIC DESCRIPTION

SILT-BEARING NANNOFOSSIL OOZE to NANNOFOSSIL OOZE

Silt-bearing nannofossil to nannofossil ooze, light-olive-gray to olive-gray (5Y 6/2 to 5Y 5/2), slightly to moderately bioturbated; interbedded with thin turbidites containing shell fragments.

SMEAR SLIDE SUMMARY (%):

	1, 130 D	3, 108 M
TEXTURE:		
Sand	20	10
Silt	20	10
Clay	60	80
COMPOSITION:		
Quartz	20	15
Foraminifers	5	5
Nannofossils	70	70
Diatoms	Tr	10
Radiolarians	—	Tr
Sponge spicules	5	Tr

SITE 657 HOLE A CORE 4 H CORED INTERVAL 4247.3-4256.8 mbsl; 26.2-35.7 mbsf

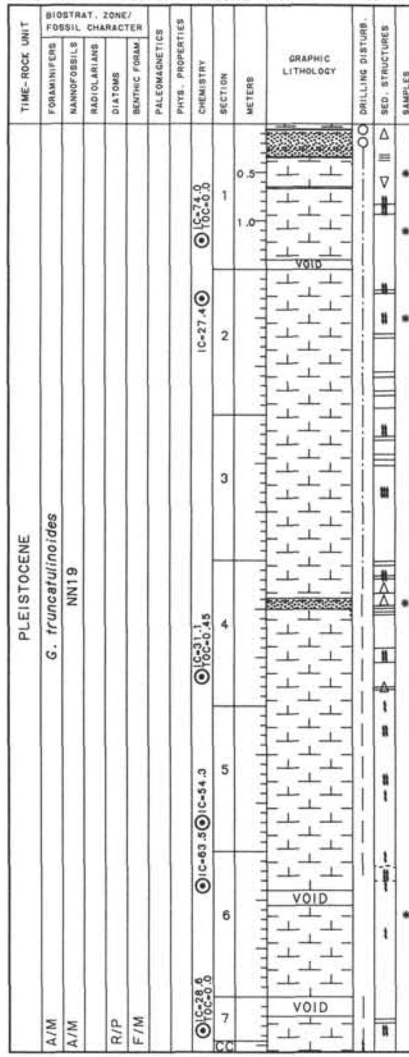

LITHOLOGIC DESCRIPTION

NANNOFOSSIL OOZE

Nannofossil ooze, white to light-gray (7.5 YR 8/0, 5Y 7/1), slightly to moderately bioturbated; thin interbedded foraminifer-bearing turbidites (in Section 1, 2–8 cm, 33–36 cm, and 60–66 cm, inverse grading!); four thin, quartz-sand turbidites in Section 4, 25 cm, 32 cm, 45 cm, and 120 cm.

SMEAR SLIDE SUMMARY (%):

	1, 50 D	1, 115 D	2, 50 D	4, 44 M	6, 75 D
TEXTURE:					
Sand	2	0	10	60	0
Silt	8	10	10	20	5
Clay	90	90	80	20	95
COMPOSITION:					
Quartz	10	10	10	60	5
Clay	5	—	—	—	—
Foraminifers	5	10	2	Tr	Tr
Nannofossils	70	80	80	40	95
Diatoms	10	Tr	3	—	Tr
Sponge spicules	—	Tr	5	Tr	Tr

SITE 657 HOLE A CORE 5 H CORED INTERVAL 4256.8-4266.3 mbsl; 35.7-45.2 mbsf

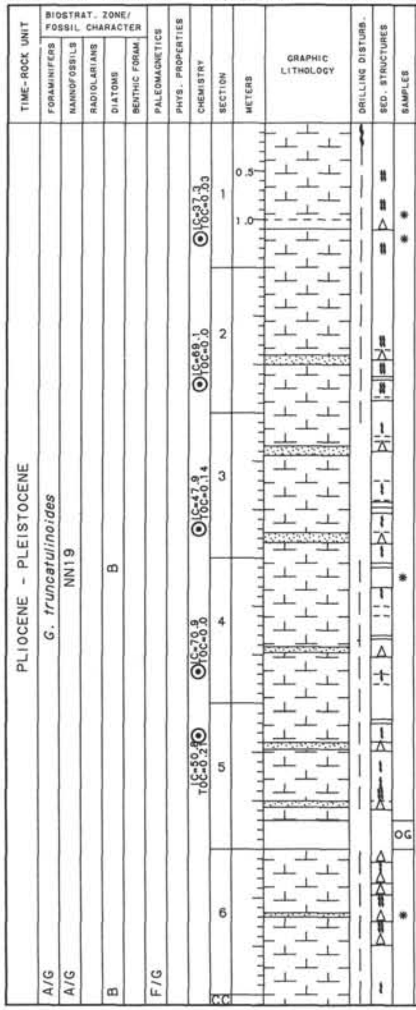

LITHOLOGIC DESCRIPTION

FORAMINIFER-BEARING NANNOFOSSIL OOZE to NANNOFOSSIL OOZE

Foraminifer-bearing nannofossil ooze to nannofossil ooze, white to light-gray (5Y 8/0, 5Y 7/1), slightly to moderately bioturbated; interbedded with thin, olive-gray to dark-gray (5Y 5/3, 5Y 4/1) quartz-silt to quartz-sand turbidites (Section 1, 110–112 cm; Section 2, 89–91 cm; Section 3, 44 and 130 cm; Section 4, 92–95 cm; Section 5, 41–43 and 100–104 cm; and Section 6, 68–70 cm).

SMEAR SLIDE SUMMARY (%):

	1, 100 D	1, 130 D	4, 30 D	6, 69 M
TEXTURE:				
Sand	10	5	5	55
Silt	10	15	5	40
Clay	80	80	90	5
COMPOSITION:				
Quartz	5	10	Tr	95
Foraminifers	10	5	10	—
Nannofossils	85	85	90	5
Diatoms	—	—	Tr	—
Sponge spicules	—	Tr	Tr	—

SITE 657 HOLE A CORE 6 H CORED INTERVAL 4266.3-4275.8 mbsl; 45.2-54.7 mbsf

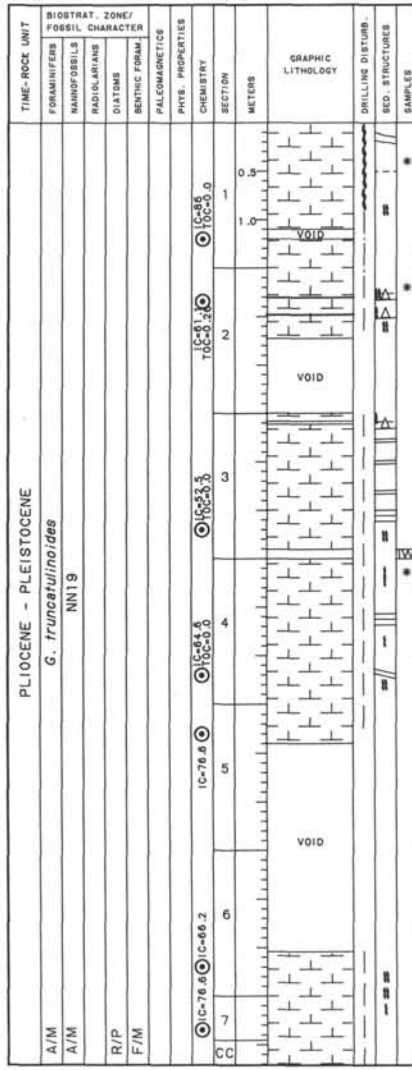

LITHOLOGIC DESCRIPTION

NANNOFOSSIL OOZE

Nannofossil ooze, white to light-gray (5Y 8/1, 5Y 7/2), slightly to moderately bioturbated; partly laminated; thin, dark-gray (5Y 4/1) quartz-sand turbidites in Section 2, 30 and 45 cm, and Section 3, 12 cm.

SMEAR SLIDE SUMMARY (%):

	1, 40 D	2, 19 D	4, 19 D
TEXTURE:			
Sand	5	0	0
Silt	5	10	10
Clay	90	90	90
COMPOSITION:			
Quartz	Tr	5	Tr
Foraminifers	5	5	5
Nannofossils	95	90	95
Sponge spicules	Tr	Tr	—

SITE 657 HOLE A CORE 7 H CORED INTERVAL 4275.8-4285.3 mbsl; 54.7-64.2 mbsf

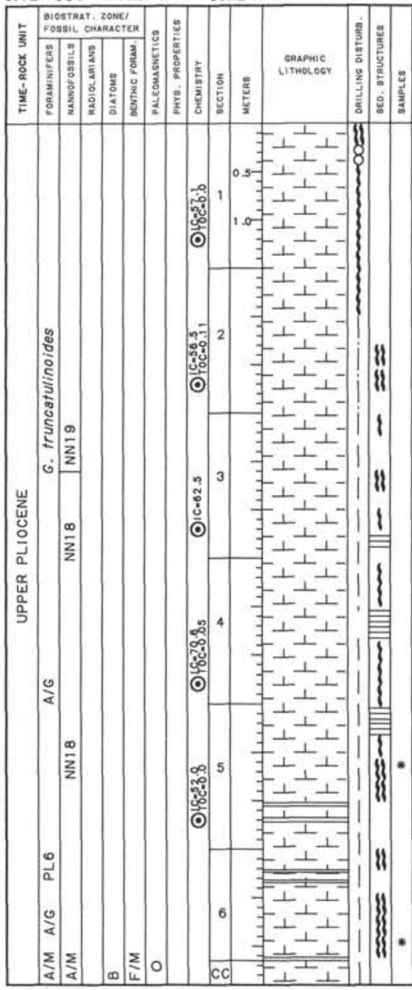

LITHOLOGIC DESCRIPTION

NANNOFOSSIL OOZE

Nannofossil ooze, generally white (7.5YR 8/0) or pale-green (5G 7/2) to light-greenish-gray (5G 7/1), distinct color laminations; rare sand-filled burrows; slightly to moderately bioturbated.

Minor lithology: Section 5, 108 and 121 cm; Section 6, 35, 43, and 116 cm: sand, light-gray (5Y 7/1) to light-olive-gray (5Y 6/2) with sharp contact at base.

SMEAR SLIDE SUMMARY (%):

	5, 66 D	6, 93 D
TEXTURE:		
Sand	0	0
Silt	10	10
Clay	90	90
COMPOSITION:		
Quartz	<5	5
Foraminifers	<5	5
Nannofossils	95	95

SITE 657 HOLE A CORE 8 H CORED INTERVAL 4285.3-4294.8 mbsl; 64.2-73.7 mbsf

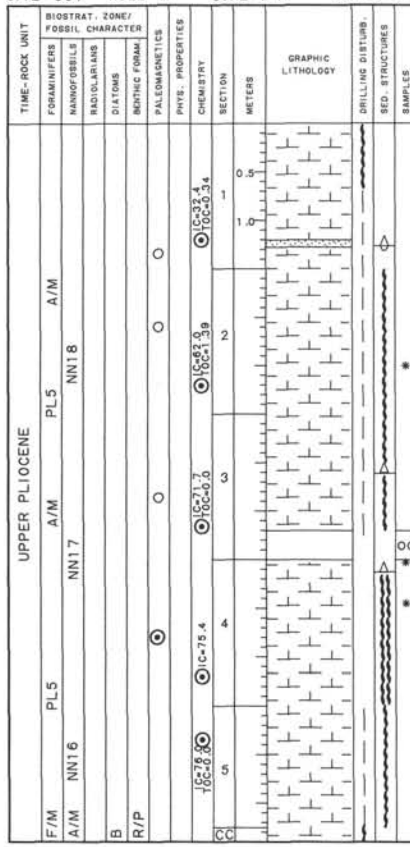

LITHOLOGIC DESCRIPTION

NANNOFOSSIL OOZE

Nannofossil ooze, generally white to light-gray or greenish-gray (5Y 8/1–6/1, 5G 6/1), color laminated; slightly to moderately bioturbated.

Minor lithology: Section 1, 121–128 cm, silty sand, olive-gray (5Y 4/2); graded, with sharp contact at base.

SMEAR SLIDE SUMMARY (%):

	2, 14 D	4, 5 M	4, 49 M
TEXTURE:			
Sand	0	0	0
Silt	2	20	20
Clay	98	80	80
COMPOSITION:			
Quartz	2	5	Tr
Foraminifers	Tr	5	5
Nannofossils	98	90	95

SITE 657 HOLE A CORE 9 H CORED INTERVAL 4294.8-4304.3 mbsl; 73.7-83.2 mbsf

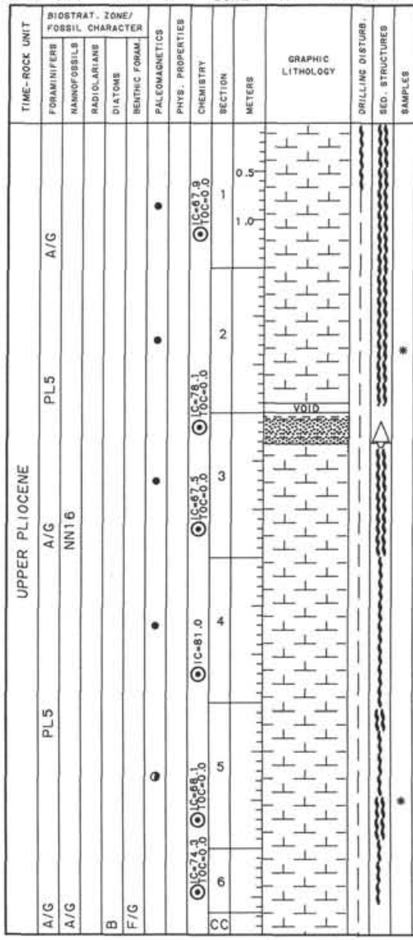

LITHOLOGIC DESCRIPTION

NANNOFOSSIL OOZE

Nannofossil ooze, generally white, light-gray to greenish-gray (5Y 8/1-6/1, 5G 6/1), color laminated; slightly to moderately bioturbated. Minor void in Section 2, 147–150 cm.

Minor lithology: Section 3, 6–33 cm: gray (5Y 6/1), graded granule sand bed; possibly a turbidite with sharp contact at base.

SMEAR SLIDE SUMMARY (%):

	2, 85 D	5, 101 M
TEXTURE:		
Sand	0	0
Silt	5	10
Clay	95	90
COMPOSITION:		
Quartz	Tr	5
Clay	—	30
Glauconite	—	5
Foraminifers	Tr	10
Nannofossils	100	50

SITE 657 HOLE A CORE 10 H CORED INTERVAL 4304.3-4313.8 mbsl; 83.2-92.7 mbsf

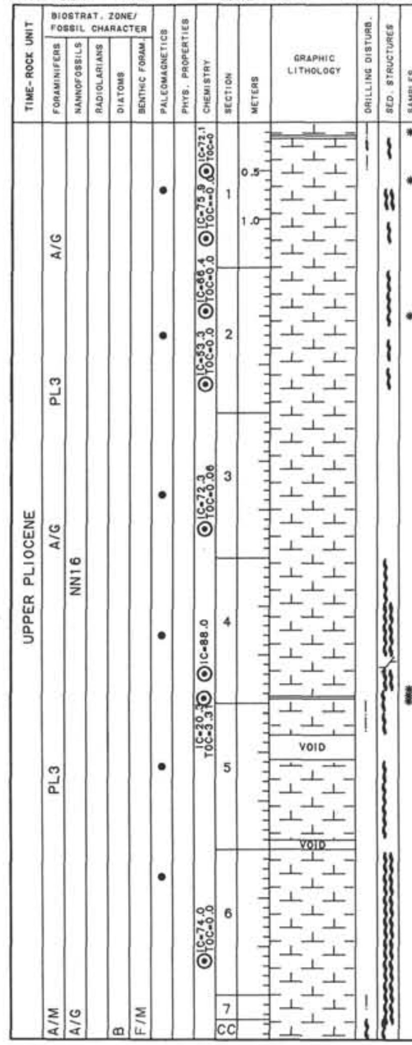

LITHOLOGIC DESCRIPTION

NANNOFOSSIL OOZE and FORAMINIFER-BEARING NANNOFOSSIL OOZE

Nannofossil and foraminifer-bearing nannofossil ooze, generally white, light-gray, or light-greenish-gray (5Y 8/1–6/1, 5GY 7/1), color laminated; slightly to moderately bioturbated.

Minor lithology: Section 1, 56 cm: minor amounts of silt; Section 4, 144 cm: major amounts of silty clay. Minor voids occur in Section 1, 17–20 cm and Section 4, 146–150 cm.

SMEAR SLIDE SUMMARY (%):

	1, 9 D	1, 56 M	2, 45 M	4, 130 D	4, 138 M	4, 144 M
TEXTURE:						
Sand	5	—	5	10	—	—
Silt	20	20	15	10	10	20
Clay	75	80	80	80	90	80
COMPOSITION:						
Quartz	10	15	Tr	Tr	Tr	15
Clay	—	—	—	—	—	15
Foraminifers	15	5	15	20	10	Tr
Nannofossils	75	80	85	80	90	70
Bioclasts	Tr	—	—	—	—	—

SITE 657 HOLE A CORE 11 H CORED INTERVAL 4313.8-4323.3 mbsl; 92.7-102.2 mbsf

TIME-ROCK UNIT: UPPER PLIOCENE

BIOSTRAT. ZONE/FOSSIL CHARACTER: FORAMINIFERS: PL3, A/M; NANNOFOSSILS: NN16, A/M; BENTHIC FORAM.: B; F/M

CHEMISTRY: IC=77.2 TOC=0.0; IC=61.9 TOC=0.0; IC=77.7 TOC=0.0; IC=80.9 TOC=0.0; IC=73.9

SECTION: 1, 2, 3, 4, 5, 6, CC

METERS: 0.5, 1.0

SAMPLES: IW, OG

LITHOLOGIC DESCRIPTION

FORAMINIFER-BEARING NANNOFOSSIL OOZE

Foraminifer-bearing nannofossil ooze, generally white (5Y 8/1), light-gray to light-greenish-gray (5Y 7/1, 5GY 7/1), or light-olive-gray (5Y 6/2) color-graded units; scattered black foraminifer tests throughout; slightly to moderately bioturbated.

SMEAR SLIDE SUMMARY (%):

	1, 122 D	1, 20 D	2, 12 D	5, 41 M	5, 48 D	6, 38 D
TEXTURE:						
Sand	—	—	—	5	15	5
Silt	20	20	30	10	10	15
Clay	80	80	70	85	75	80
COMPOSITION:						
Quartz	Tr	Tr	10	10	5	10
Foraminifers	5	10	10	10	25	10
Nannofossils	95	90	80	80	70	80

SITE 657 HOLE A CORE 12 H CORED INTERVAL 4323.3-4332.8 mbsl; 102.7-111.7 mbsf

TIME-ROCK UNIT: LOWER PLIOCENE

BIOSTRAT. ZONE/FOSSIL CHARACTER: FORAMINIFERS: PL2, A/M; NANNOFOSSILS: NN16, A/M; DIATOMS: B; BENTHIC FORAM.: F/M

SECTION: 1, 2, CC

METERS: 0.5, 1.0

GRAPHIC LITHOLOGY: VOID

LITHOLOGIC DESCRIPTION

NANNOFOSSIL OOZE

Nannofossil ooze, generally white (5Y 8/1) or light-gray (5Y 7/1, 7/2); core badly disturbed; slight bioturbation rarely apparent.

SITE 657 HOLE A CORE 13 H CORED INTERVAL 4332.8-4342.3 mbsl; 111.7-121.2 mbsf

TIME-ROCK UNIT: LOWER PLIOCENE

BIOSTRAT. ZONE/FOSSIL CHARACTER: FORAMINIFERS: PL2, A/G; NANNOFOSSILS: NN15, A/M; DIATOMS: R/P; BENTHIC FORAM.: F/M

SECTION: 1, 2, CC

METERS: 0.5, 1.0

GRAPHIC LITHOLOGY: VOID, VOID

LITHOLOGIC DESCRIPTION

NANNOFOSSIL OOZE

Nannofossil ooze, generally light-gray (5Y 7/1), light-greenish-gray (5GY 7/1), or pale-yellowish-green (5GY 7/2) in color; scattered black-stained foraminifer tests. Core badly disturbed by drilling.

Minor lithology: Section 1, 40–46 cm: silty quartz sand, light-olive-green (5Y 6/2).

SMEAR SLIDE SUMMARY (%):

	1, 46 M
TEXTURE:	
Sand	60
Silt	25
Clay	15
COMPOSITION:	
Quartz	60
Feldspar	Tr
Clay	15
Pyrite	Tr
Foraminifers	15
Nannofossils	10

SITE 657 HOLE A CORE 14 H CORED INTERVAL 4342.3-4351.8 mbsl; 121.2-130.7 mbsf

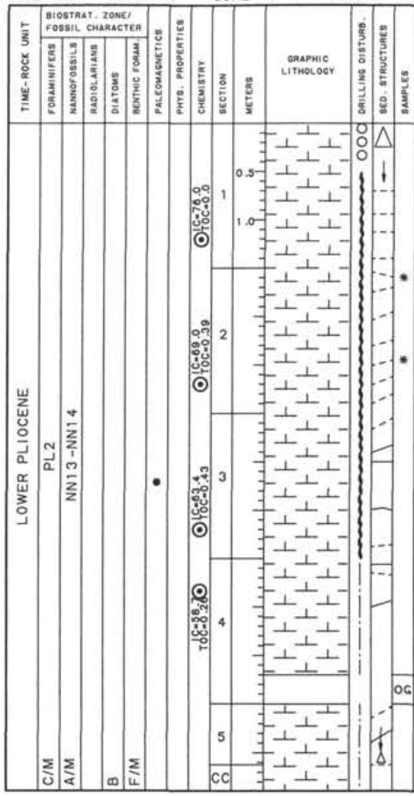

LITHOLOGIC DESCRIPTION

Repeated 3–20-cm-thick cycles of SILT-BEARING FORAMINIFER-BEARING NANNOFOSSIL OOZE, grading upward to FORAMINIFER-BEARING NANNOFOSSIL OOZE

Silt-bearing, foraminifer-bearing nannofossil ooze, generally light-greenish-gray (5GY 7/1) with minor amounts of sand in some cycles; foraminifer-bearing nannofossil ooze, generally light-gray (5Y 7/1) in color.

Both lithologies contain scattered black-stained foraminifer tests.

SMEAR SLIDE SUMMARY (%):

	2, 94 D	2, 10 D
TEXTURE:		
Sand	—	35
Silt	20	15
Clay	80	50
COMPOSITION:		
Quartz	5	15
Foraminifers	5	25
Nannofossils	90	60

SITE 657 HOLE A CORE 15 H CORED INTERVAL 4351.8-4361.3 mbsl; 130.7-140.2 mbsf

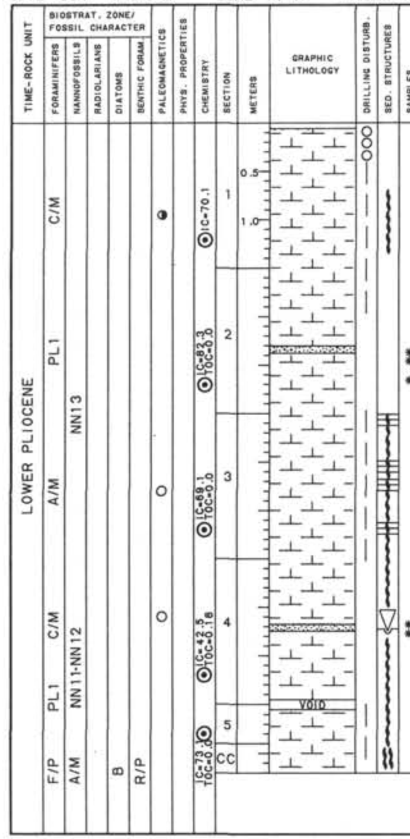

LITHOLOGIC DESCRIPTION

NANNOFOSSIL OOZE

Nannofossil ooze, generally alternating cycles of light-gray (5Y 7/1) with white (5Y 8/1) sediment, some dark-greenish-gray (5GY 4/1) foraminifer-rich sediment; darker sediment commonly grades into lighter units. Darker units often contain minor amounts of silt, clay, and spicules; lighter units usually contain minor amounts of foraminifers; scattered black-stained foraminifer tests common throughout; sediment slightly to moderately bioturbated.

Minor lithology: Section 2, 88–90 cm and Section 4, 73–76 cm: dark-greenish-gray (5GY 4/1) silty sand with reverse-graded bed and sharp bottom contact. Minor void in Section 4, 148–150 cm.

SMEAR SLIDE SUMMARY ():

	2, 80 D	2, 90 M	2, 117 D	4, 73 M	4, 76 M
TEXTURE:					
Sand	—	40	—	40	30
Silt	15	30	10	30	10
Clay	85	30	90	30	60
COMPOSITION:					
Quartz	15	50	Tr	70	50
Rock Fragments	—	—	—	10	5
Clay	—	10	—	—	—
Foraminifers	—	—	10	Tr	5
Nannofossils	85	30	90	20	40
Sponge Spicules	—	10	—	—	—

SITE 657 HOLE A CORE 16 H CORED INTERVAL 4361.3-4370.8 mbsl; 140.2-149.7 mbsf

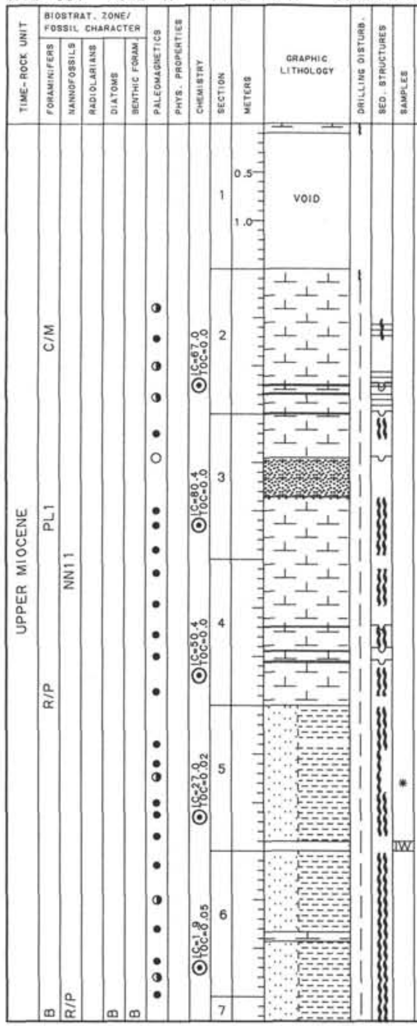

LITHOLOGIC DESCRIPTION

NANNOFOSSIL OOZE and NANNOFOSSIL-BEARING SILTY CLAY

Nannofossil ooze, generally white, light-gray, or gray (7.5YR 8/0, 7/0, 6/0, 10YR 7/2); slightly to moderately bioturbated.

Nannofossil-bearing silty clay, generally gray (N6), light-gray (5Y 7/1), olive (5Y 7/3), light-olive-brown (2.5Y 5/4), or light-reddish-brown (5YR 6/3); slightly to moderately bioturbated.

Minor lithology: Section 2, 120, 126, and 150 cm; Section 3, 45–83 cm; and Section 4, 70, 97, and 107 cm: sand, possibly turbidite with sharp contact at base.

SMEAR SLIDE SUMMARY (%):

	5, 70 D
TEXTURE:	
Sand	—
Silt	40
Clay	60
COMPOSITION:	
Quartz	30
Rock Fragments	5
Clay	50
Nannofossils	15

SITE 657 HOLE A CORE 17 X CORED INTERVAL 4370.8-4380.3 mbsl; 149.7-159.2 mbsf

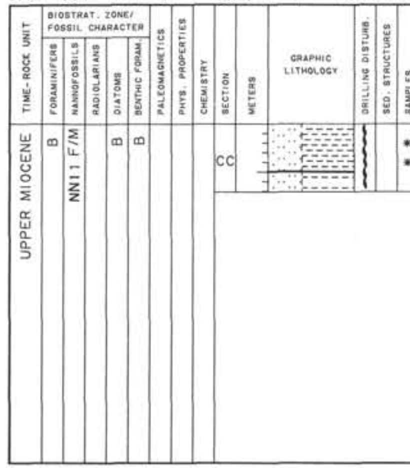

LITHOLOGIC DESCRIPTION

NANNOFOSSIL-BEARING SILTY CLAY

Nannofossil-bearing silty clay, olive-gray (5Y 4/2) to gray (10Y 5/1); core badly disturbed.

Minor lithology: CC, 50 cm: quartz sand layer, dark-gray (7.5YR 4/0).

SMEAR SLIDE SUMMARY (%):

	CC, 25 D	CC, 45 M
TEXTURE:		
Sand	—	70
Silt	20	25
Clay	80	5
COMPOSITION:		
Quartz	30	80
Feldspar	—	Tr
Rock Fragments	—	20
Clay	60	—
Nannofossils	10	Tr

SITE 657 HOLE A CORE 18 X CORED INTERVAL 4380.3-4389.8 mbsl; 4389.8 mbsf

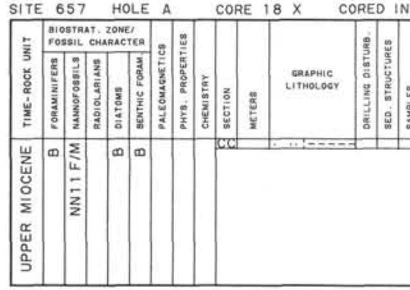

LITHOLOGIC DESCRIPTION

NANNOFOSSIL-BEARING SILTY CLAY

Nannofossil-bearing silty clay, olive-gray (5Y 4/2); badly disturbed by drilling.

SITE 657 HOLE A CORE 19 X CORED INTERVAL 4389.8-4399.3 mbsl; 168.7-178.2 mbsf

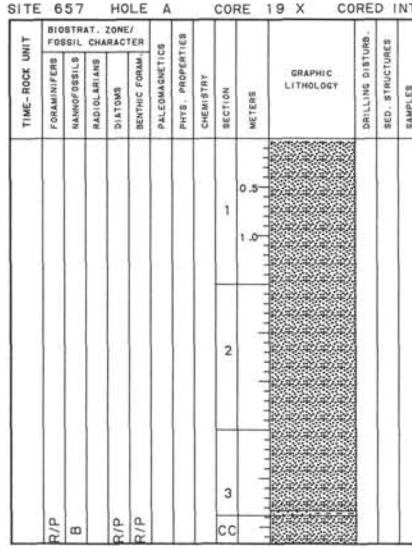

LITHOLOGIC DESCRIPTION

SAND

Sand, dark-gray (5Y 4/1); quartzose.

Minor lithology: Section 3, 84–88 cm: silty clay, grayish-brown (2Y 5/2).

SITE 657 HOLE B CORE 1 H CORED INTERVAL 4221.1-4223.8 mbsl; 0-2.7 mbsf

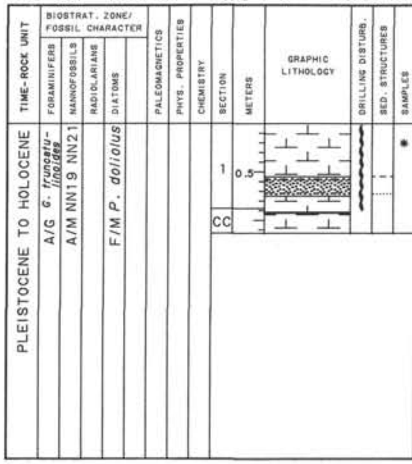

LITHOLOGIC DESCRIPTION

FORAMINIFER-BEARING NANNOFOSSIL OOZE

Foraminifer-bearing nannofossil ooze, light-gray (5Y 7/1), quite disturbed by drilling.

Minor lithology: Section 1, 61–83 cm and CC, 0–5 cm, dark-gray (5Y 4/1) silty clay.

SMEAR SLIDE SUMMARY (%):

	1, 29 D
TEXTURE:	
Sand	—
Silt	10
Clay	90
COMPOSITION:	
Quartz	Tr
Foraminifers	10
Nannofossils	90

SITE 657 HOLE B CORE 2 H CORED INTERVAL 4223.8-4233.3 mbsl; 2.7-12.2 mbsf

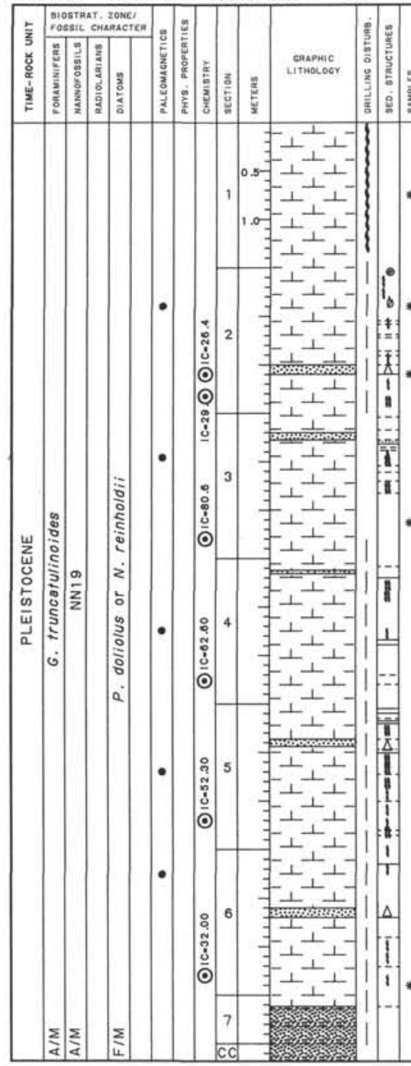

LITHOLOGIC DESCRIPTION

NANNOFOSSIL OOZE and FORAMINIFER-BEARING NANNOFOSSIL OOZE

Nannofossil ooze and foraminifer-bearing nannofossil ooze, generally white to light-gray (5Y 7/1); minor to moderate bioturbation.

Minor lithologies: Section 3, 28-29 cm; Section 4, 12–19 cm; Section 5, 47–51 cm; and Section 6, 57–59 cm: quartz sand turbidites, light-gray or greenish-gray (5GY 4/1, 5Y 4/1). Section 7, 18–50 cm: foraminifer-bearing silty sand containing shell fragments at base.

SMEAR SLIDE SUMMARY (%):

	1, 80 D	2, 40 D	2, 110 M	3, 130 D	6, 130 M
TEXTURE:					
Sand	5	5	60	5	10
Silt	10	10	30	10	10
Clay	85	85	10	85	80
COMPOSITION:					
Quartz	5	10	85	Tr	10
Feldspar	—	—	Tr	—	—
Rock Fragments	—	—	3	—	Tr
Clay	5	10	—	—	—
Glauconite	—	—	—	—	5
Foraminifers	5	5	2	5	Tr
Nannofossils	85	75	10	95	80

SITE 657 HOLE B CORE 3 H CORED INTERVAL 4233.3-4242.8 mbsl; 12.2-21.7 mbsf

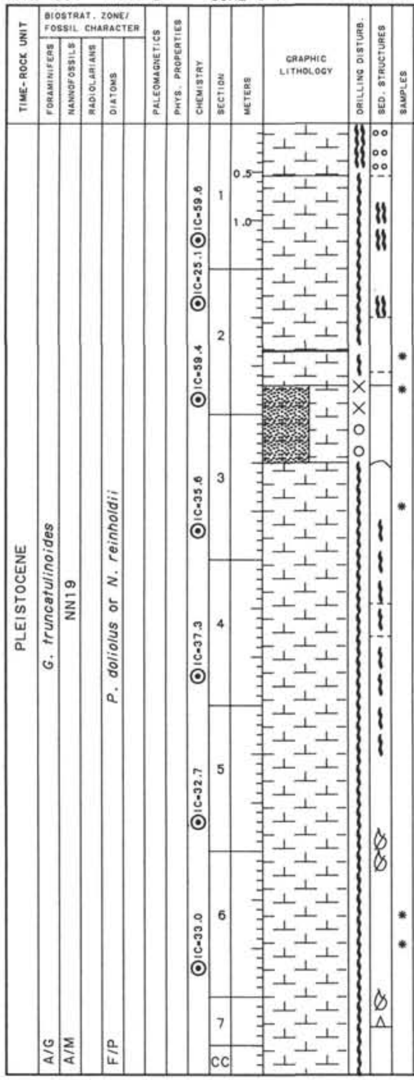

LITHOLOGIC DESCRIPTION

NANNOFOSSIL OOZE and FORAMINIFER-BEARING NANNOFOSSIL OOZE

Nannofossil ooze and foraminifer-bearing nannofossil ooze, light-gray (10Y 5/2); moderate bioturbation and drilling disturbance.

Minor lithology: Section 1, 0–55 cm; Section 2, 120 cm; Section 3, 50 cm: drilling breccia of nannofossil ooze and quartz sand. Minor void in Section 2, 80–85 cm.

SMEAR SLIDE SUMMARY (%):

	2, 90 D	2, 125 M	3, 92 D	6, 67 D	6, 90 D
TEXTURE:					
Sand	5	60	—	5	5
Silt	10	20	40	35	35
Clay	85	20	60	60	60
COMPOSITION:					
Quartz	5	30	10	10	20
Feldspar	—	Tr	—	—	—
Mica	—	10	Tr	Tr	Tr
Accessory Minerals	Tr	Tr	—	—	Tr
Foraminifers	15	10	5	10	10
Nannofossils	80	10	60	60	50
Diatoms	—	—	10	—	—
Radiolarians	—	—	Tr	—	—
Sponge Spicules	Tr	—	15	15	20
Bioclasts	—	40	—	—	—

SITE 657 HOLE B CORE 4 H CORED INTERVAL 4242.8-4252.3 mbsl; 21.7-31.2 mbsf

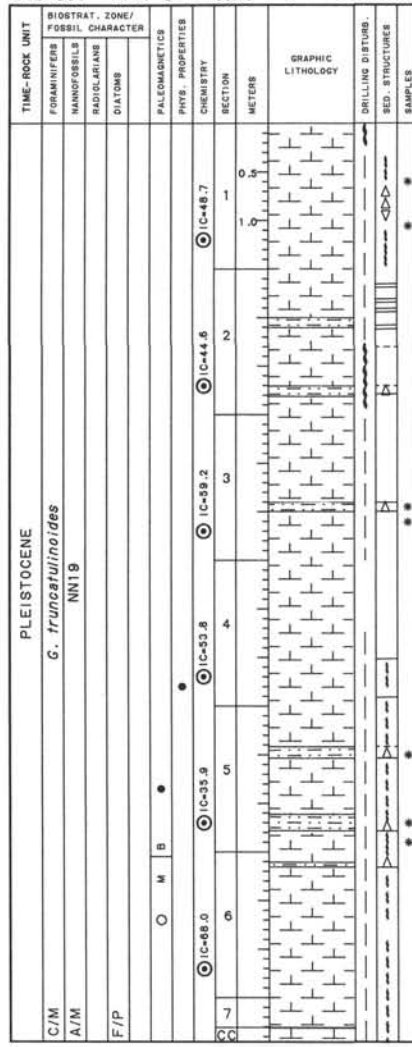

LITHOLOGIC DESCRIPTION

NANNOFOSSIL OOZE and FORAMINIFER-BEARING NANNOFOSSIL OOZE

Nannofossil ooze and foraminifer-bearing nannofossil ooze, light-gray to white (5Y 7/1 to 5Y 8/0) with minor to moderate bioturbation.

Minor lithology: Section 2, 55–62 and 121–132 cm; Section 3, 96–100 cm; Section 5, 41–52 and 111–124 cm; and Section 6, 10–15 cm: interbedded quartz-silt and quartz-clay sequences with graded bedding (turbidites), light-gray to greenish-gray (5Y 6/2, 5GY 6/2).

SMEAR SLIDE SUMMARY (%):

	1, 65 M	1, 118 M	3, 100 M	3, 105 D	5, 53 M	5, 125 M	5, 130 M
TEXTURE:							
Sand	30	—	10	10	15	5	30
Silt	30	40	30	10	45	45	30
Clay	40	60	60	80	40	50	40
COMPOSITION:							
Quartz	30	20	5	Tr	30	15	35
Feldspar	—	—	—	—	—	Tr	—
Mica	—	—	—	—	Tr	5	Tr
Accessory Minerals	—	—	—	—	5	Tr	Tr
Glauconite	—	—	—	—	—	Tr	Tr
Foraminifers	30	5	25	15	15	10	15
Nannofossils	40	60	70	55	40	50	40
Sponge Spicules	—	15	—	—	15	15	10

SITE 657 HOLE B CORE 5 H CORED INTERVAL 4252.3-4261.8 mbsl; 31.2-40.7 mbsf

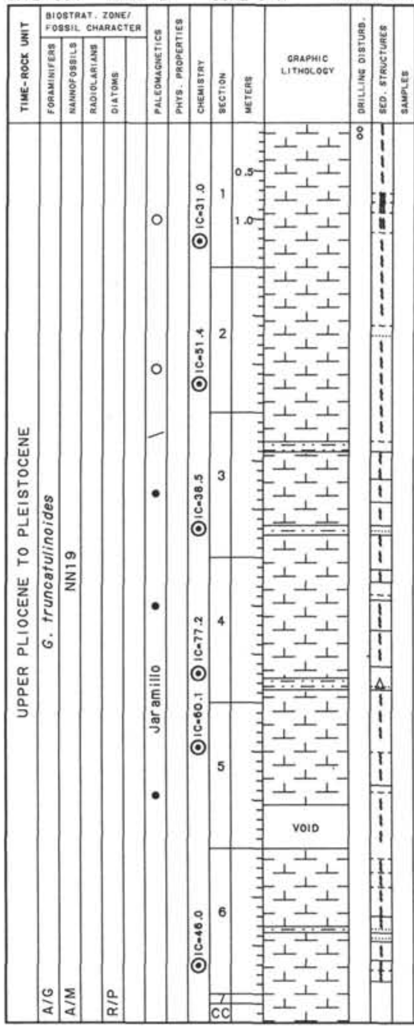

LITHOLOGIC DESCRIPTION

NANNOFOSSIL OOZE and FORAMINIFER-BEARING NANNOFOSSIL OOZE

Nannofossil ooze and foraminifer-bearing nannofossil ooze, light-gray to white (5Y 7/1, 5Y 8/0) with minor to moderate bioturbation.

Minor lithology: *Section 3, 40 and 125 cm; Section 4, 130 cm;* and *Section 6,* 80 and 90 cm: interbedded quartz-silt and quartz-clay sequences with graded bedding (turbidites), light-gray to greenish-gray (5Y 6/2, 5GY 6/2).

SITE 657 HOLE B CORE 6 H CORED INTERVAL 4261.8-4271.3 mbsl; 40.7-50.2 mbsf

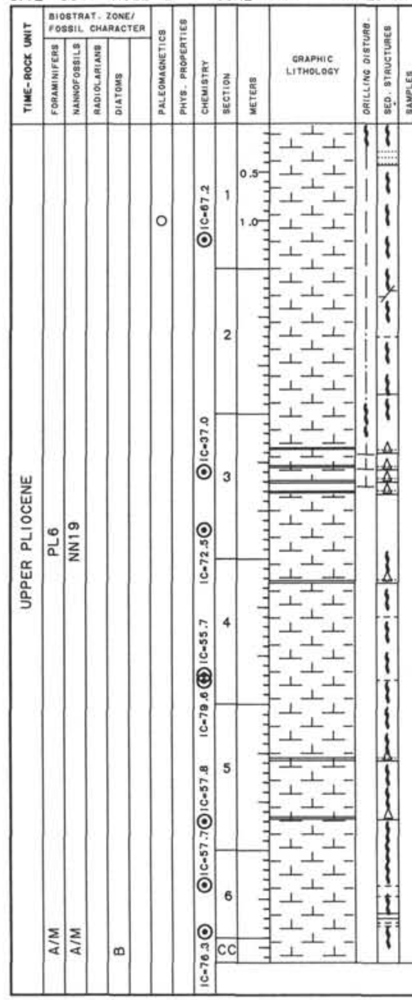

LITHOLOGIC DESCRIPTION

NANNOFOSSIL OOZE and FORAMINIFER-BEARING NANNOFOSSIL OOZE

Nannofossil ooze and foraminifer-bearing nannofossil ooze, light-gray to white (5Y 7/1, 5Y 8/0) with minor to moderate bioturbation.

Minor lithology: Section 3, 43, 55, 68, and 85 cm; Section 4, 27 cm; and Section 5, 65, 84, and 119 cm; interbedded quartz-silt and quartz-clay sequences with graded bedding (turbidites), light-gray to greenish-gray (5Y 6/2, 5GY 6/2).

SITE 657 HOLE B CORE 7 H CORED INTERVAL 4271.3-4280.8 mbsl; 50.2-59.7 mbsf

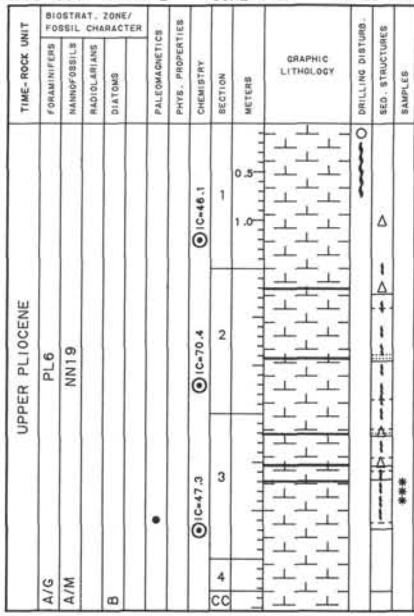

LITHOLOGIC DESCRIPTION

NANNOFOSSIL OOZE and FORAMINIFER-BEARING NANNOFOSSIL OOZE

Nannofossil ooze and foraminifer-bearing nannofossil ooze, light-gray to white (5Y 7/1, 5Y 8/0) with minor to moderate bioturbation.

Minor lithology: Section 2, 26 and 98 cm; Section 3, 27, 53 and 72 cm; interbedded quartz-silt and quartz-clay sequences with graded bedding (turbidites), light-gray to greenish-gray (5Y 6/2, 5GY 6/2).

SMEAR SLIDE SUMMARY (%):

	3, 75 M	3, 85 M	3, 90 M
TEXTURE:			
Sand	—	40	—
Silt	10	40	30
Clay	90	20	70
COMPOSITION:			
Quartz	10	65	15
Foraminifers	5	10	15
Nannofossils	85	20	70
Sponge spicules	—	5	—

SITE 657 HOLE B CORE 8 H CORED INTERVAL 4280.8-4290.3 mbsl; 59.7-69.2 mbsf

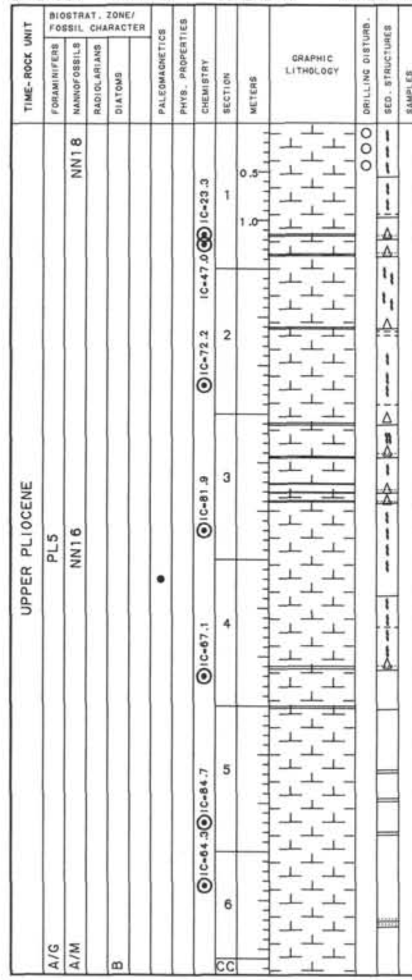

LITHOLOGIC DESCRIPTION

NANNOFOSSIL OOZE and FORAMINIFER-BEARING NANNOFOSSIL OOZE

Nannofossil ooze and foraminifer-bearing nannofossil ooze, light-gray to white (5Y 7/1, 5Y 8/0) with minor to moderate bioturbation.

Minor lithology: Section 1, 120 and 135 cm; Section 2, 63 cm; and Section 3, 13, 45, 70, 80 and 90 cm; interbedded quartz-silt and quartz-clay sequences with graded bedding, light-gray to greenish-gray (5Y 6/2, 5GY 6/2).

SITE 657 HOLE B CORE 9 H CORED INTERVAL 4290.3-4299.8 mbsl; 69.2-78.7 mbsf

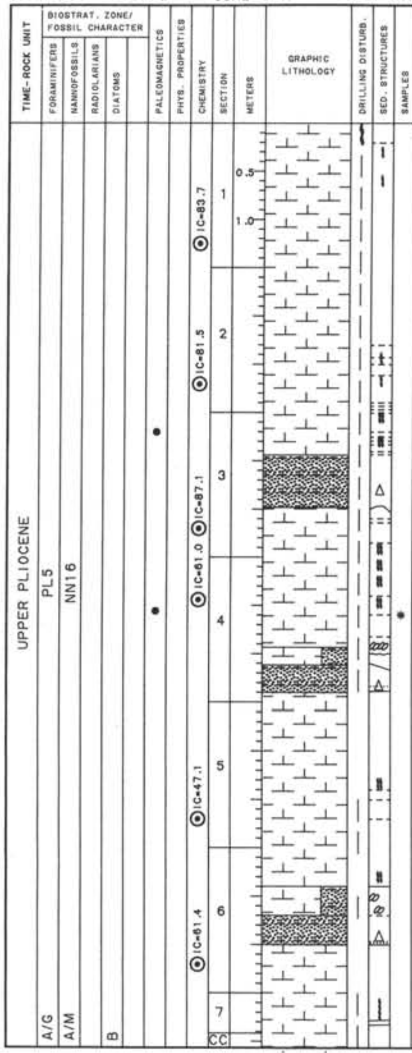

LITHOLOGIC DESCRIPTION

NANNOFOSSIL OOZE

Nannofossil ooze, generally white, light-gray or light-grayish-green (5Y 8/0, 5Y 7/1, 5GY 7/1); moderately bioturbated.

Minor lithologies: Section 3, 45–100 cm; Section 4, 114–141 cm; Section 6, 70–101 cm; quartz-sand turbidites. Section 4, 94–109 cm; Section 6, 44–70 cm; nannofossil ooze "biscuits" in shell-bearing quartz-sand.

SMEAR SLIDE SUMMARY (%):

	4, 60 D
TEXTURE:	
Sand	2
Silt	3
Clay	95
COMPOSITION:	
Quartz	3
Foraminifers	2
Nannofossils	95

SITE 657 HOLE B CORE 10 H CORED INTERVAL 4299.8-4309.3 mbsl; 78.7-88.2 mbsf

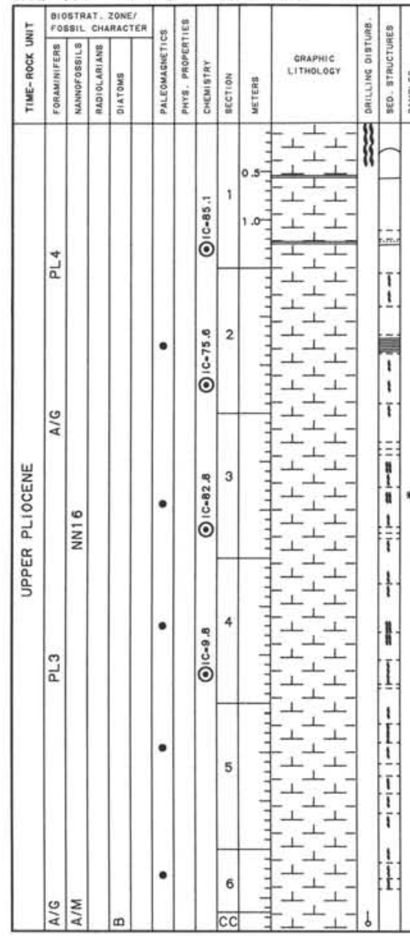

LITHOLOGIC DESCRIPTION

FORAMINIFER-BEARING NANNOFOSSIL OOZE to NANNOFOSSIL OOZE

Foraminifer-bearing nannofossil ooze to nannofossil ooze, light-gray (7.5YR 8/0, 7.5YR 7/1), slightly bioturbated; interbedded with sandy quartz turbidites in Section 1, 55 and 120 cm.

SMEAR SLIDE SUMMARY (%):

	3, 100 D	5, 50 D
TEXTURE:		
Sand	2	2
Silt	8	8
Clay	90	90
COMPOSITION:		
Quartz	5	2
Clay	—	3
Glauconite	—	3
Foraminifers	5	2
Nannofossils	90	90

SITE 657 HOLE B CORE 11 H CORED INTERVAL 4309.3-4318.8 mbsl; 88.2-97.7 mbsf

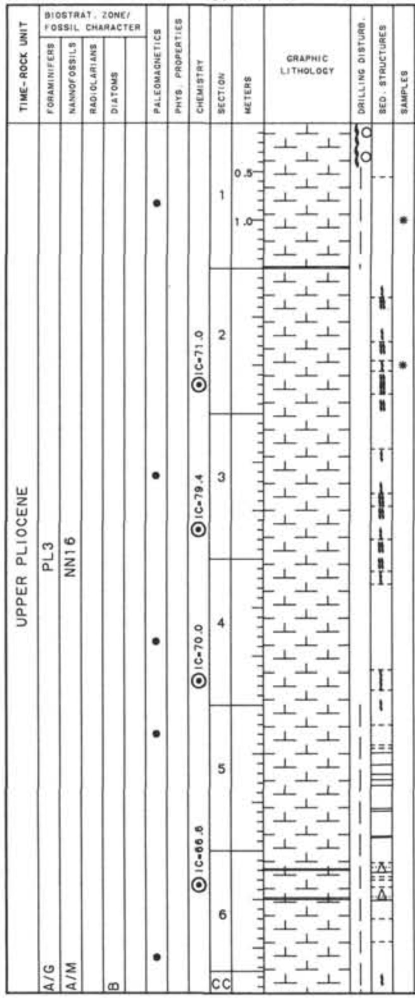

LITHOLOGIC DESCRIPTION

FORAMINIFER-BEARING NANNOFOSSIL OOZE to NANNOFOSSIL OOZE

Foraminifer-bearing nannofossil ooze to nannofossil ooze, light-gray (7.5YR 7/1), slightly to moderately bioturbated; interbedded sandy quartz turbidites in Section 6, 15 and 45 cm. Minor void in Section 1, 145–150 cm.

SMEAR SLIDE SUMMARY (%):

	1, 100 D	2, 100 D
TEXTURE:		
Sand	—	1
Silt	5	4
Clay	95	95
COMPOSITION:		
Quartz	Tr	Tr
Foraminifers	5	5
Nannofossils	95	95

SITE 657 HOLE B CORE 12 H CORED INTERVAL 4318.8-4328.3 mbsl; 97.7-102.2 mbsf

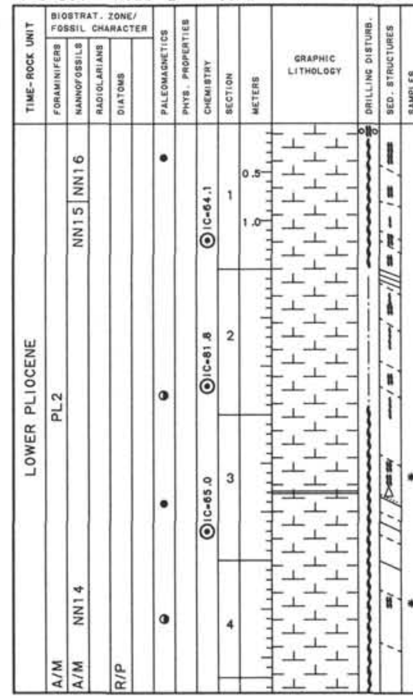

LITHOLOGIC DESCRIPTION

NANNOFOSSIL OOZE

Nannofossil ooze, light-gray (7.5Y 7/1), slightly to moderately bioturbated; one silty quartz turbidite in Section 3, 80 cm. Minor void in Section 1, 147–150 cm.

SMEAR SLIDE SUMMARY (%):

	3, 65 M	4, 90 D
TEXTURE:		
Sand	—	—
Silt	5	5
Clay	95	95
COMPOSITION:		
Quartz	5	Tr
Foraminifers	Tr	5
Nannofossils	95	95

SITE 657 HOLE B CORE 13 H CORED INTERVAL 4328.3-4337.8 mbsl; 107.2-116.7 mbsf

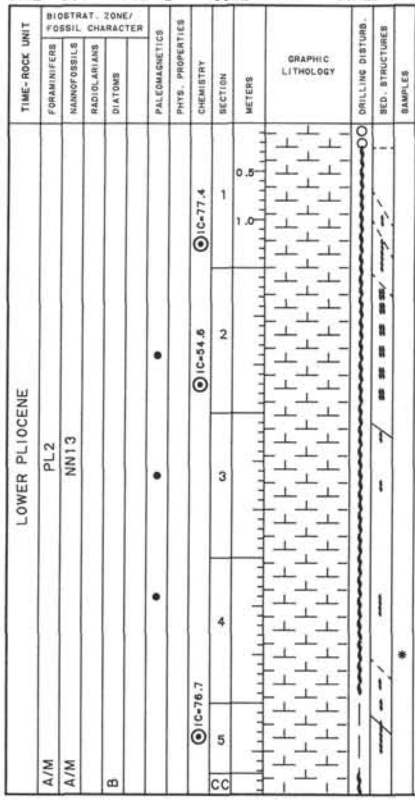

LITHOLOGIC DESCRIPTION

NANNOFOSSIL OOZE

Nannofossil ooze, light-gray (7.5YR 7/1); moderately bioturbated.

SMEAR SLIDE SUMMARY ():

	4, 100 D
TEXTURE:	
Sand	—
Silt	5
Clay	95
COMPOSITION:	
Quartz	3
Foraminifers	2
Nannofossils	95

SITE 657 HOLE B CORE 14 H CORED INTERVAL 4337.8-4347.3 mbsl; 116.7-126.2 mbsf

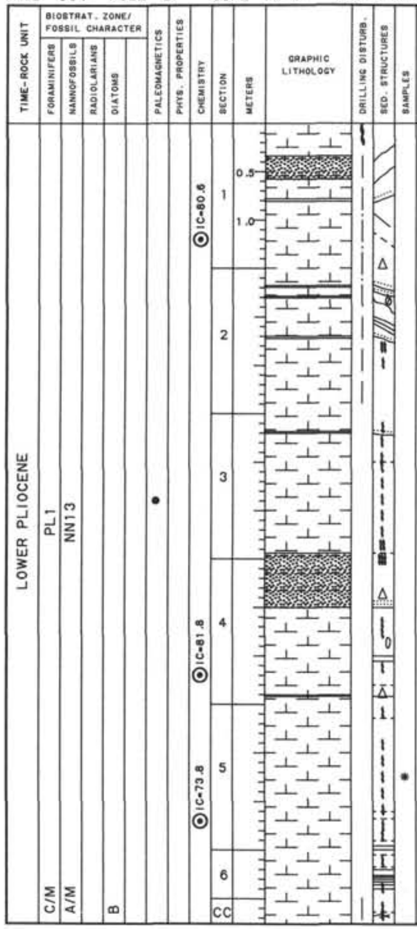

LITHOLOGIC DESCRIPTION

NANNOFOSSIL OOZE and FORAMINIFER-BEARING NANNOFOSSIL OOZE

Nannofossil ooze and foraminifer-bearing nannofossil ooze, light-gray to white (10Y 7/1, 7.5YR 8/0, 5Y 6/1); moderately bioturbated; extremely contorted in Sects. 1 and 2.

Minor lithologies: Section 1, 19–50, 72–75, and 146–147 cm; Section 2, 2, 29, 31, and 176 cm; Section 3, 22 and 150 cm; and Section 4, 0–53, 102–106, and 146–148 cm; quartz-bearing sand sequences with graded bedding (turbidites).

SMEAR SLIDE SUMMARY (%):

	5, 80 D
TEXTURE:	
Sand	—
Silt	10
Clay	90
COMPOSITION:	
Quartz	5
Foraminifers	5
Nannofossils	90

SITE 657 HOLE B CORE 15 H CORED INTERVAL 4347.3-4356.8 mbsl; 126.2-135.7 mbsf

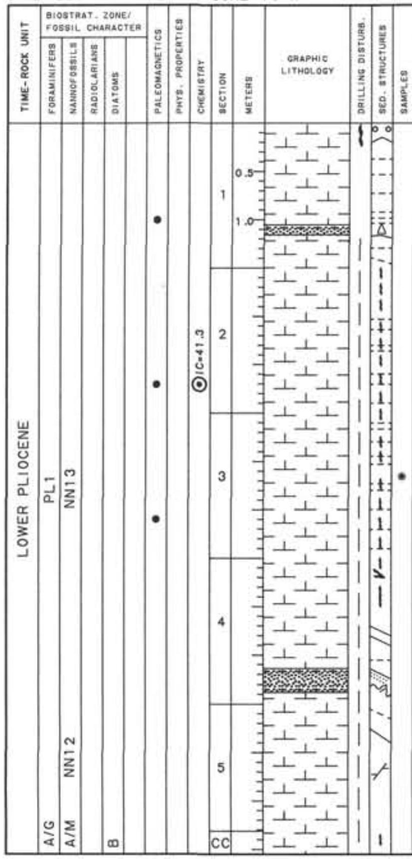

LITHOLOGIC DESCRIPTION

NANNOFOSSIL OOZE

Nannofossil ooze, generally white to light-gray (5Y 8/0, 5Y 6/1); slightly bioturbated; highly contorted.

Minor lithologies: Section 1, 105 cm: sandy quartz turbidites. Section 4, 115 cm: sandy quartz sequence with reverse-graded bedding.

SMEAR SLIDE SUMMARY (%):

	3, 70 D
TEXTURE:	
Sand	—
Silt	3
Clay	97
COMPOSITION:	
Quartz	2
Clay	2
Foraminifers	1
Nannofossils	95

SITE 657 HOLE B CORE 16 H CORED INTERVAL 4356.8-4366.3 mbsl; 135.7-145.2 mbsf

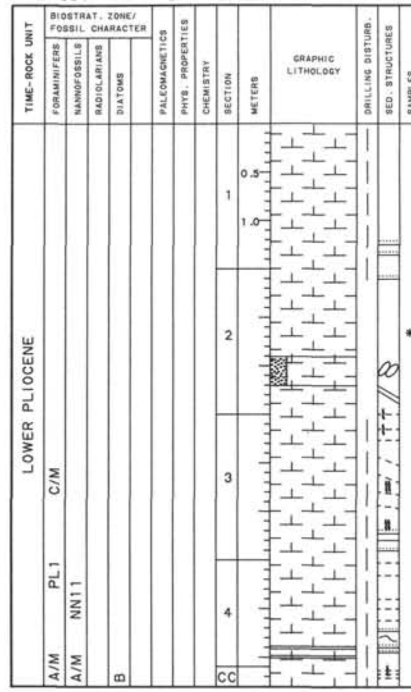

LITHOLOGIC DESCRIPTION

NANNOFOSSIL OOZE

Nannofossil ooze, light-gray to white (5Y 6/1, 5Y 8/1, 10Y 8/1); highly converted; intercalated with thin, sandy silts (turbidites ?) in Section 2, 90–130 cm and Section 4, 83–87 and 100 cm. Minor voids in Section 1, 146–150 cm and Section 2, 147–150 cm.

SITE 657 HOLE B CORE 17 H CORED INTERVAL 4366.3-4375.8 mbsl; 145.2-154.7 mbsf

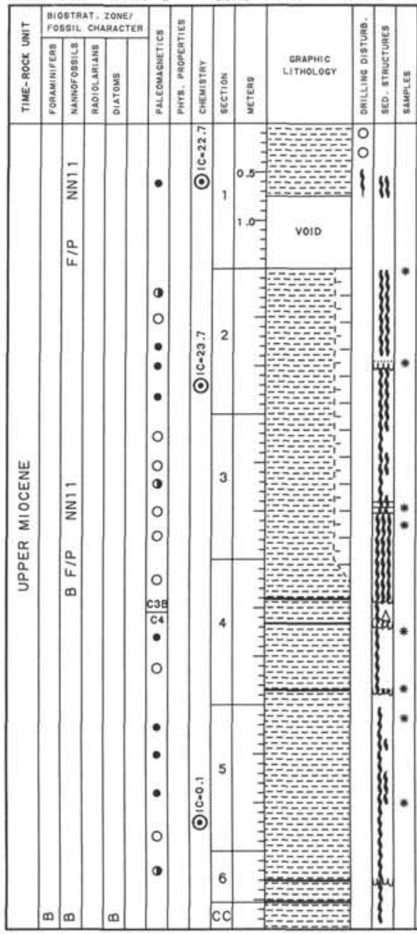

LITHOLOGIC DESCRIPTION

NANNOFOSSIL-BEARING CLAY and NANNOFOSSIL CLAY

Nannofossil-bearing clay and nannofossil clay, generally brownish-red or grayish-green (7.5YR 5/4, 2.5Y 5/4, 5Y 5/2); slightly to moderately bioturbated with few nannofossils.

Minor lithologies: Section 2, 119 cm; Section 4, 37–40, 68–70, and 136–138 cm; and Section 6, 28–30 cm: clayey sand and clayey, sandy silt, dark-colored.

SMEAR SLIDE SUMMARY (%):

	2, 8 M	2, 119 M	3, 92 D	3, 108 D	4, 71 D	4, 132 D	5, 110 D
TEXTURE:							
Sand	—	30	—	5	—	60	—
Silt	20	40	25	20	10	10	25
Clay	80	30	75	75	90	30	75
COMPOSITION:							
Quartz	5	60	5	10	10	60	25
Clay	70	20	15	75	90	35	70
Accessory Minerals	—	—	—	—	—	5	—
Foraminifers	—	5	—	—	—	—	—
Nannofossils	25	15	80	10	—	—	—

SITE 657 HOLE B CORE 18H CORED INTERVAL 4375.8-4385.3 mbsl; 154.7-164.2 mbsf

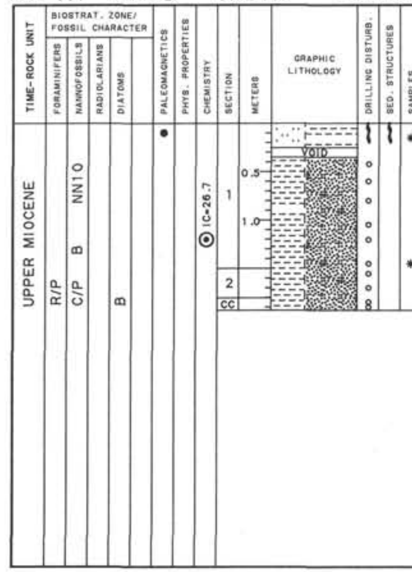

LITHOLOGIC DESCRIPTION

NANNOFOSSIL-BEARING, SILTY, CLAYEY, CALCAREOUS and QUARTZOSE SAND

Nannofossil-bearing, silty, clayey, calcareous, and quartzose sand, gray (5Y 5/1) with many large bioclasts (broken shell debris).

Minor lithology: Section 1, 0–20 cm: nannofossil-bearing, quartzose, silty clay, olive-gray (5Y 5/2).

SMEAR SLIDE SUMMARY (%):

	1, 20 D	1, 145 D
TEXTURE:		
Sand	—	60
Silt	30	10
Clay	70	30
COMPOSITION:		
Quartz	30	40
Clay	50	10
Nannofossils	20	20
Bioclasts	—	30

SITE 657 HOLE B CORE 19H CORED INTERVAL 4385.3-4394.8 mbsl; 164.2-173.7 mbsf

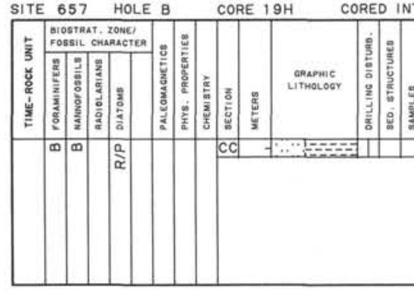

LITHOLOGIC DESCRIPTION

NANNOFOSSIL-BEARING, QUARTZOSE, SILTY CLAY

Nannofossil-bearing, quartzose, silty clay, olive-gray (5Y 5/2).

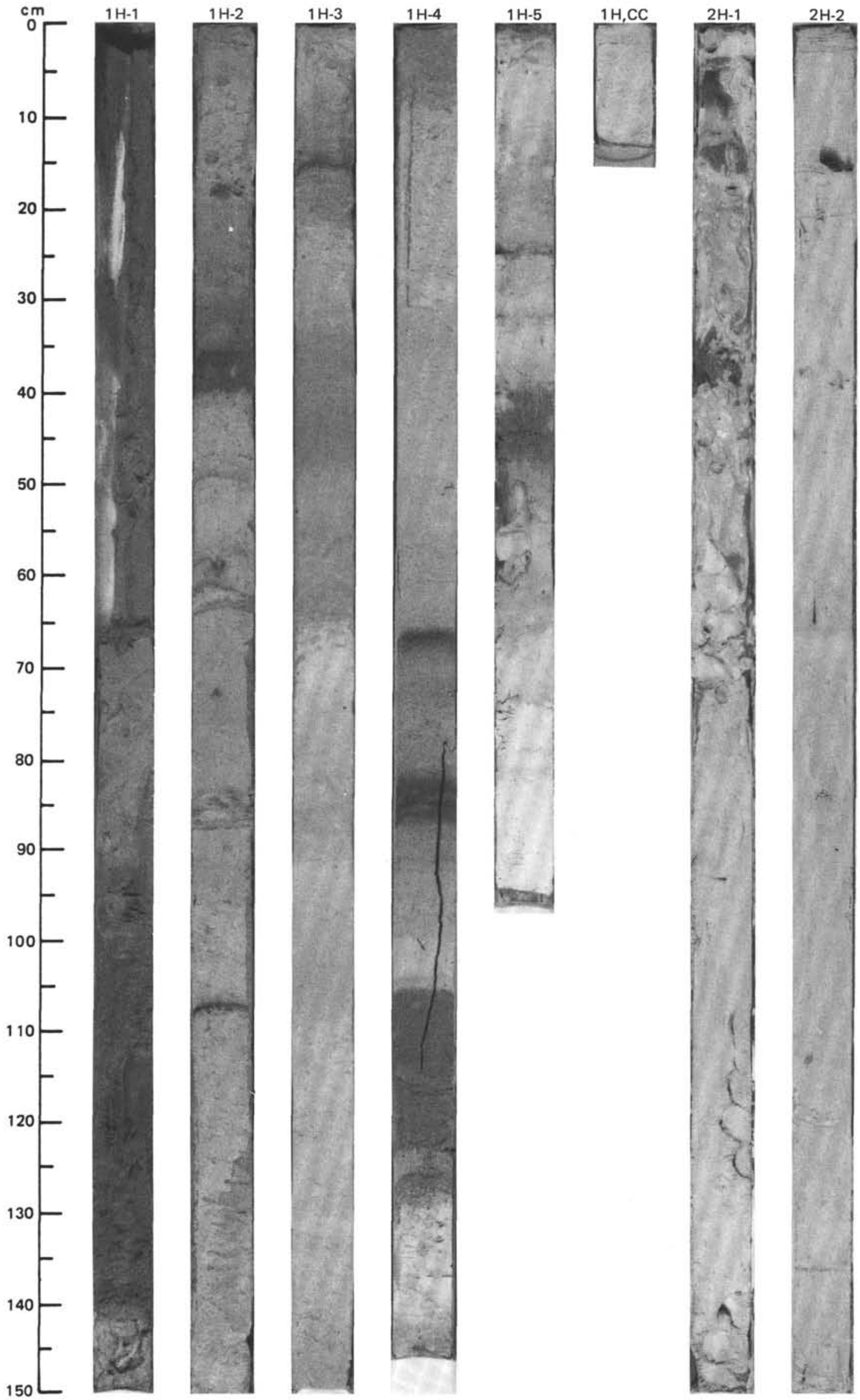
cm
0
10
20
30
40
50
60
70
80
90
100
110
120
130
140
150
1H-1
1H-2
1H-3
1H-4
1H-5
1H,CC
2H-1
2H-2

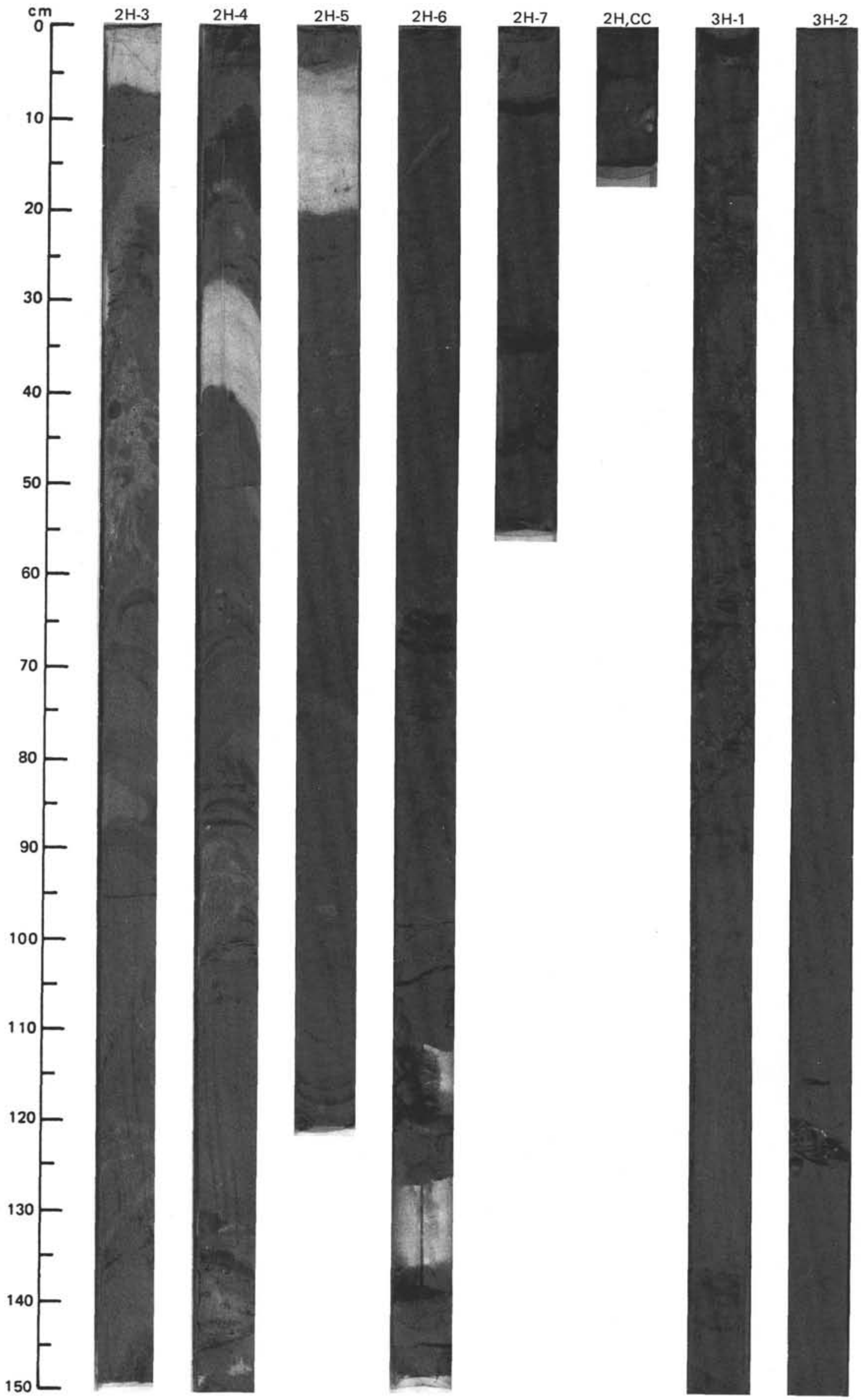
cm
0
10
20
30
40
50
60
70
80
90
100
110
120
130
140
150
2H-3
2H-4
2H-5
2H-6
2H-7
2H,CC
3H-1
3H-2

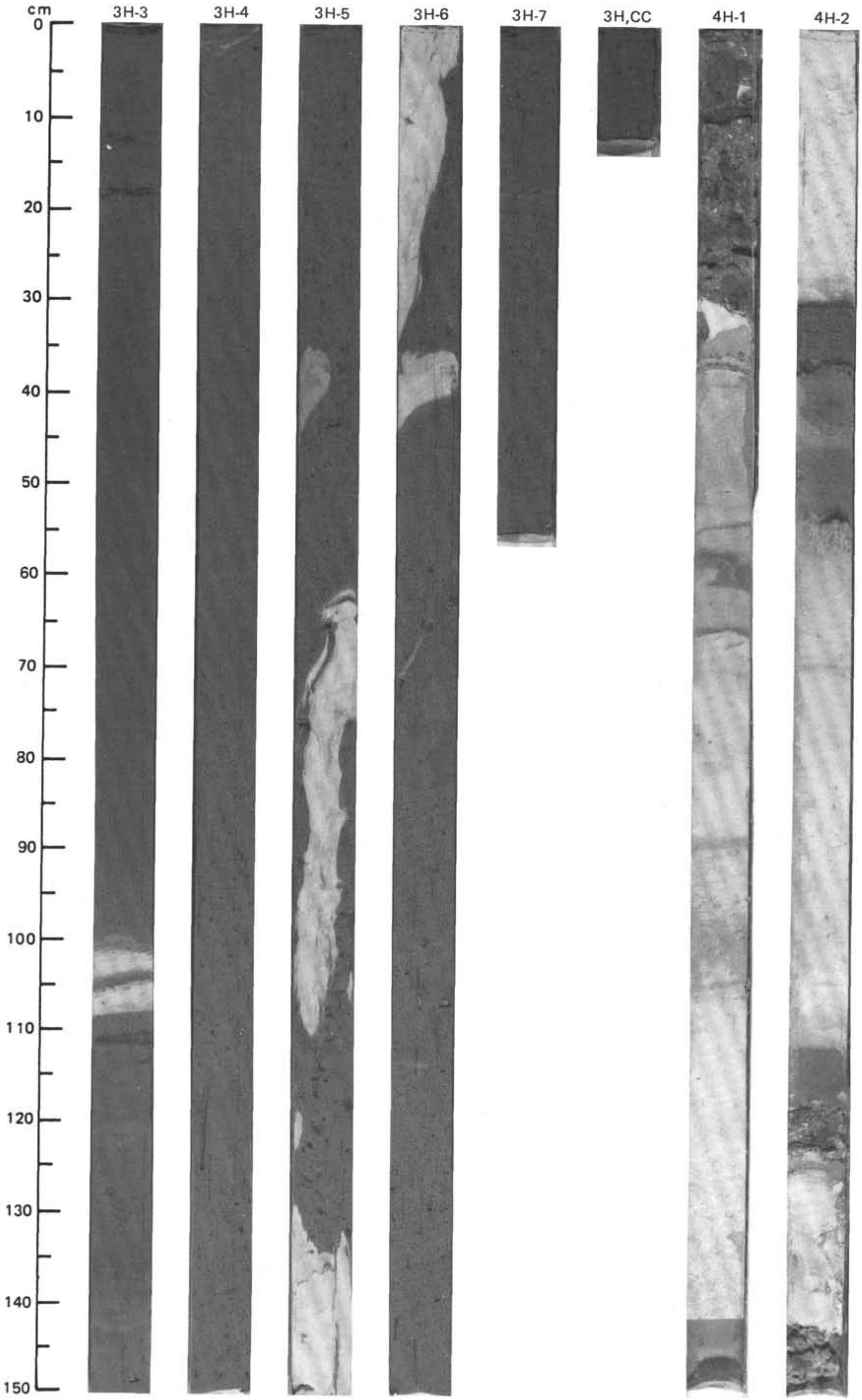
cm
0
10
20
30
40
50
60
70
80
90
100
110
120
130
140
150
3H-3
3H-4
3H-5
3H-6
3H-7
3H,CC
4H-1
4H-2

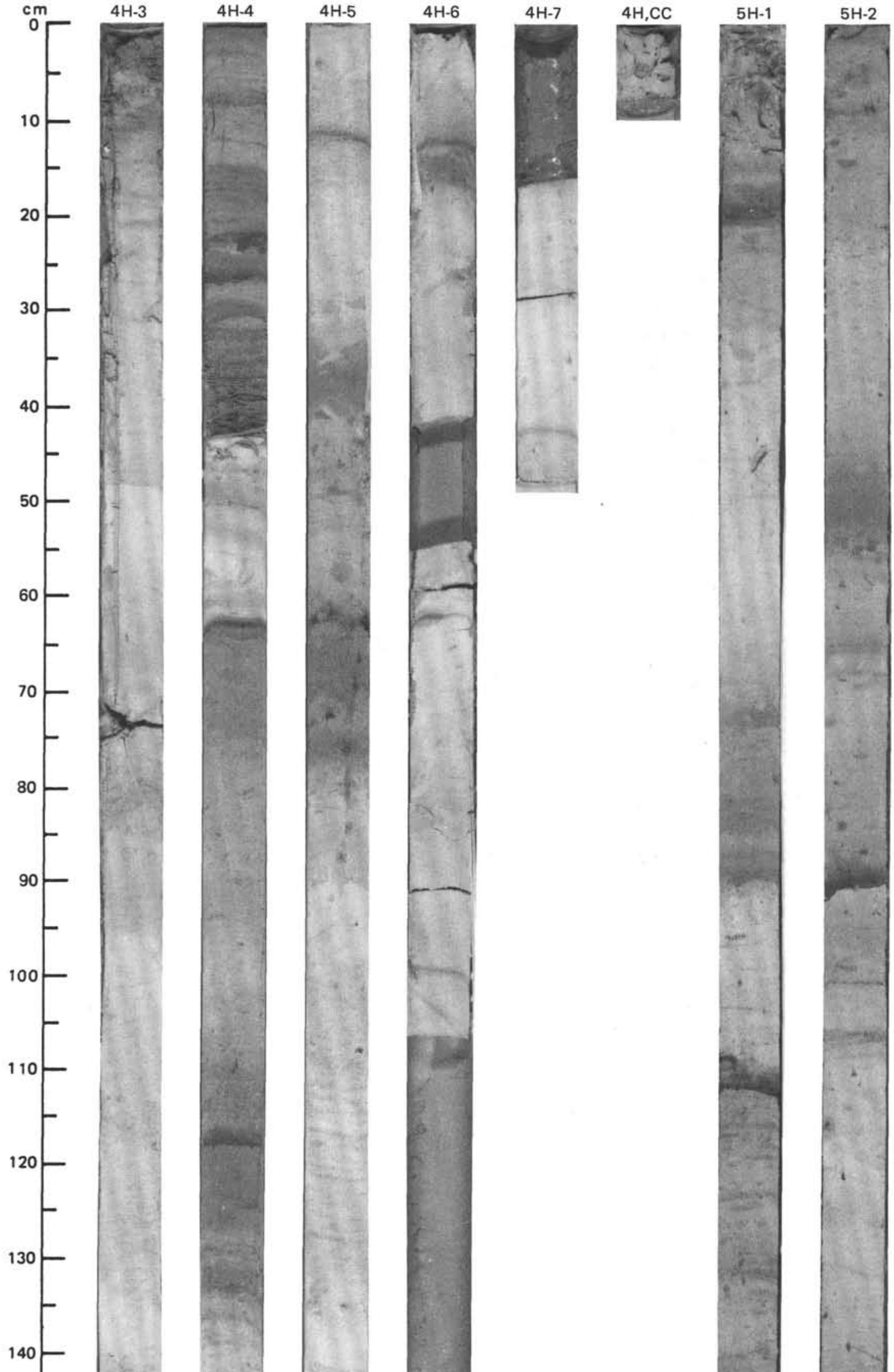
cm
0
10
20
30
40
50
60
70
80
90
100
110
120
130
140
150
4H-3
4H-4
4H-5
4H-6
4H-7
4H,CC
5H-1
5H-2

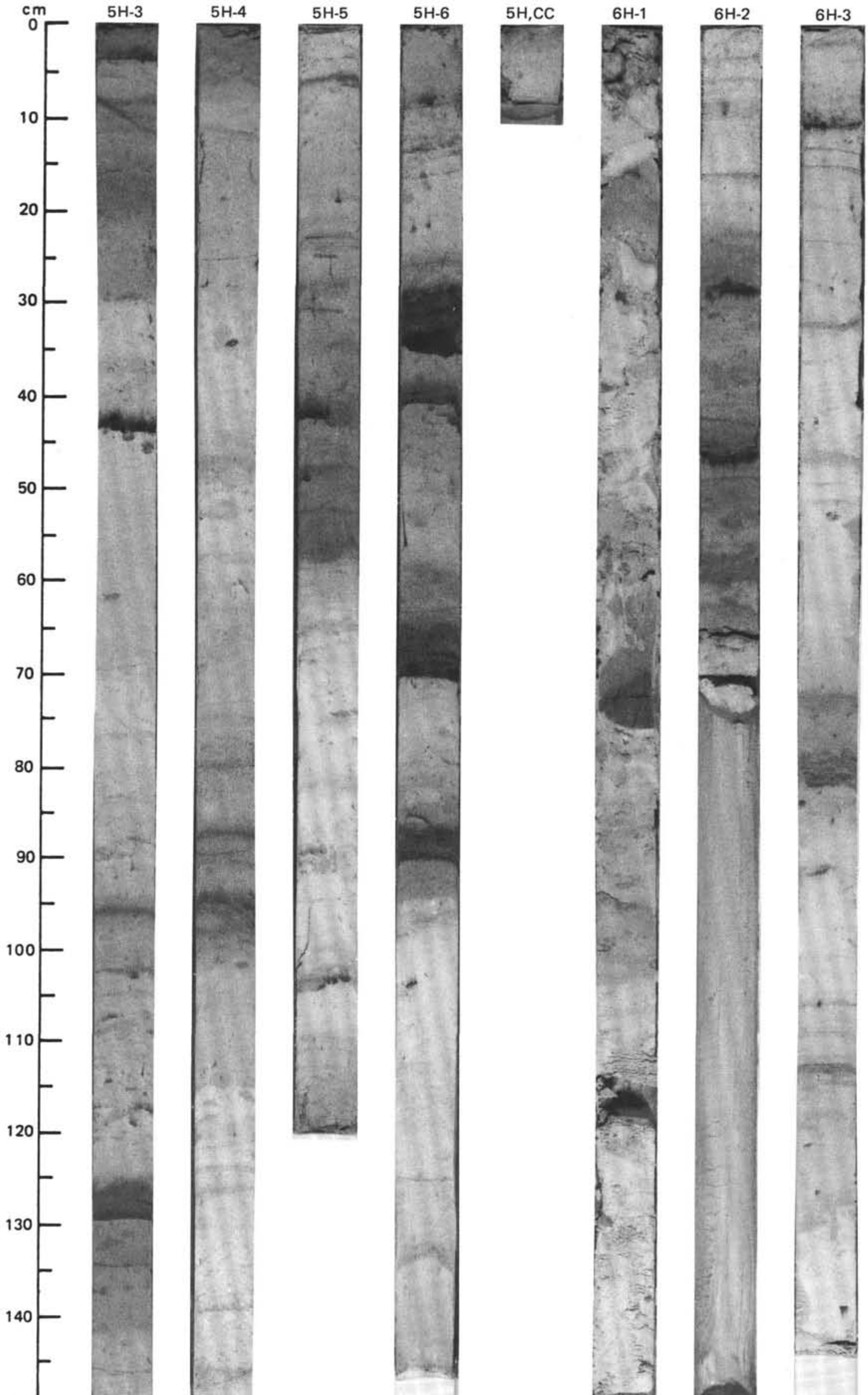
cm
0
10
20
30
40
50
60
70
80
90
100
110
120
130
140
150
5H-3
5H-4
5H-5
5H-6
5H,CC
6H-1
6H-2
6H-3


cm
0
10
20
30
40
50
60
70
80
90
100
110
120
130
140
150
6H-4
6H-5
6H-6
6H-7
6H,CC
7H-1
7H-2
7H-3

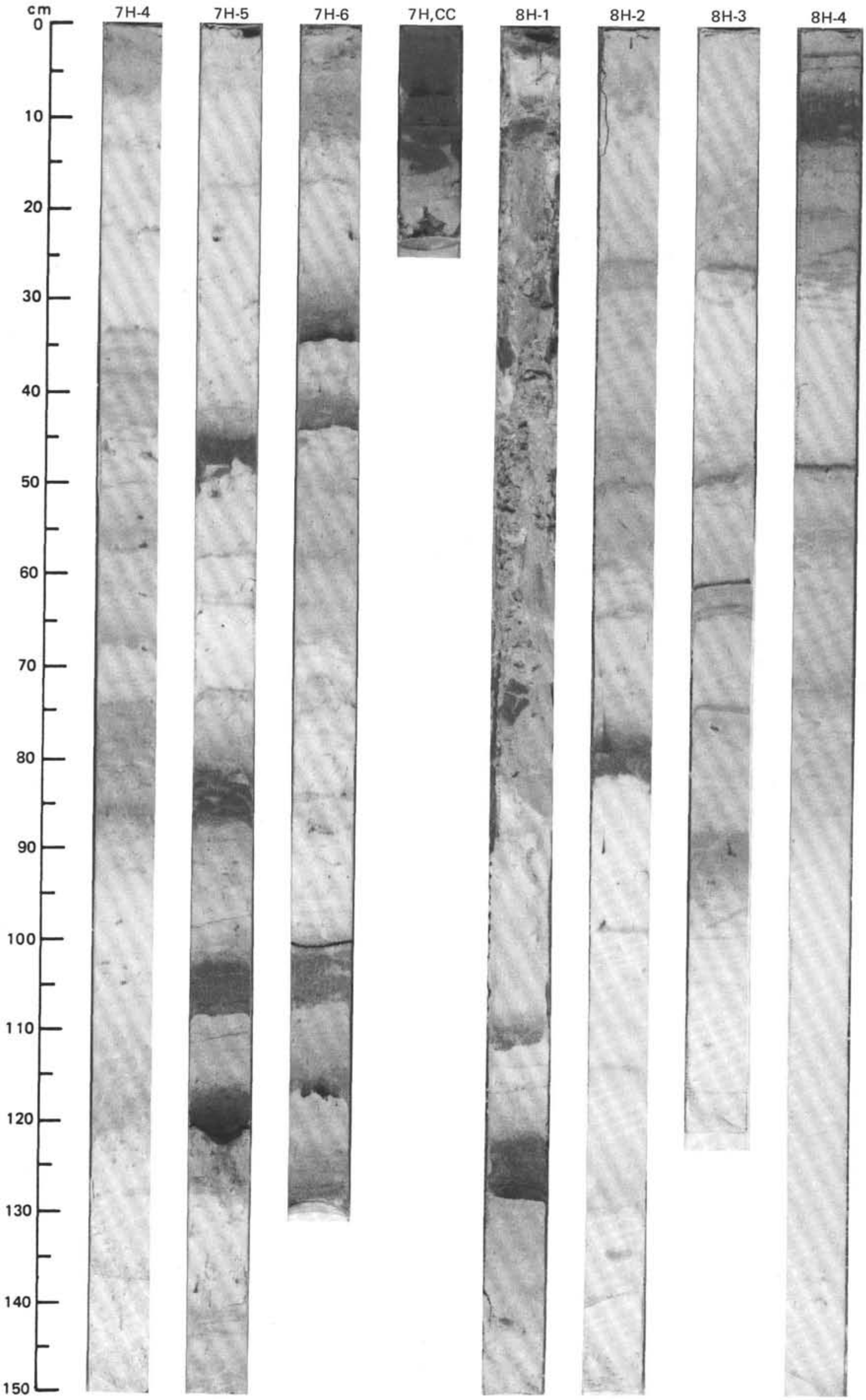
cm
0
10
20
30
40
50
60
70
80
90
100
110
120
130
140
150
7H-4
7H-5
7H-6
7H,CC
8H-1
8H-2
8H-3
8H-4

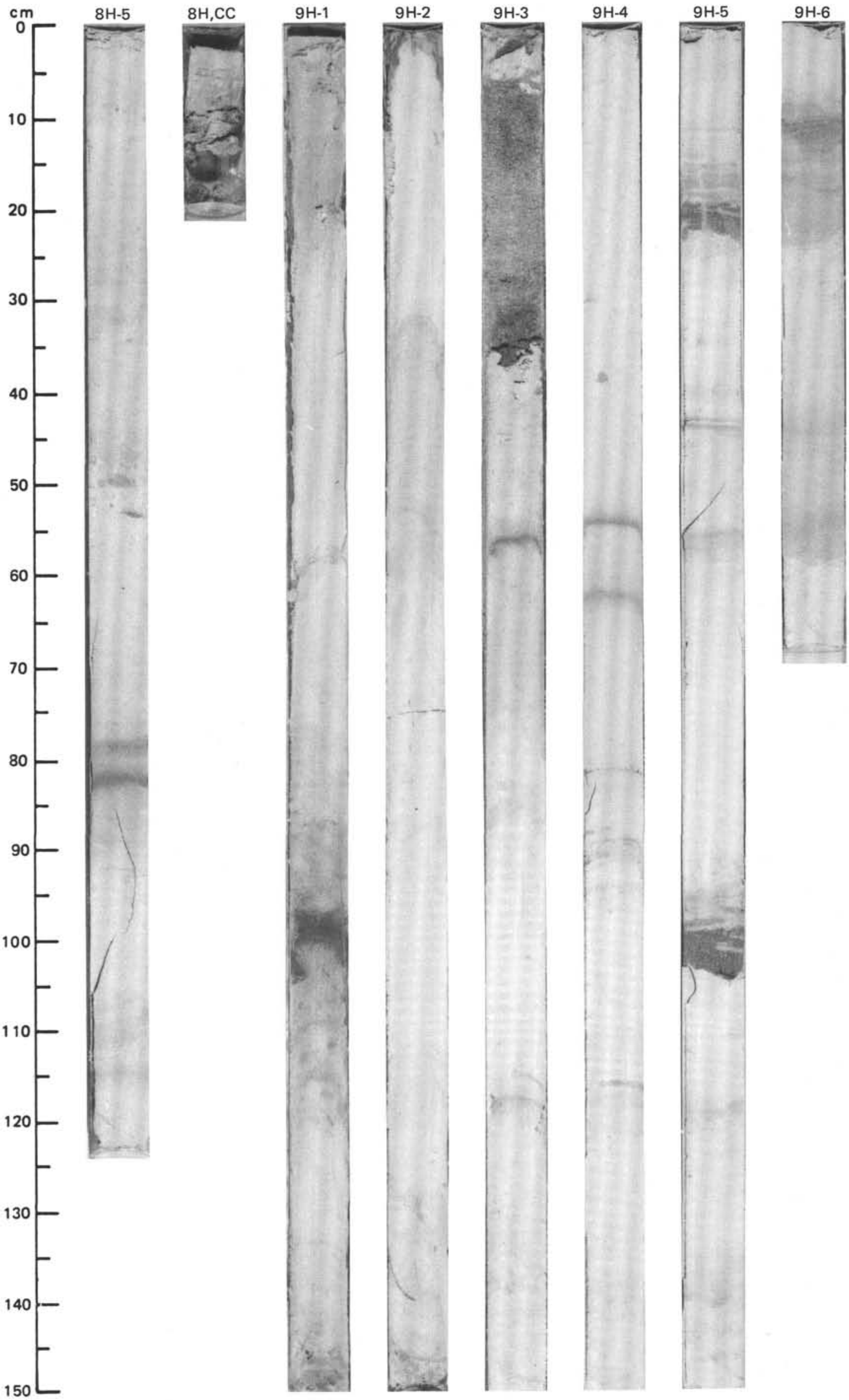
cm
0
10
20
30
40
50
60
70
80
90
100
110
120
130
140
150
8H-5
8H,CC
9H-1
9H-2
9H-3
9H-4
9H-5
9H-6

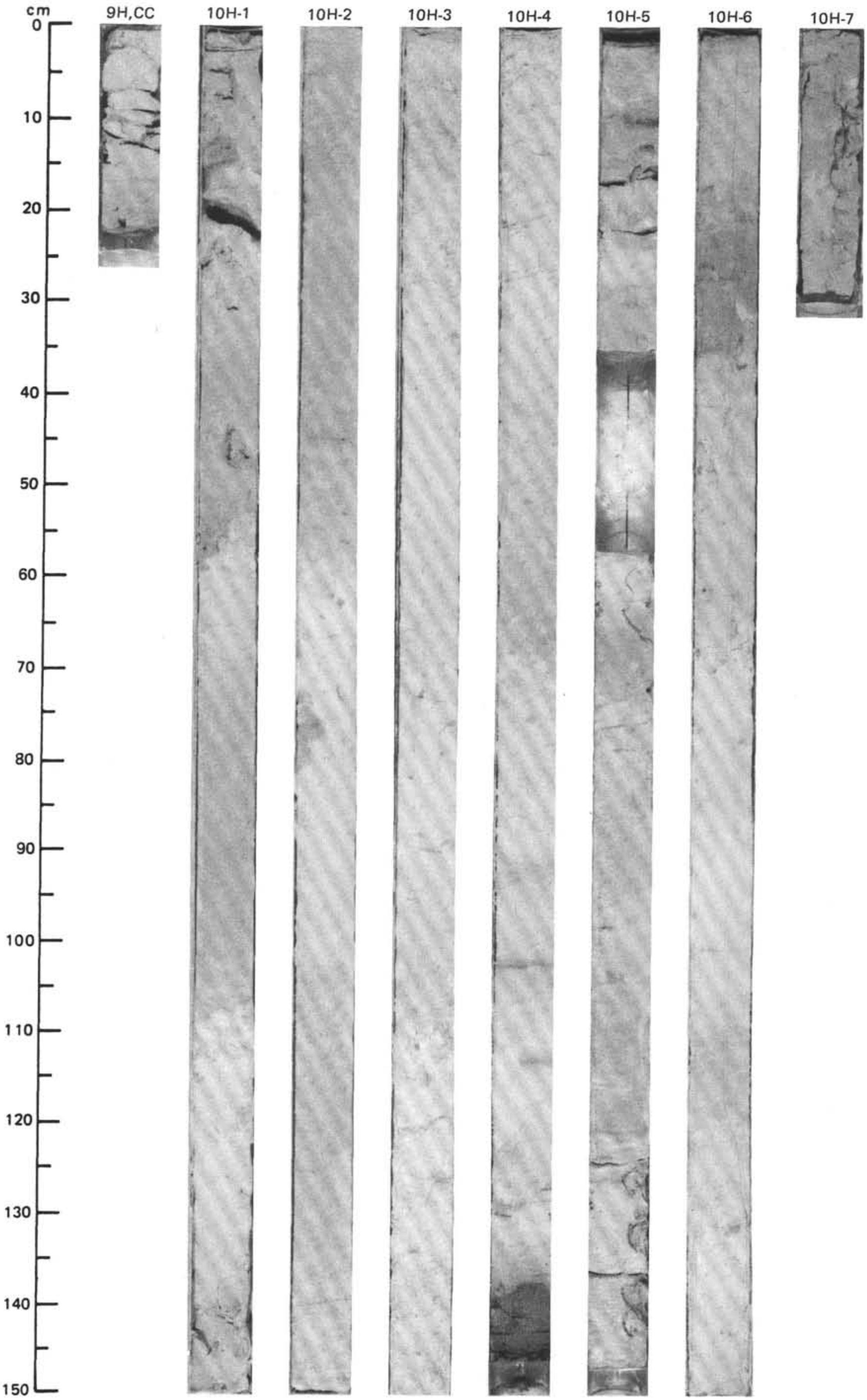
cm
0
10
20
30
40
50
60
70
80
90
100
110
120
130
140
150
9H,CC
10H-1
10H-2
10H-3
10H-4
10H-5
10H-6
10H-7

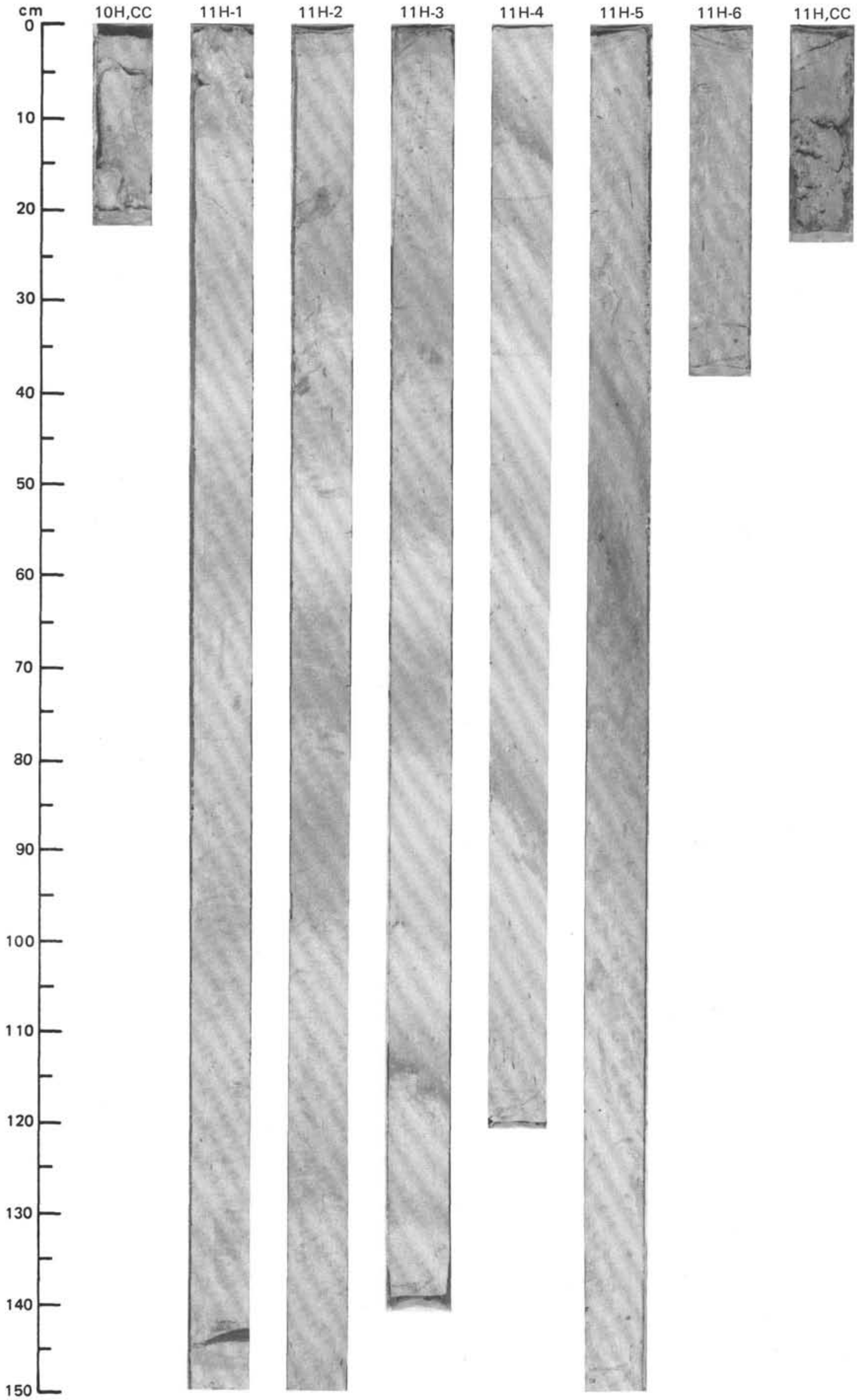
cm
0
10
20
30
40
50
60
70
80
90
100
110
120
130
140
150
10H,CC
11H-1
11H-2
11H-3
11H-4
11H-5
11H-6
11H,CC

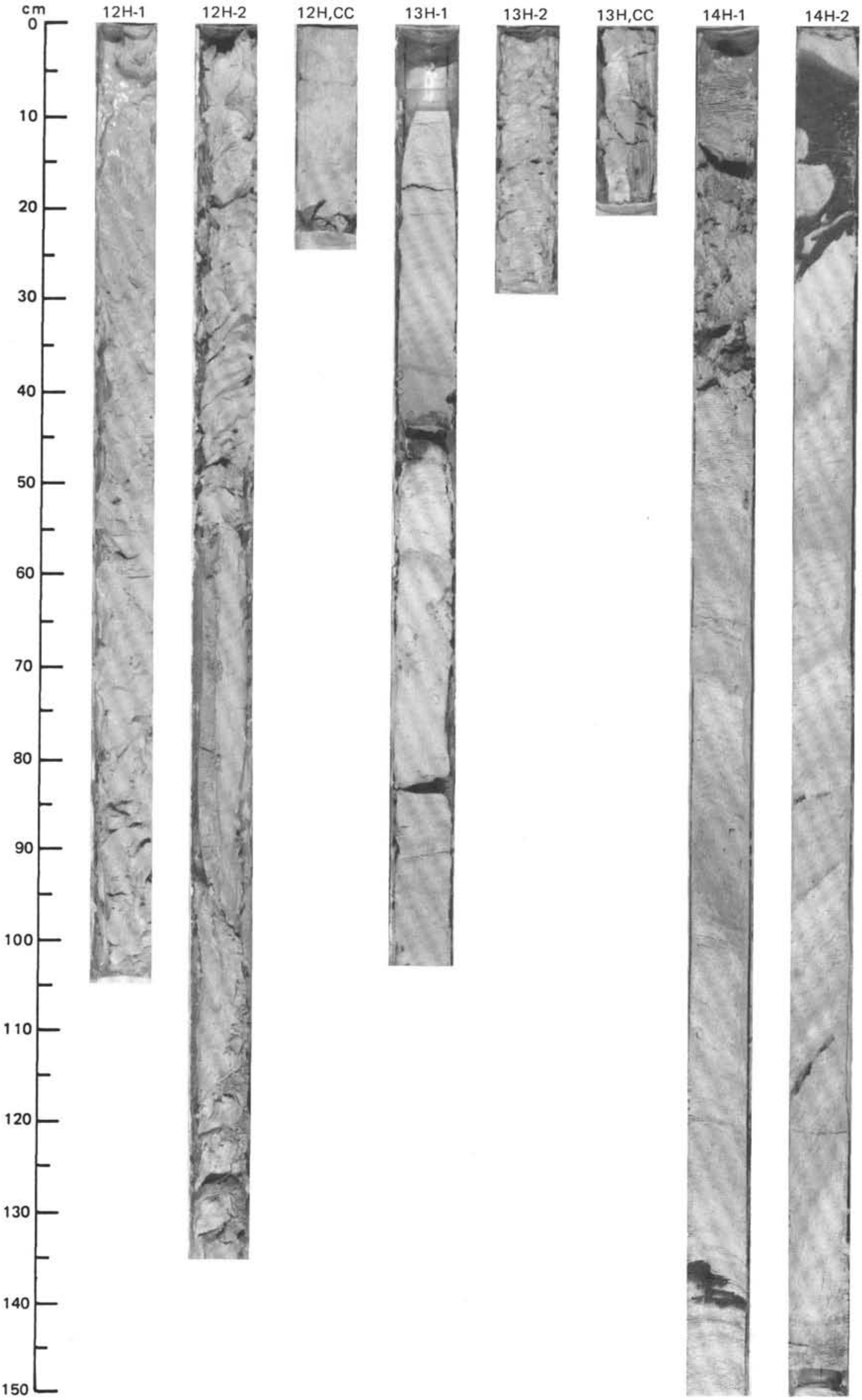
cm
0
10
20
30
40
50
60
70
80
90
100
110
120
130
140
150
12H-1
12H-2
12H,CC
13H-1
13H-2
13H,CC
14H-1
14H-2

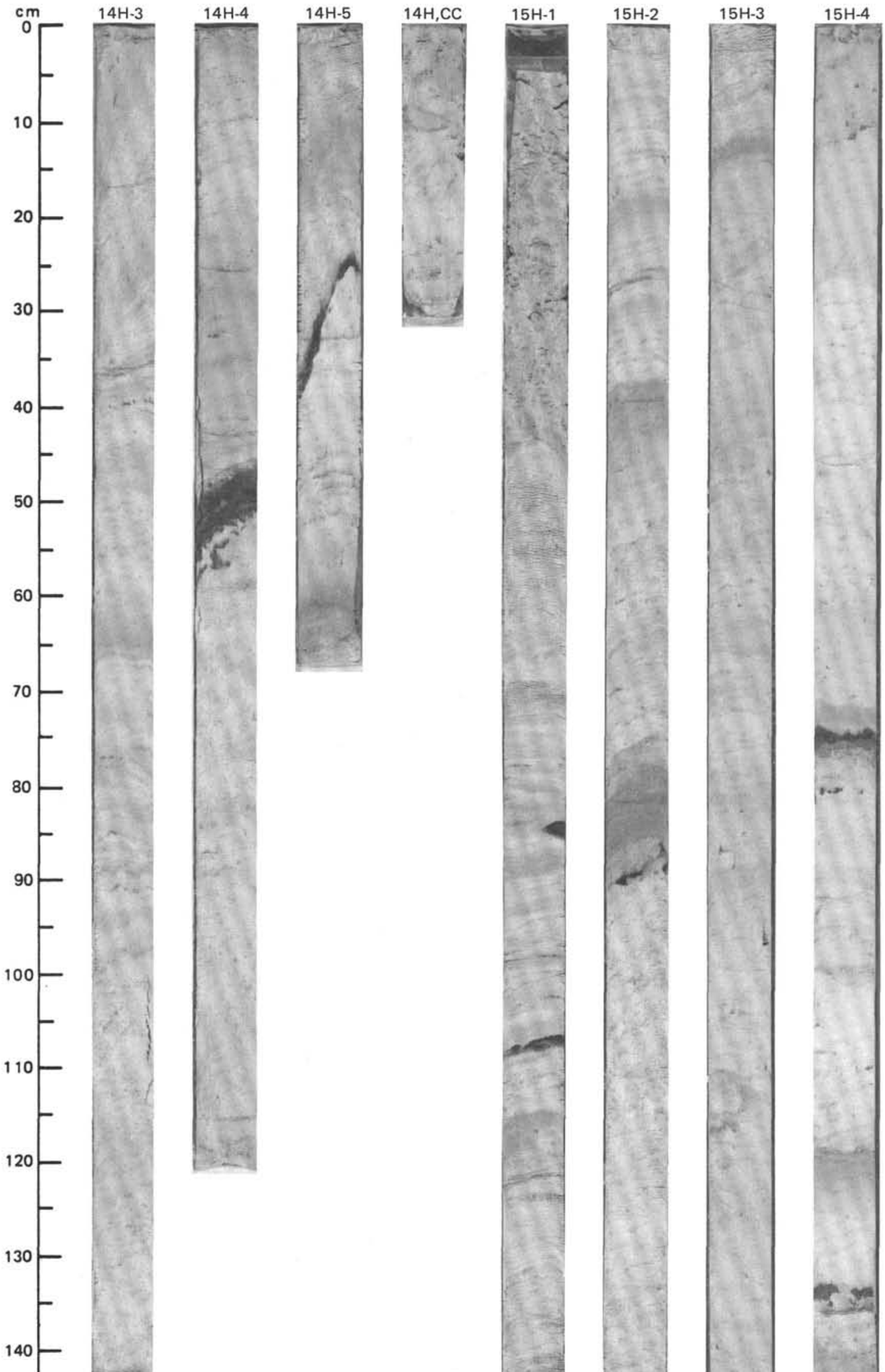
cm
0
10
20
30
40
50
60
70
80
90
100
110
120
130
140
150
14H-3
14H-4
14H-5
14H,CC
15H-1
15H-2
15H-3
15H-4

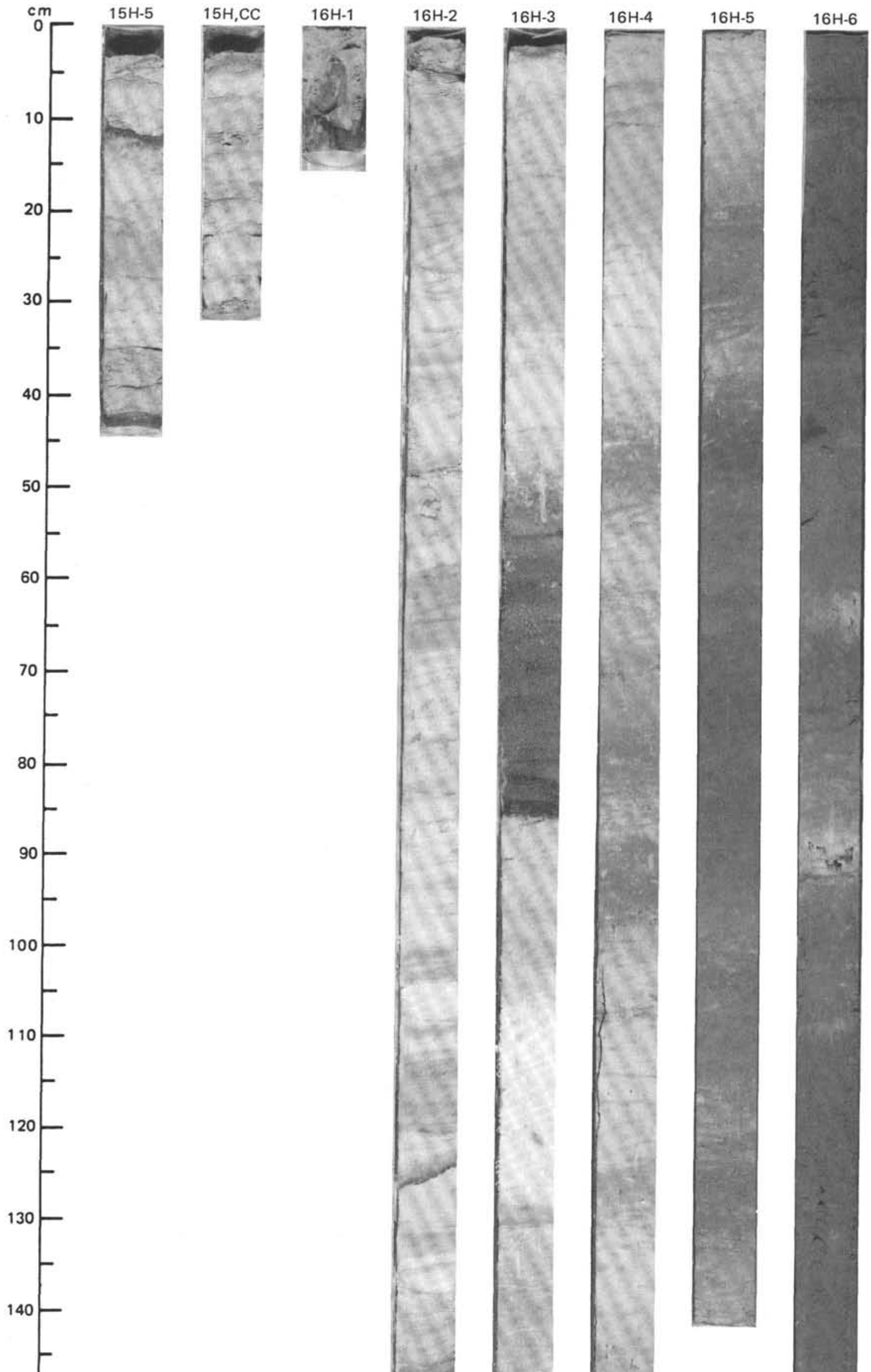
cm
0
10
20
30
40
50
60
70
80
90
100
110
120
130
140
150
15H-5
15H,CC
16H-1
16H-2
16H-3
16H-4
16H-5
16H-6

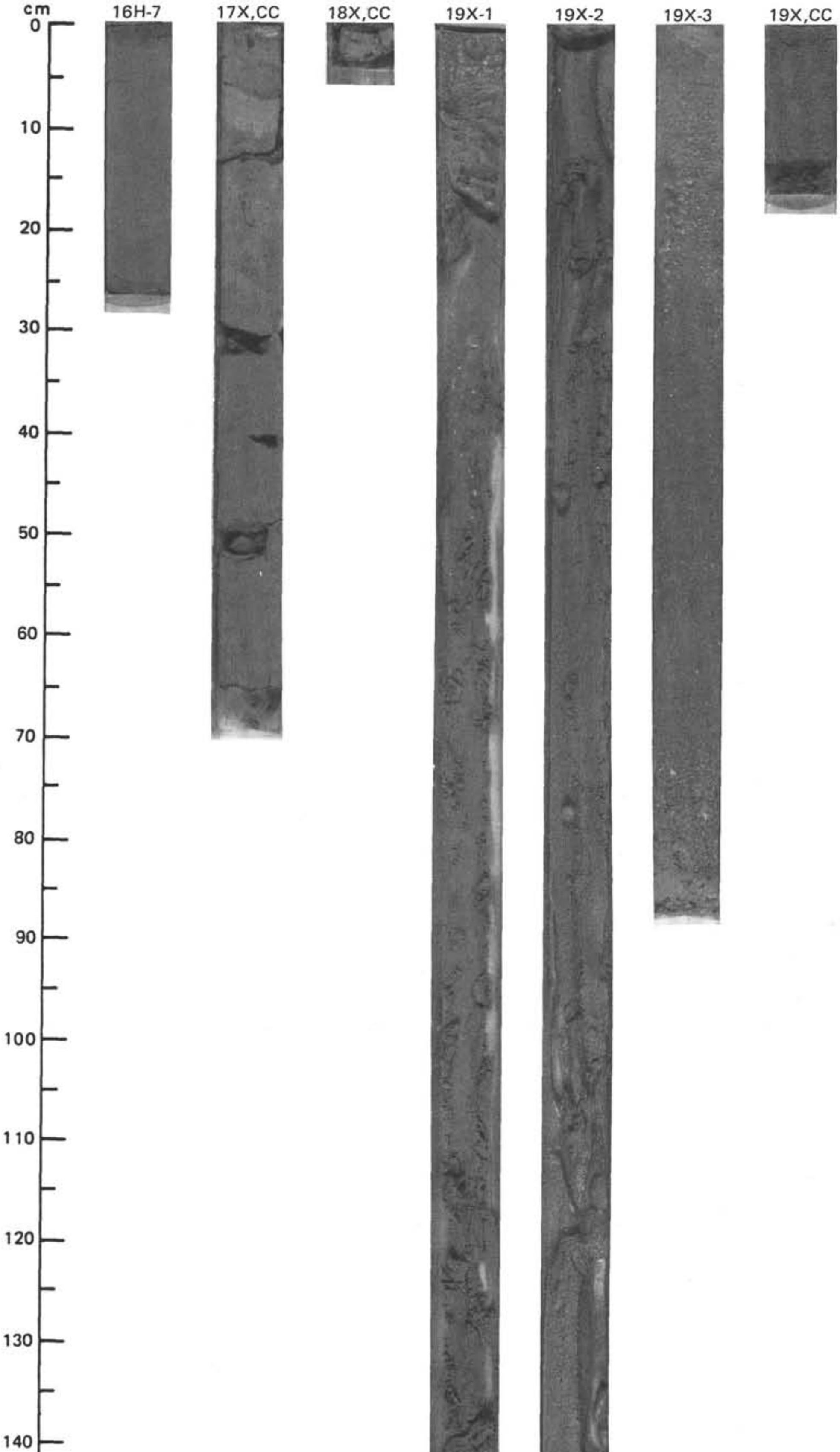
cm
16H-7
17X,CC
18X,CC
19X-1
19X-2
19X-3
19X,CC
0
10
20
30
40
50
60
70
80
90
100
110
120
130
140
150

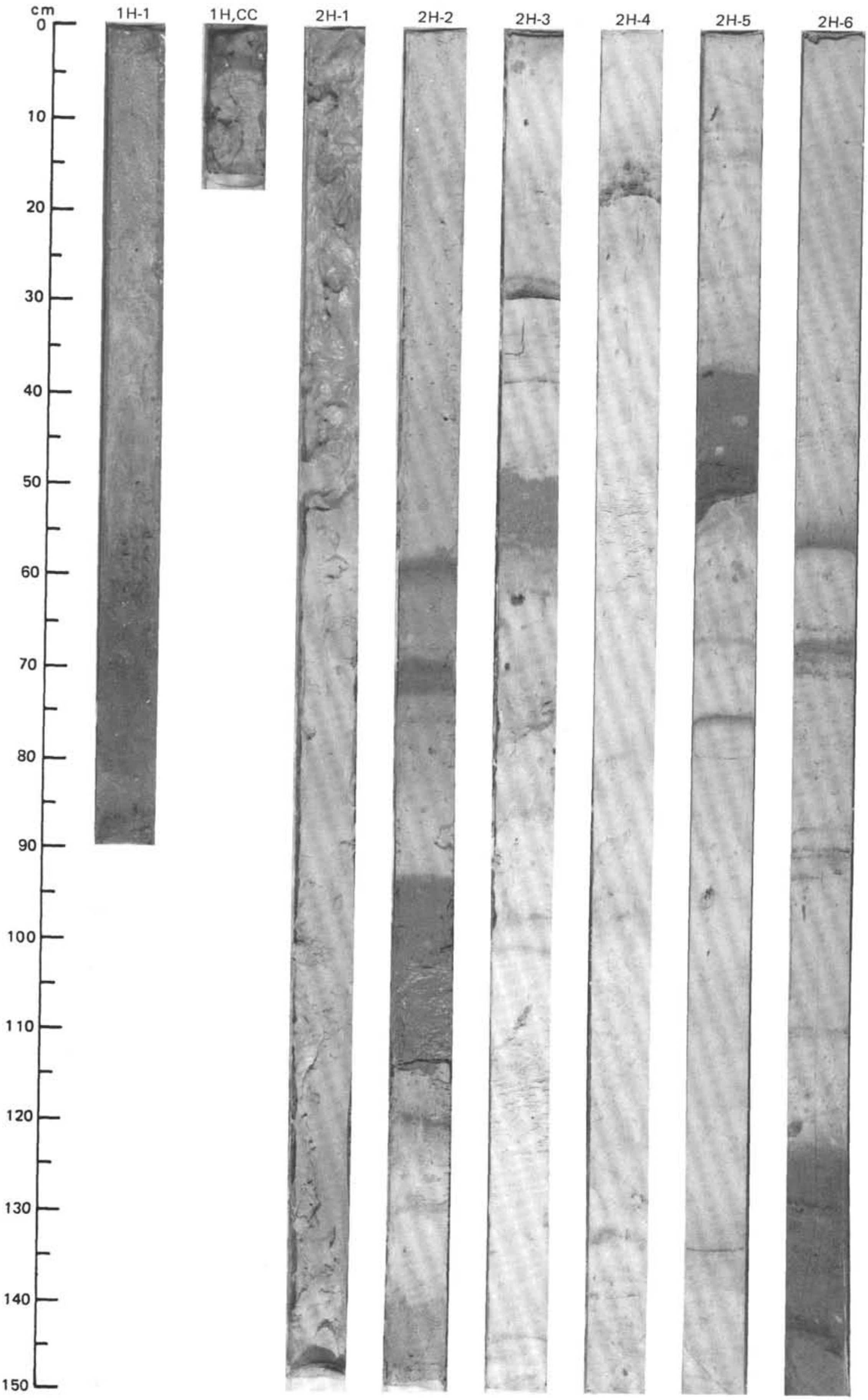
cm
0
10
20
30
40
50
60
70
80
90
100
110
120
130
140
150
1H-1
1H,CC
2H-1
2H-2
2H-3
2H-4
2H-5
2H-6

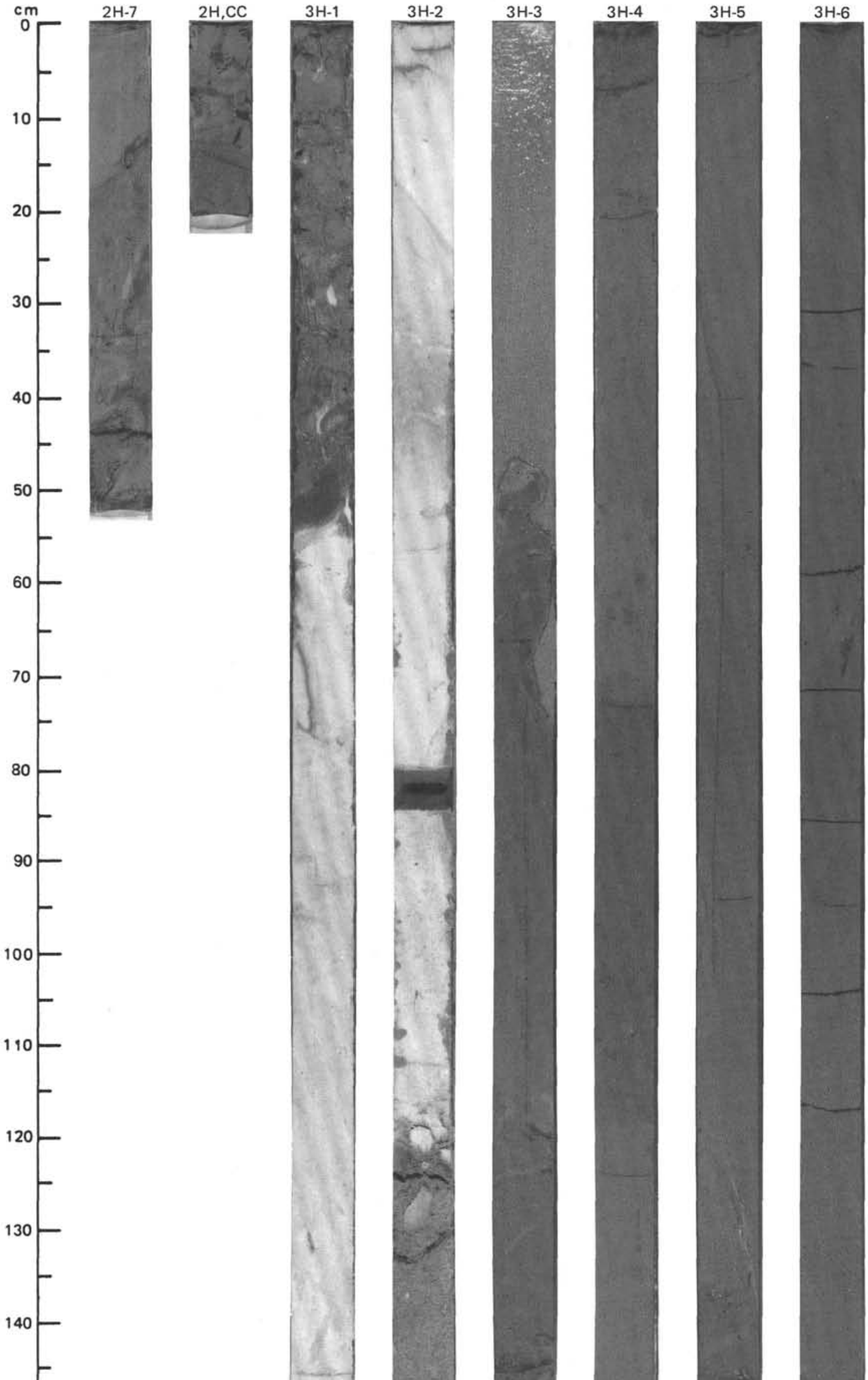
cm
0
10
20
30
40
50
60
70
80
90
100
110
120
130
140
150
2H-7
2H,CC
3H-1
3H-2
3H-3
3H-4
3H-5
3H-6

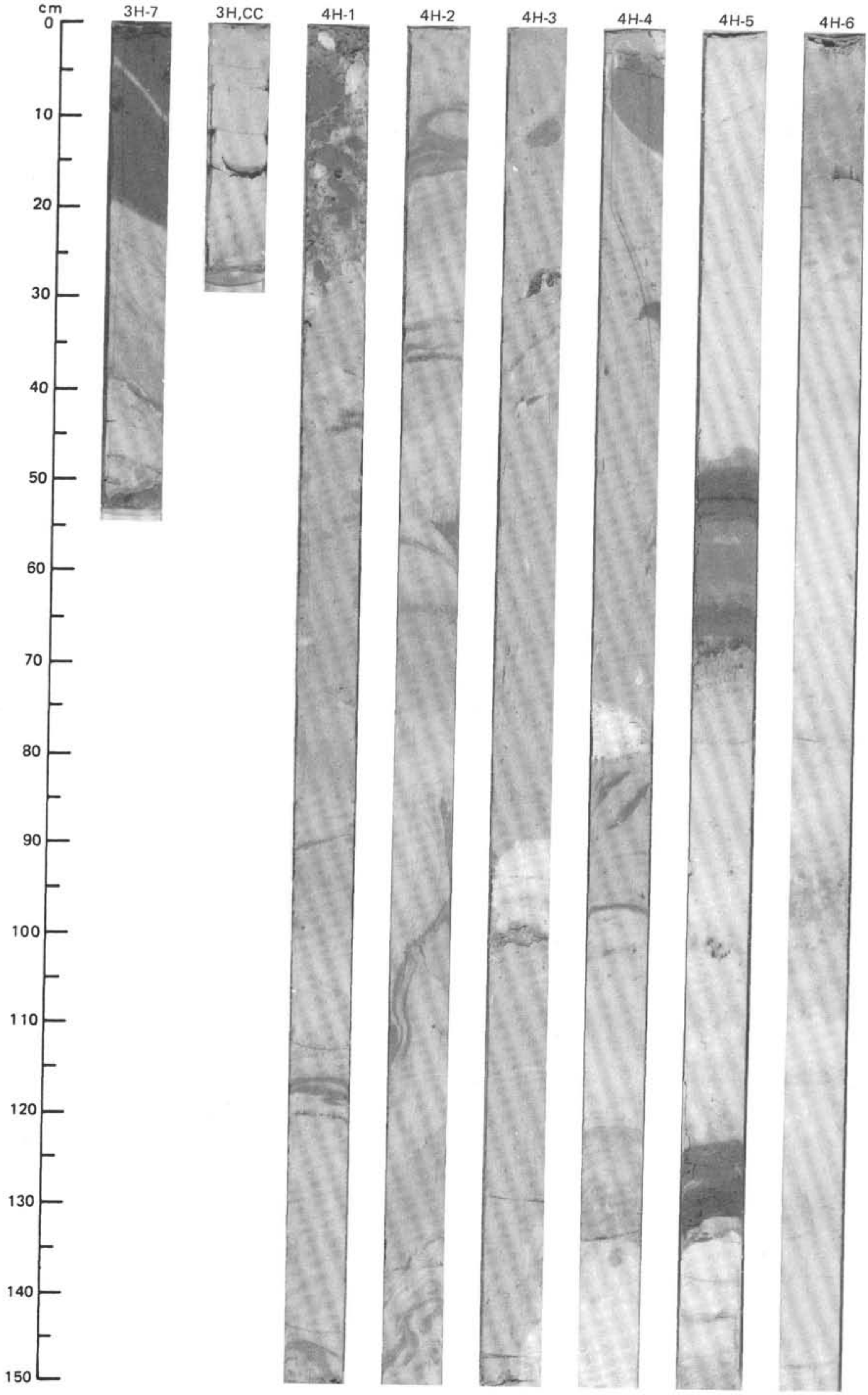
cm
0
10
20
30
40
50
60
70
80
90
100
110
120
130
140
150
3H-7
3H,CC
4H-1
4H-2
4H-3
4H-4
4H-5
4H-6

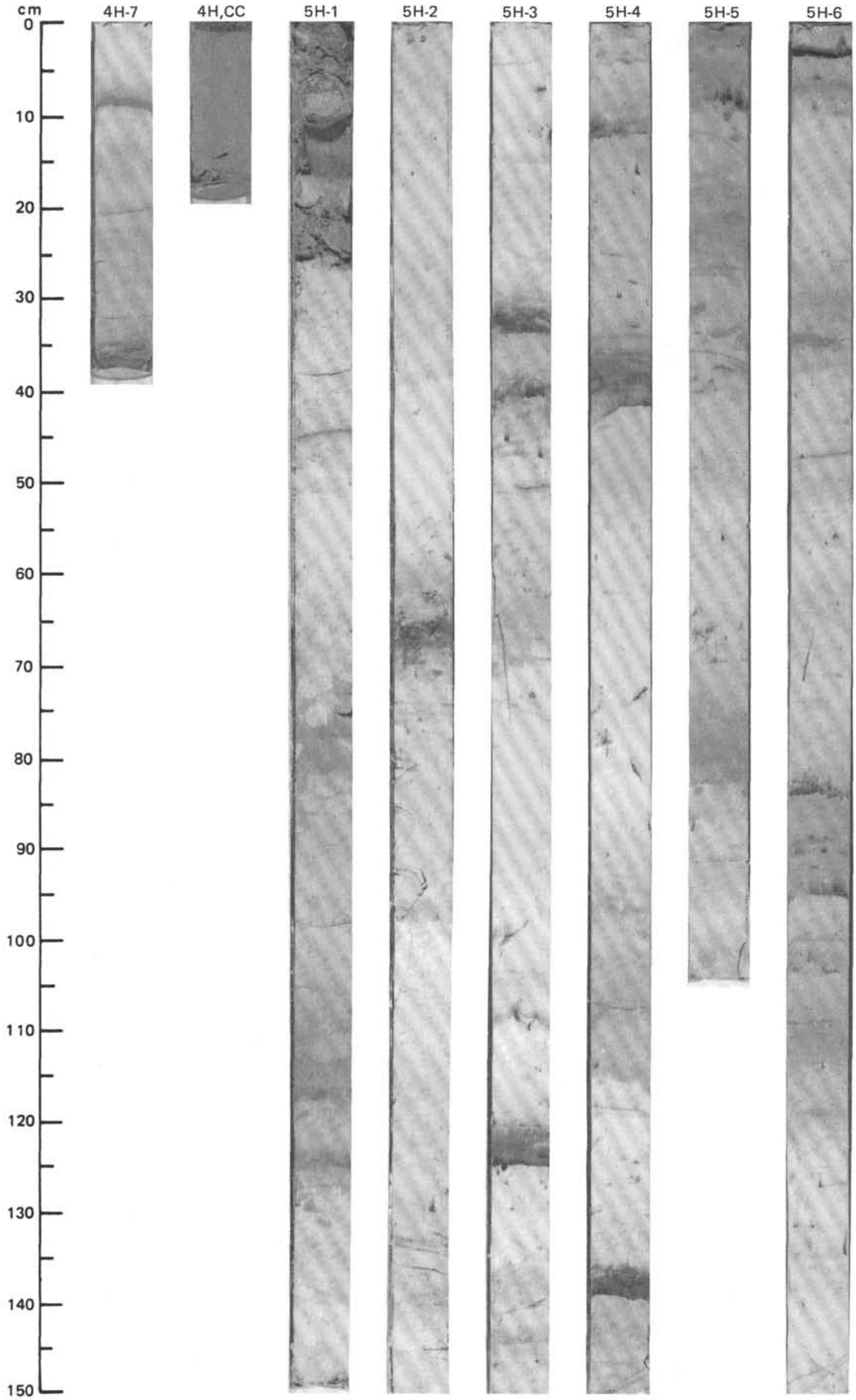
cm
0
10
20
30
40
50
60
70
80
90
100
110
120
130
140
150
4H-7
4H,CC
5H-1
5H-2
5H-3
5H-4
5H-5
5H-6

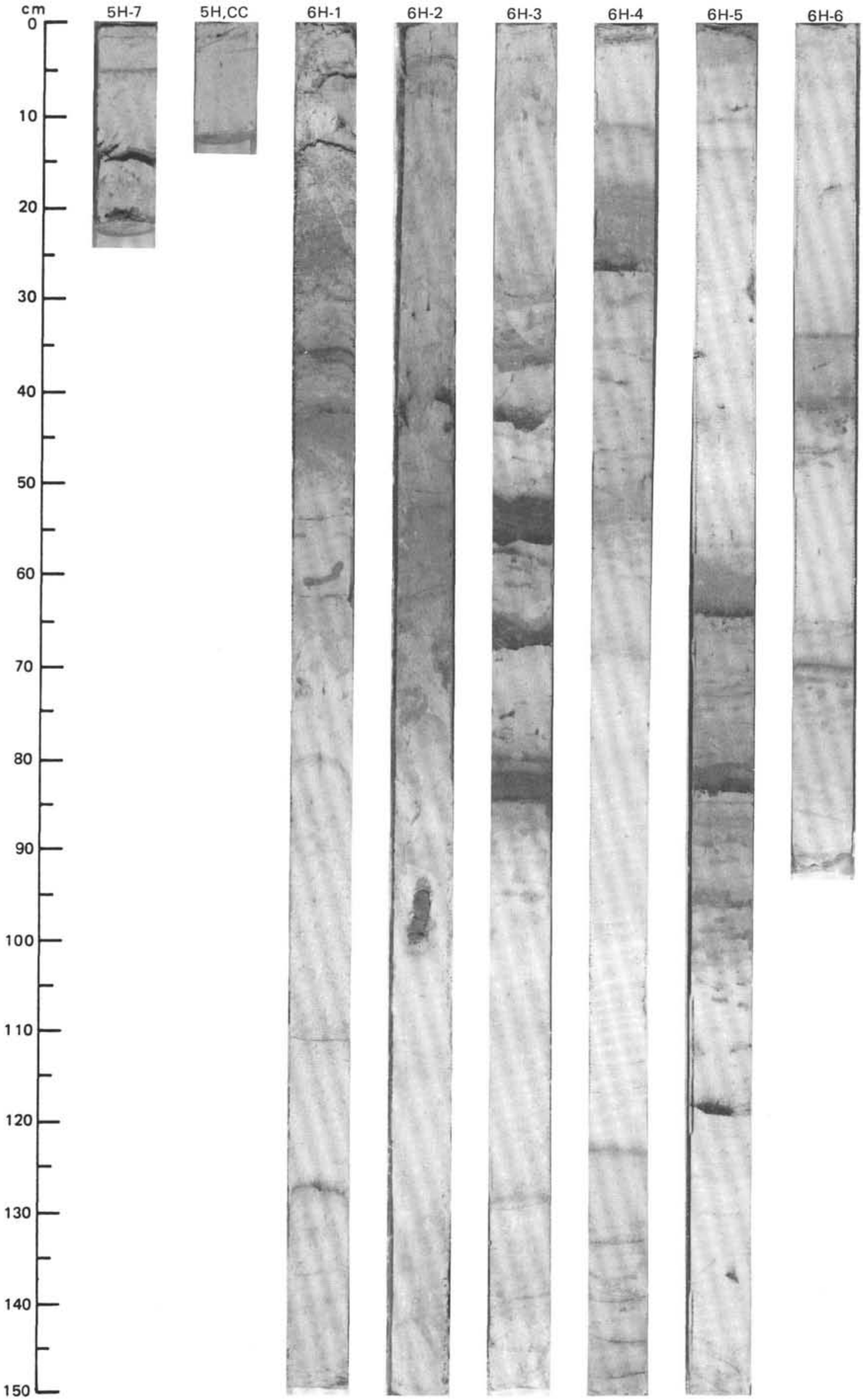
cm
0
10
20
30
40
50
60
70
80
90
100
110
120
130
140
150
5H-7
5H,CC
6H-1
6H-2
6H-3
6H-4
6H-5
6H-6

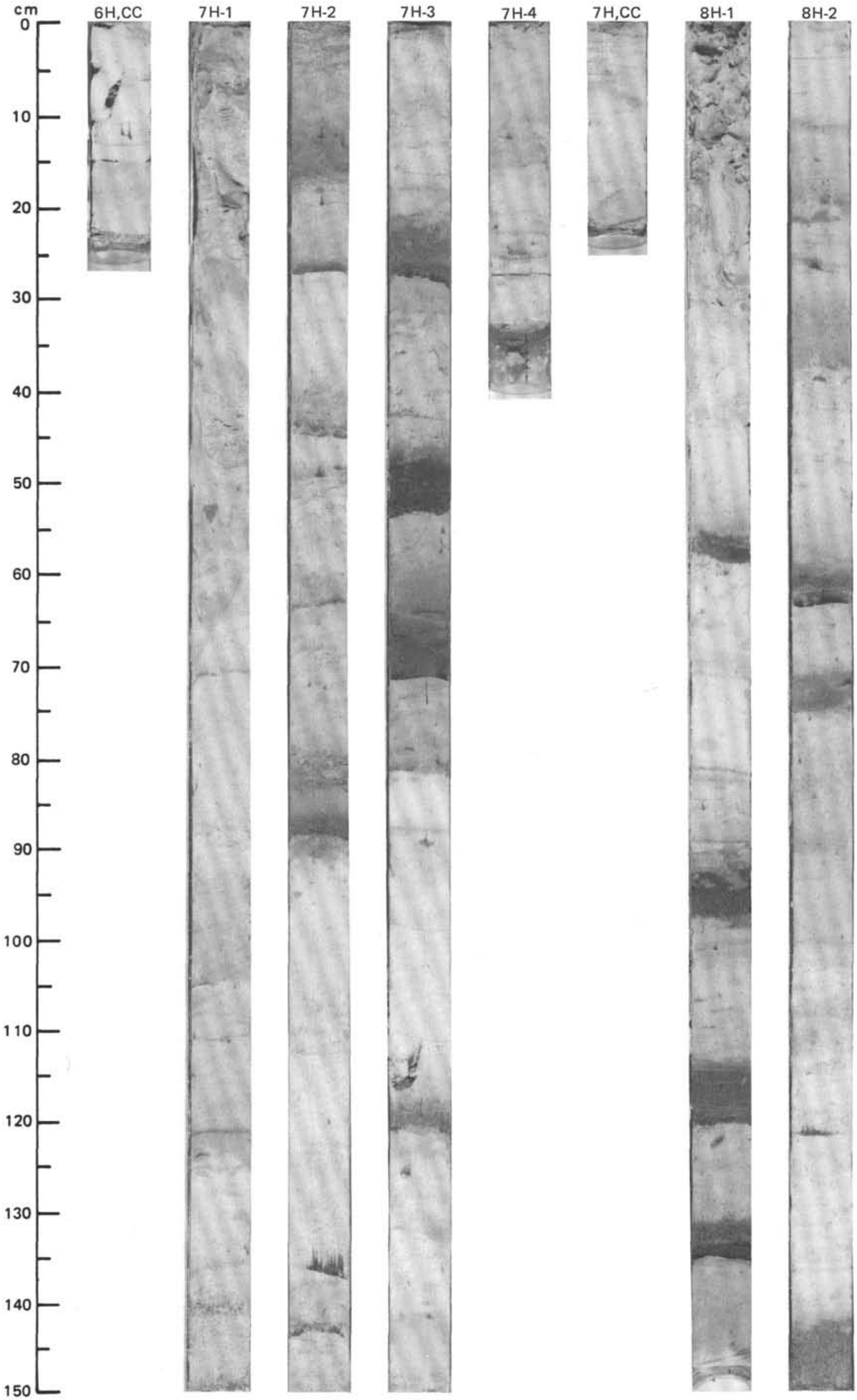
cm
0
10
20
30
40
50
60
70
80
90
100
110
120
130
140
150
6H,CC
7H-1
7H-2
7H-3
7H-4
7H,CC
8H-1
8H-2

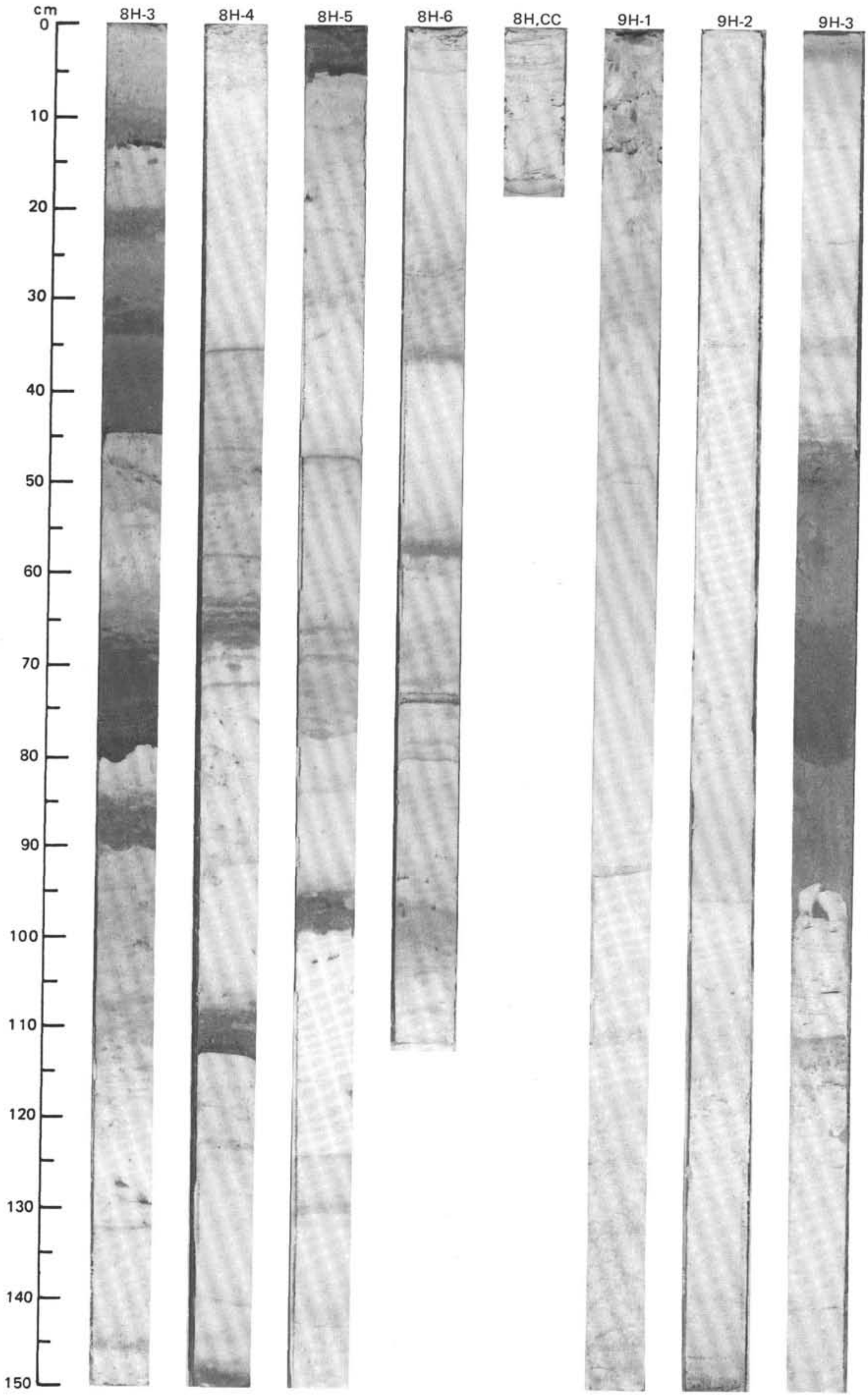
cm
0
10
20
30
40
50
60
70
80
90
100
110
120
130
140
150
8H-3
8H-4
8H-5
8H-6
8H,CC
9H-1
9H-2
9H-3

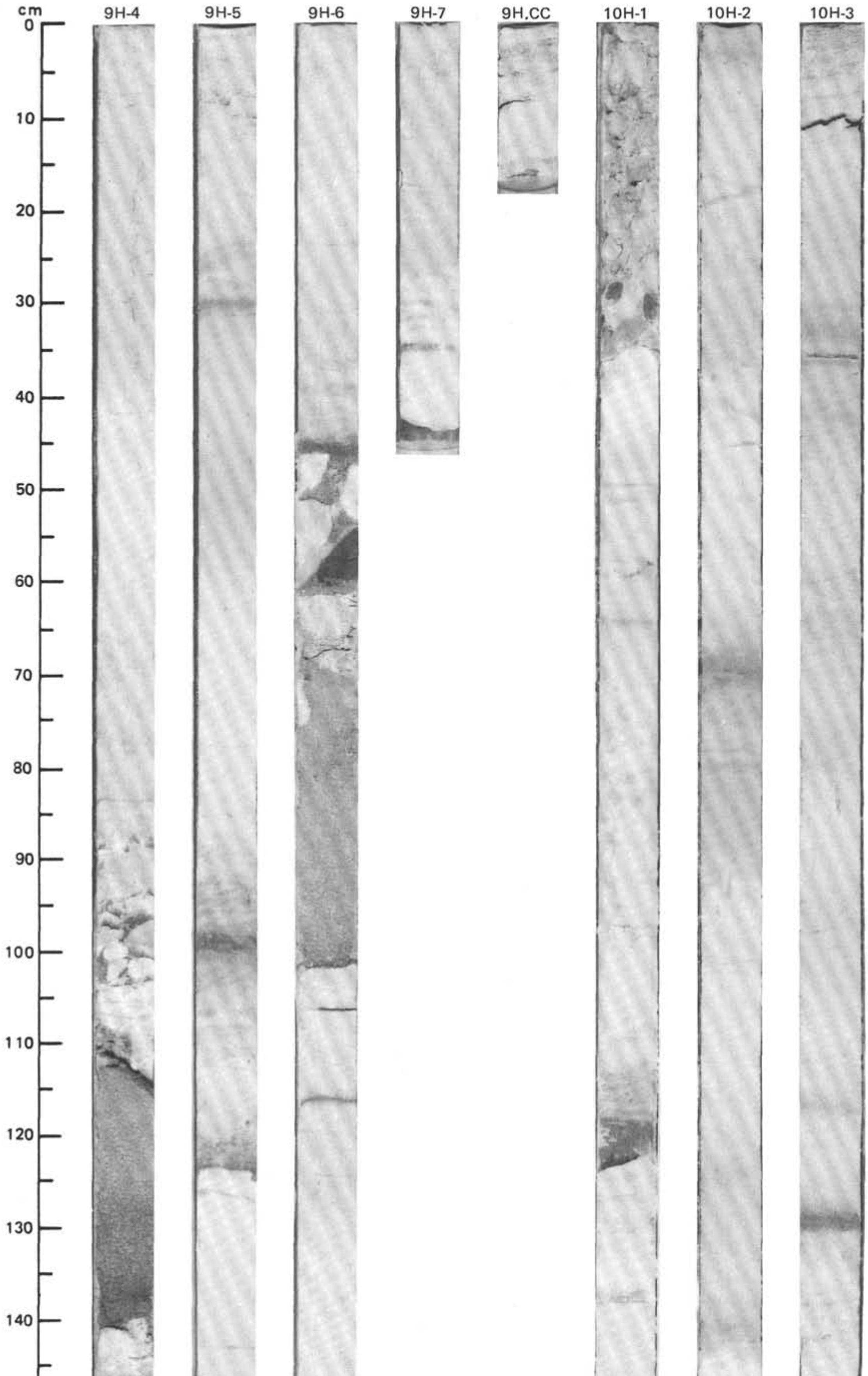
cm
0
10
20
30
40
50
60
70
80
90
100
110
120
130
140
150
9H-4
9H-5
9H-6
9H-7
9H,CC
10H-1
10H-2
10H-3

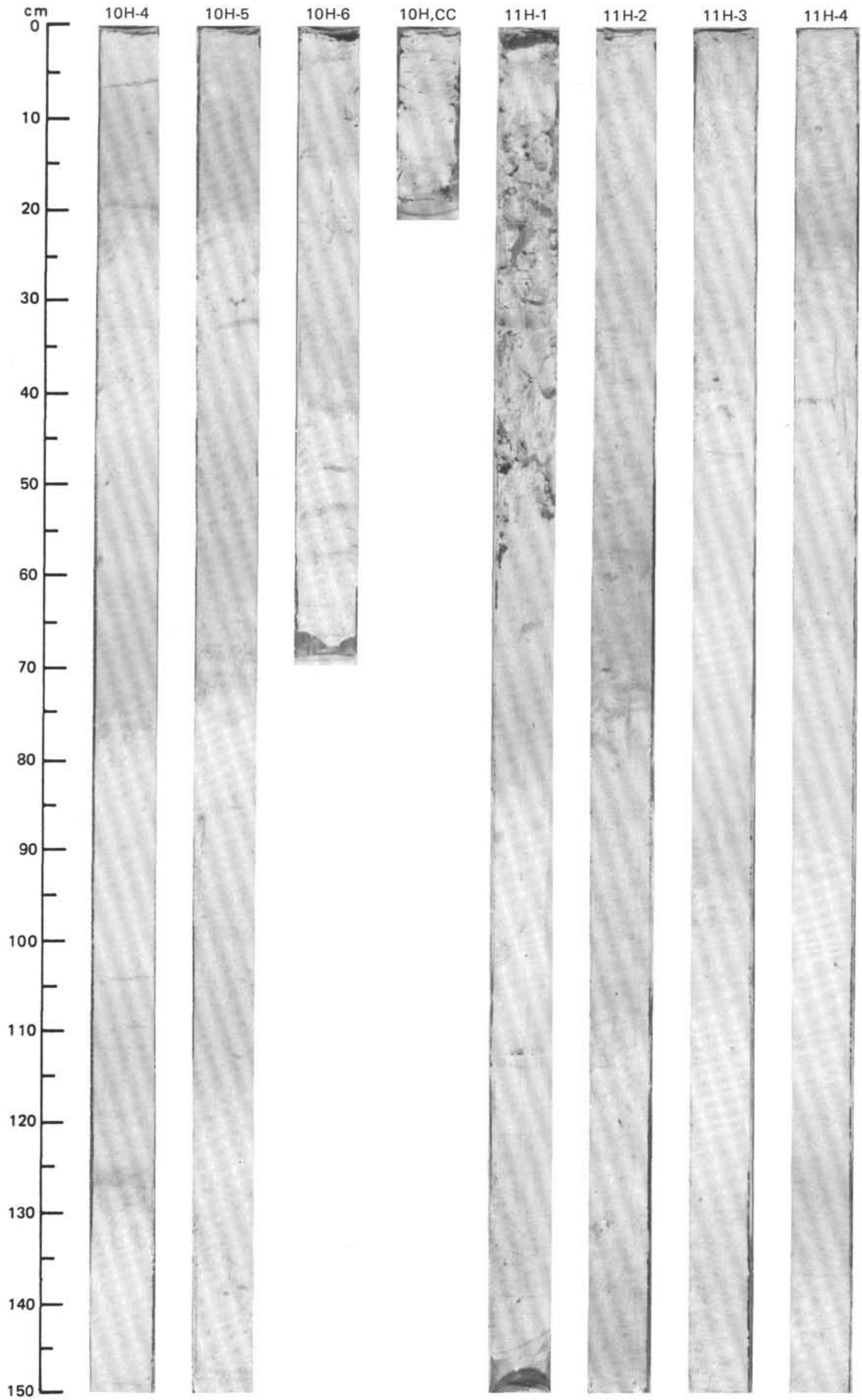
cm
0
10
20
30
40
50
60
70
80
90
100
110
120
130
140
150
10H-4
10H-5
10H-6
10H,CC
11H-1
11H-2
11H-3
11H-4

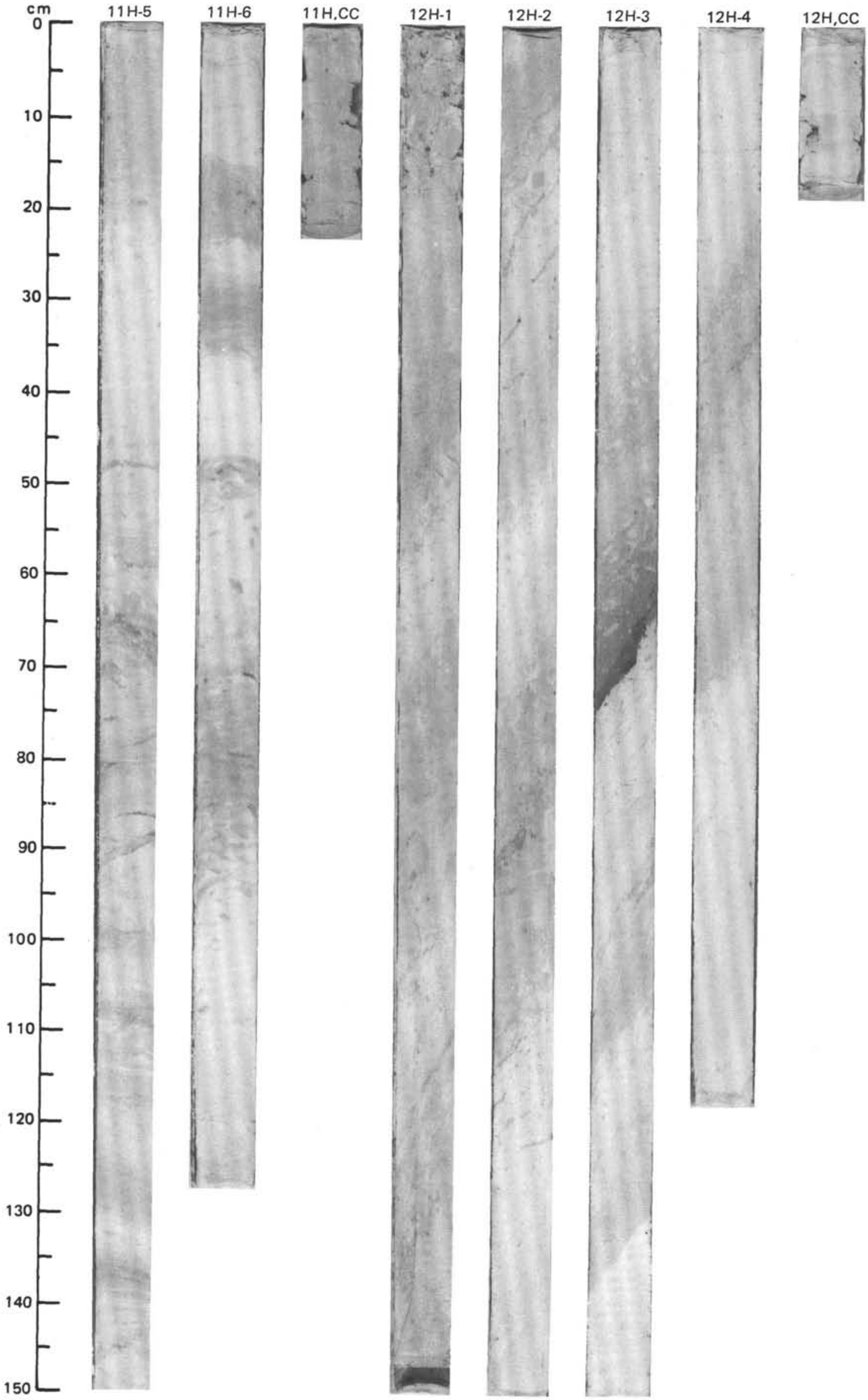
cm
0
10
20
30
40
50
60
70
80
90
100
110
120
130
140
150
11H-5
11H-6
11H,CC
12H-1
12H-2
12H-3
12H-4
12H,CC

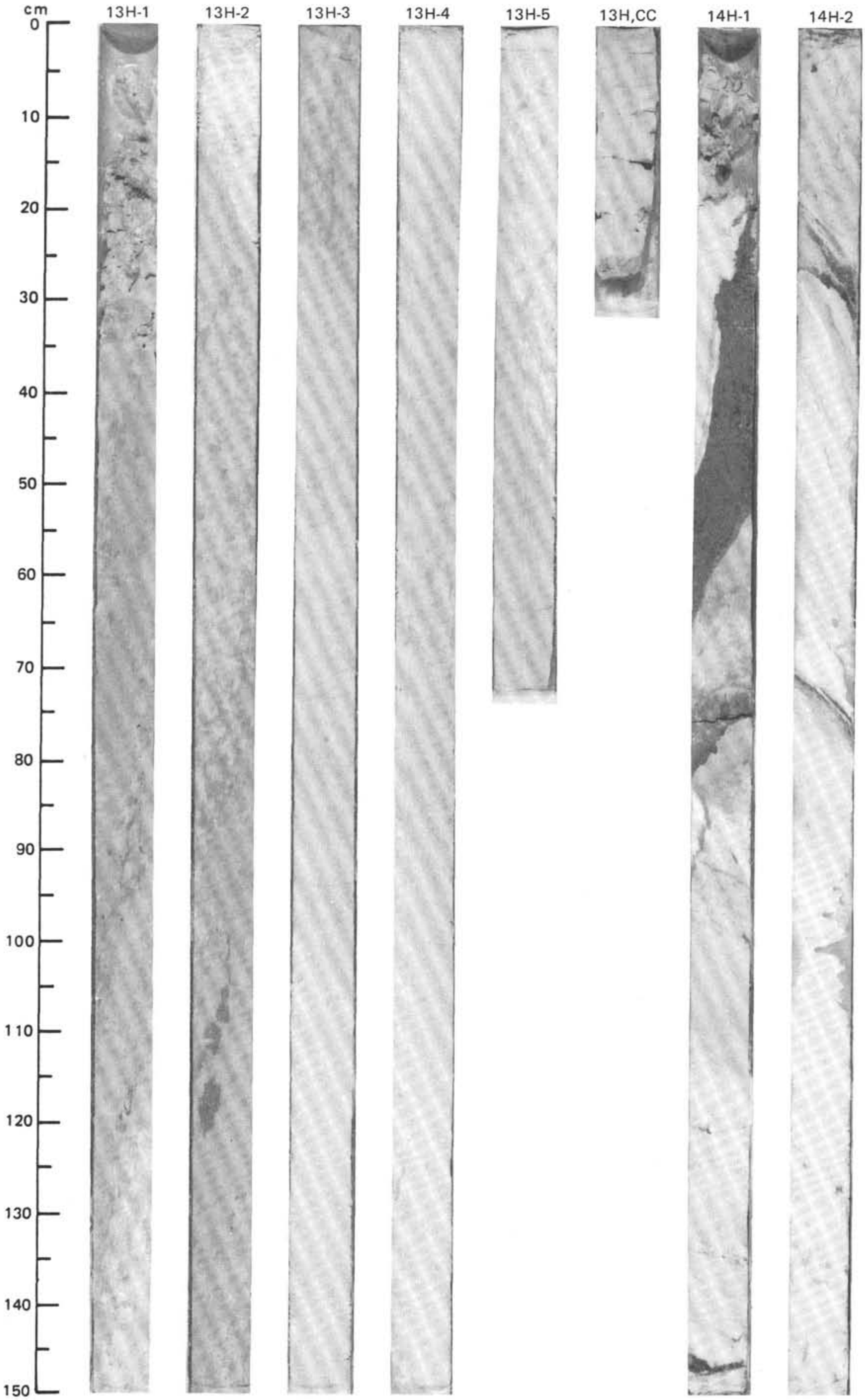
cm
0
10
20
30
40
50
60
70
80
90
100
110
120
130
140
150
13H-1
13H-2
13H-3
13H-4
13H-5
13H,CC
14H-1
14H-2

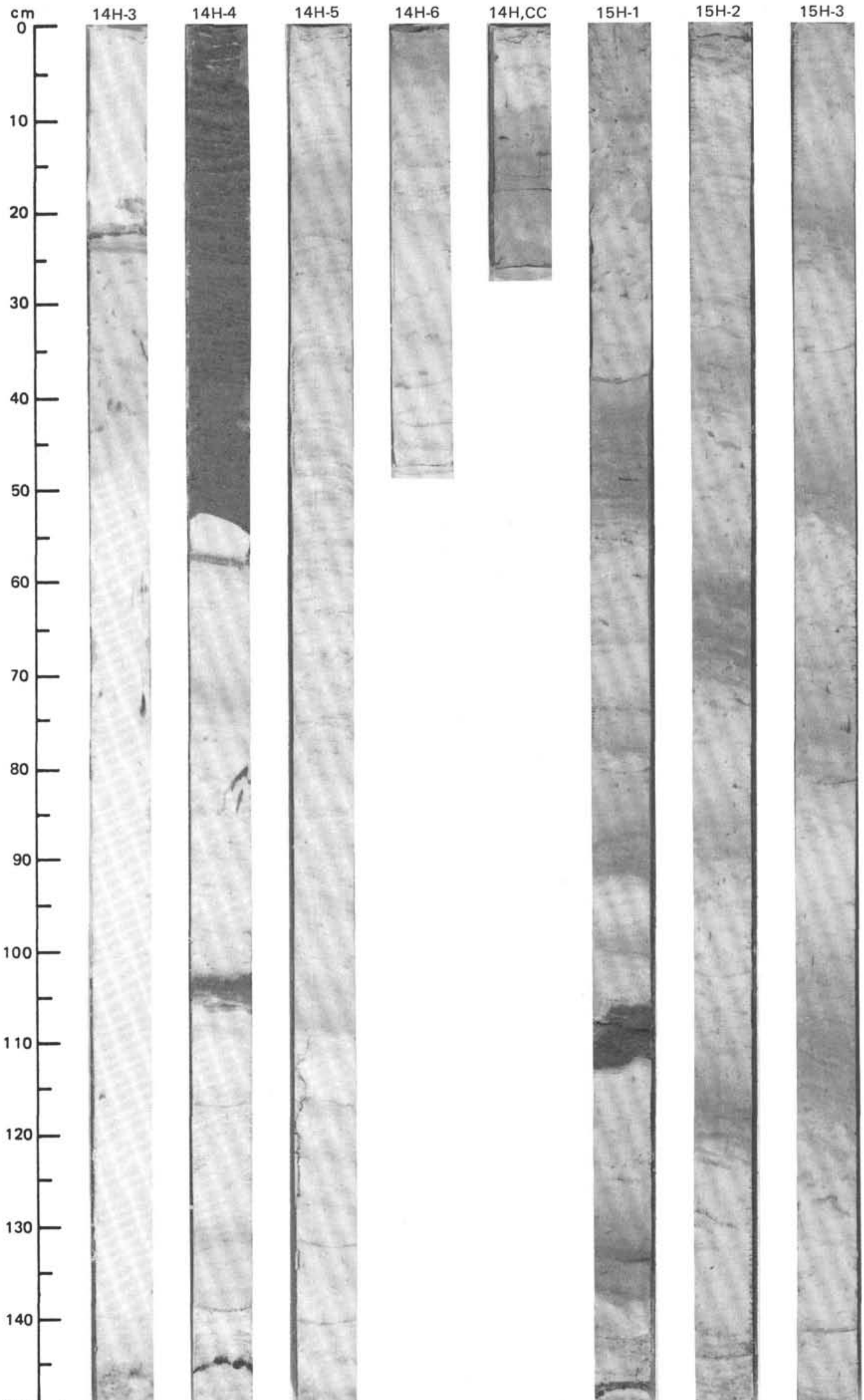
cm
0
10
20
30
40
50
60
70
80
90
100
110
120
130
140
150
14H-3
14H-4
14H-5
14H-6
14H,CC
15H-1
15H-2
15H-3

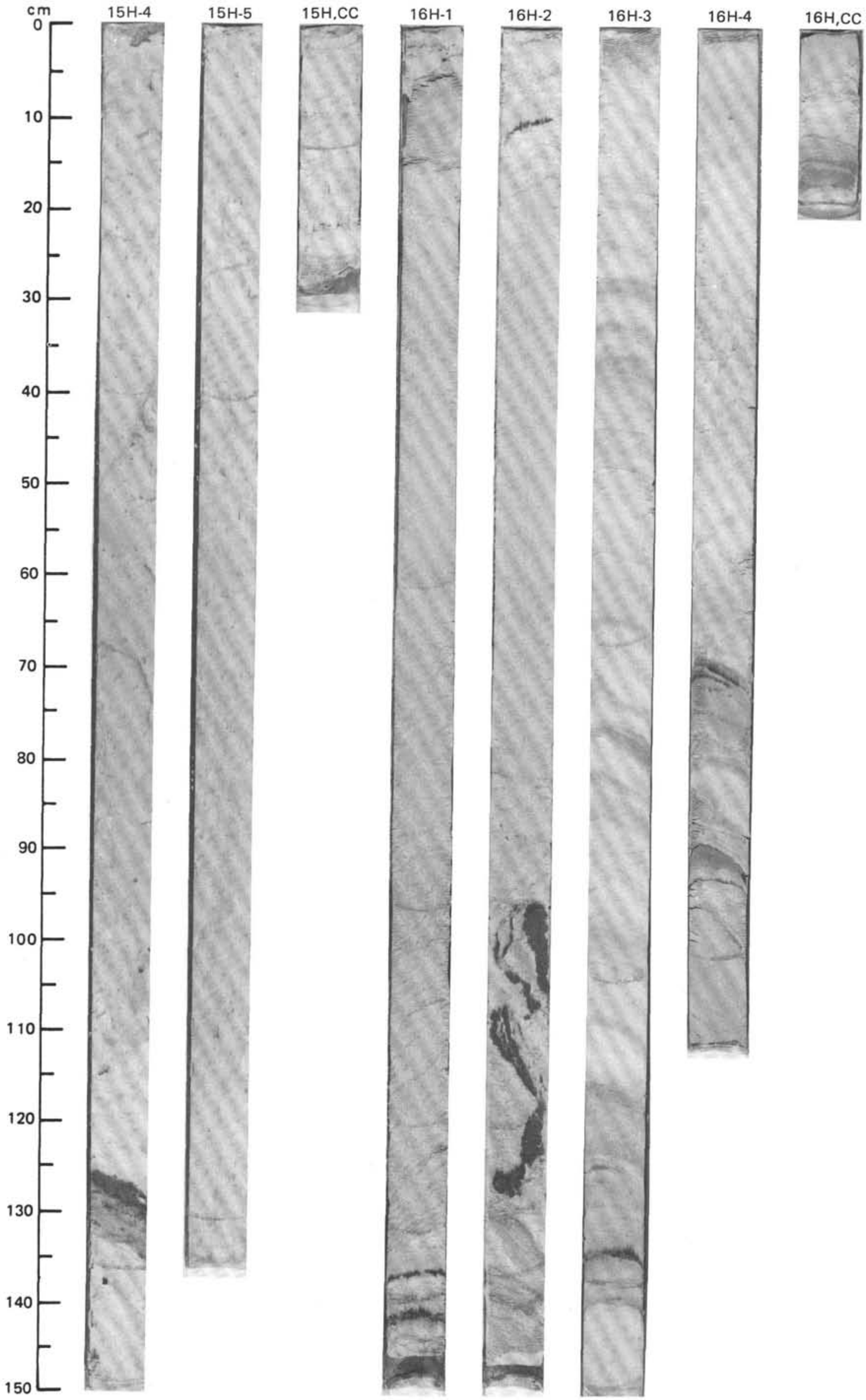
cm
0
10
20
30
40
50
60
70
80
90
100
110
120
130
140
150
15H-4
15H-5
15H,CC
16H-1
16H-2
16H-3
16H-4
16H,CC

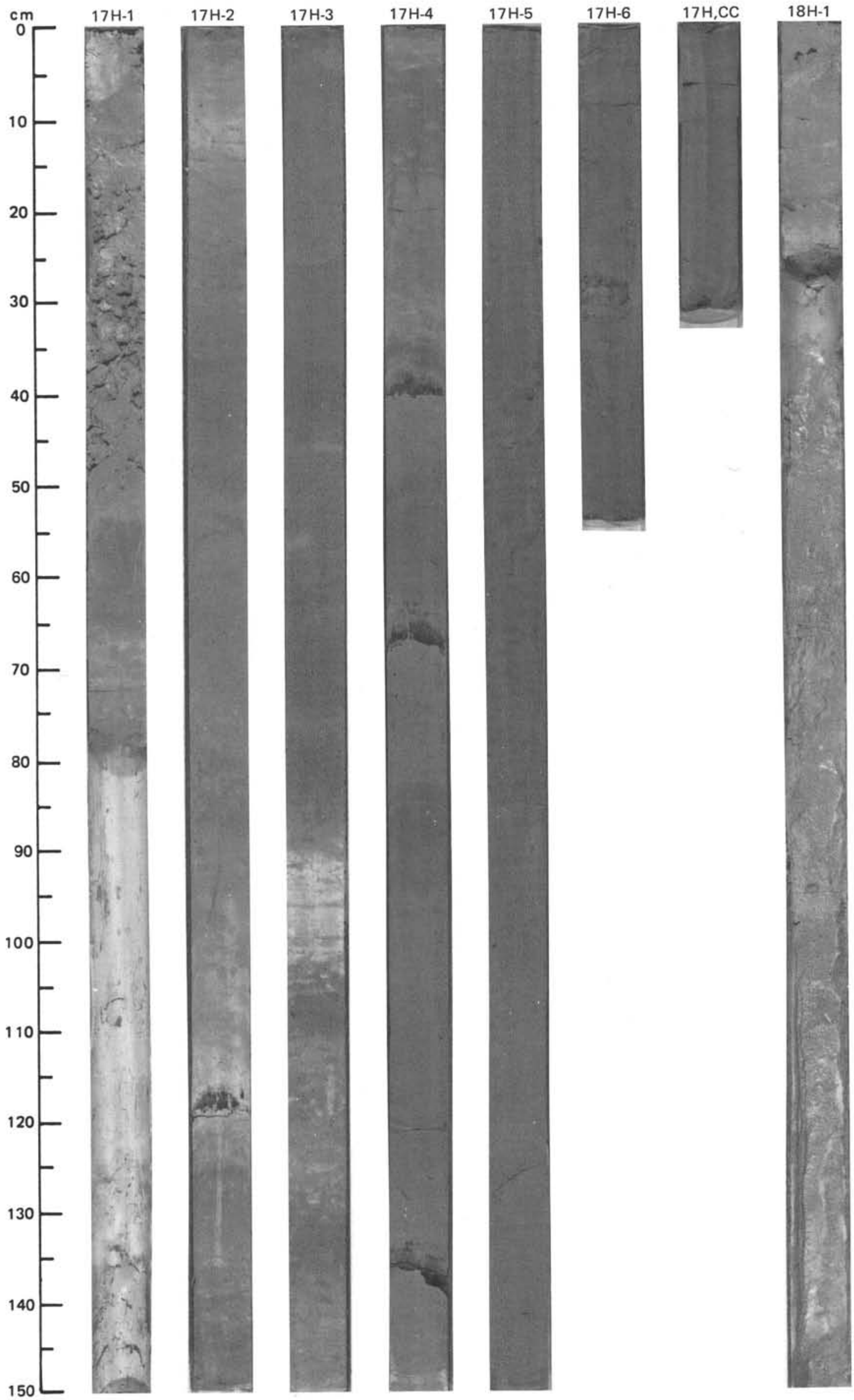
cm
0
10
20
30
40
50
60
70
80
90
100
110
120
130
140
150
17H-1
17H-2
17H-3
17H-4
17H-5
17H-6
17H,CC
18H-1

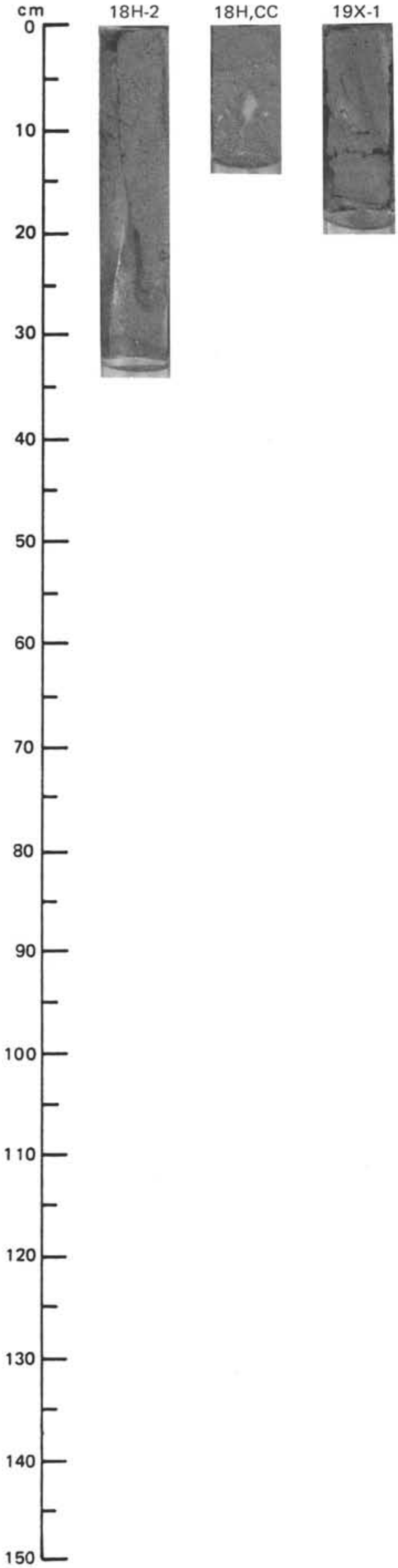
cm
18H-2
18H,CC
19X-1
0
10
20
30
40
50
60
70
80
90
100
110
120
130
140
150